

Discrete flavour and CP symmetries in light of JUNO and neutrino global fit

Gui-Jun Ding^{a,b*}, Cai-Chang Li^{c,d,e†}, Jun-Nan Lu^{a‡}, S. T. Petcov^{f,g§}

^a*Department of Modern Physics and Anhui Center for fundamental sciences in theoretical physics, University of Science and Technology of China, Hefei, Anhui 230026, China*

^b*College of Physics, Guizhou University, Guiyang 550025, China*

^c*School of Physics, Northwest University, Xi'an 710127, China*

^d*Shaanxi Key Laboratory for Theoretical Physics Frontiers, Xi'an 710127, China*

^e*NSFC-SPTP Peng Huanwu Center for Fundamental Theory, Xi'an 710127, China*

^f*INFN/SISSA, Via Bonomea 265, 34136 Trieste, Italy*

^g*Kavli IPMU (WPI), University of Tokyo, 5-1-5 Kashiwanoha, 277-8583 Kashiwa, Japan*

Abstract

Working within the reference three-neutrino mixing framework, we confront the lepton mixing predictions derived using non-Abelian discrete flavour and CP symmetries with the first JUNO data on the solar neutrino mixing parameters $\sin^2 \theta_{12}$ and with the results of the latest global neutrino data analysis. We focus on symmetry breaking patterns for which the lepton PMNS mixing matrix depends only on one or two free real parameters. Performing a comprehensive statistical analysis in each of the considered cases, we report the best fit values, the 3σ C.L. allowed ranges and the χ^2 -distributions of the lepton mixing observables - the three mixing angles and the three CP-violation phases. We find that the JUNO measurements can disfavour or rule out a number of the mixing patterns associated with specific types of breakings of the discrete flavour and CP symmetries. The synergy of JUNO, DUNE and T2HK data can provide an exhaustive test of the considered approach to lepton mixing based on non-Abelian discrete lepton flavour symmetries combined with the CP symmetry.

*E-mail: dinggj@ustc.edu.cn

†E-mail: ccli@nwu.edu.cn

‡E-mail: junnanlu@ustc.edu.cn

§E-mail: petcov@sisssa.it Also at Institute of Nuclear Research and Nuclear Energy, Bulgarian Academy of Sciences, 1784 Sofia, Bulgaria.

Contents

1	Introduction	2
2	Theoretical approach and master formulas	5
2.1	$\mathcal{G}_\ell = Z_n$ ($n \geq 3$) or K_4 and $\mathcal{G}_\nu = Z_2 \times H_{CP}^\nu$	6
2.2	$\mathcal{G}_\ell = Z_2 \times H_{CP}^\ell$ and $\mathcal{G}_\nu = Z_2 \times H_{CP}^\nu$	8
3	Lepton mixing with one free parameter	9
4	Lepton mixing with two free parameters	16
4.1	The breaking patterns of $A_5 \rtimes H_{CP}$	17
4.2	The breaking patterns of $\Sigma(168) \rtimes H_{CP}$	19
4.3	The breaking patterns of $\Delta(6n^2) \rtimes H_{CP}$	21
5	Numerical analysis	26
5.1	Lepton mixing matrix depending on one free parameter	27
5.2	Lepton mixing matrix depending on two free parameters	30
6	Summary and conclusion	37
A	Group theory of A_5, $\Sigma(168)$ and $\Delta(6n^2)$	46
A.1	The group A_5	46
A.2	The group $\Sigma(168)$	46
A.3	The series group $\Delta(6n^2)$	47
A.4	The series group D_n	48
B	Allowed ranges of lepton mixing observables for viable one- and two-parameter patterns	49
C	The symmetry breaking pattern $\mathcal{G}_\ell = Z_2$, $\mathcal{G}_\nu = K_4 \times H_{CP}^\nu$ and lepton flavour mixing	49

1 Introduction

The neutrino oscillation data accumulated over many years of measurements following the discovery of neutrino oscillations [1,2] revealed the existence of three-flavour neutrino mixing involving three light massive neutrinos (see, e.g., [3]). In this reference three-neutrino mixing framework the unitary PMNS neutrino matrix is parametrised by three angles and, depending on whether the massive neutrinos are Dirac or Majorana particles, by one Dirac or one Dirac and two Majorana CP-violation (CPV) phases. In the so-called “standard” parametrisation we will employ in the present study, the Pontecorvo–Maki–Nakagawa–Sakata (PMNS) matrix has the form [3,4]:

$$U = \begin{pmatrix} c_{12}c_{13} & s_{12}c_{13} & s_{13}e^{-i\delta_{CP}} \\ -s_{12}c_{23} - c_{12}s_{13}s_{23}e^{i\delta_{CP}} & c_{12}c_{23} - s_{12}s_{13}s_{23}e^{i\delta_{CP}} & c_{13}s_{23} \\ s_{12}s_{23} - c_{12}s_{13}c_{23}e^{i\delta_{CP}} & -c_{12}s_{23} - s_{12}s_{13}c_{23}e^{i\delta_{CP}} & c_{13}c_{23} \end{pmatrix} \text{diag}(1, e^{i\frac{\alpha_{21}}{2}}, e^{i\frac{\alpha_{31}}{2}}), \quad (1.1)$$

where $c_{ij} \equiv \cos \theta_{ij}$, $s_{ij} \equiv \sin \theta_{ij}$, δ_{CP} is the Dirac CP-violation phase and $\alpha_{21,31}$ are the two Majorana CPV phases [5]. As is well known, the three-flavour neutrino oscillation probabilities depend, in addition to the three neutrino mixing angles, on the two neutrino

mass squared differences $\Delta m_{21}^2 \equiv m_2^2 - m_1^2$ and $\Delta m_{31}^2 \equiv m_3^2 - m_1^2$, and on the Dirac CP violating (CPV) phase. The five parameters θ_{12} , θ_{13} , θ_{23} , Δm_{21}^2 and $|\Delta m_{31}^2|$ have been measured in neutrino oscillation experiments with high precision. However, the sign of Δm_{31}^2 cannot be determined from the existing data, the two possible signs corresponding to two types of neutrino mass spectra: with normal ordering (NO) if $\Delta m_{31}^2 > 0$, and with inverted ordering (IO) for $\Delta m_{31}^2 < 0$. The data on the Dirac CPV phase is inconclusive having large uncertainties [3]. There is no experimental information on the values of the Majorana phases, which play important role, e.g., in the phenomenology of neutrinoless double beta decay (see, e.g., [4]).

For the solar, reactor and atmospheric neutrino mixing angles θ_{12} , θ_{13} and θ_{23} , it was obtained in the latest analysis of the global neutrino oscillation data [6]:

$$\sin^2 \theta_{12} = 0.308_{-0.011}^{+0.012}, \quad \sin^2 \theta_{13} = 0.02215_{-0.00058}^{+0.00056}, \quad (1.2)$$

$$\sin^2 \theta_{23} = 0.470_{-0.013}^{+0.017} \text{ for NO}, \quad \sin^2 \theta_{23} = 0.550_{-0.015}^{+0.012} \text{ for IO with SuperKamiokande}, \quad (1.3)$$

$$\sin^2 \theta_{23} = 0.561_{-0.015}^{+0.012} \text{ for NO}, \quad \sin^2 \theta_{23} = 0.562_{-0.015}^{+0.012} \text{ for IO without SuperKamiokande} \quad (1.4)$$

where the 1σ C.L. uncertainties are given and ‘‘SuperKamiokande’’ refers to SuperKamiokande atmospheric neutrino data. Similar results have been obtained in the global analyses performed by the Valencia group [7] and Bari group [8, 9]. Thus, the neutrino oscillation experiments have revealed that the neutrino or lepton mixing involves two large and one small angles. This is in strong contrast with the quark mixing exhibiting three small angles.

Understanding the origin of the peculiar pattern of lepton mixing is one of the major problems in today’s particle physics. It is part of the more general formidable and still unresolved fundamental problem of uncovering the origin(s) of the lepton and quark flavours. Several possible mechanisms of generating the observed pattern of lepton mixing have been proposed in the literature (see, e.g., [10] for a review). Among the most simple and elegant, if not the most simple and elegant, is arguably the mechanism based on non-Abelian discrete flavour symmetries, which have been extensively explored, see, e.g., [11–21] for reviews. Combining non-Abelian discrete flavour symmetries with the generalized CP (gCP) symmetry proved to be a very effective approach to address the lepton mixing problem leading to testable predictions. In this approach, the underlying flavour theory is assumed to be invariant under certain non-Abelian discrete flavour symmetry G_f and gCP symmetry denoted as H_{CP} , which should be compatible with G_f [22, 23]. Thus the full symmetry group is $G_f \times H_{CP}$ [24]. The three generation of leptons fields are assigned to transform non-trivially as some irreducible representations under the action of G_f , so that different entries of the Yukawa couplings are correlated with each other. The lepton flavour mixing arises from the non-trivial breaking of the flavour and CP symmetry group $G_f \times H_{CP}$. The residual symmetries $\mathcal{G}_\ell = G_\ell \times H_{CP}^\ell$ and $\mathcal{G}_\nu = G_\nu \times H_{CP}^\nu$ ¹ are preserved by charged lepton and neutrino sectors, respectively, where G_ℓ , G_ν are subgroups of G_f and analogously H_{CP}^ℓ , H_{CP}^ν are subsets of H_{CP} . It is remarkable that the form of the lepton mixing matrix as well as the values of the mixing angles and CPV phases are completely fixed by the groups \mathcal{G}_ℓ , \mathcal{G}_ν and their relative embedding into $G_f \times H_{CP}$, the details of the symmetry breaking dynamics being irrelevant. Most importantly, this approach is very predictive since the lepton mixing matrix can only depend on very few parameters.

Recently the Jiangmen Underground Neutrino Observatory (JUNO) experiment [25], considered originally in [26–29], reported a high-precision determination of the solar oscillation parameters $\sin^2 \theta_{12}$ and Δm_{21}^2 using the first 59.1 days of data [30]:

$$\sin^2 \theta_{12} = 0.3092 \pm 0.0087, \quad \Delta m_{21}^2 = (7.50 \pm 0.12) \times 10^{-5} \text{eV}^2. \quad (1.5)$$

¹If neutrinos are Majorana particle, the residual flavour and CP symmetries of neutrino sector would be commutable, so that \mathcal{G}_ν would reduce to the direct product $\mathcal{G}_\nu = G_\nu \times H_{CP}^\nu$.

where we have given also 1σ uncertainties in the best fit values. This remarkable results improve the precision on $\sin^2 \theta_{12}$ and Δm_{21}^2 , reached in the global analyses using data accumulated over at least several years of measurements, by reducing the respective 1σ uncertainties by the factors of 1.6 and 1.3, respectively. It is estimated that after six years of data collection, the JUNO experiment will measure the oscillation parameters Δm_{21}^2 , $\sin^2 \theta_{12}$ and Δm_{31}^2 with an 1σ uncertainty respectively of 0.3%, 0.5% and 0.2% [31] - unprecedented precision that cannot be matched by any other experiment, and can also determine the neutrino mass ordering. Different aspects of the implication of JUNO's first results have been already discussed in [9, 32–44].

The approach to the lepton mixing problem based on non-Abelian discrete flavour symmetries combined with the gCP symmetry can lead to sharp predictions for lepton mixing angles and CPV phases. In this work, we shall confront the theoretical predictions of models based on this approach with the first JUNO results and the results of latest analysis of global neutrino data NuFIT-v6.0 [6], and we will perform statistical analysis of the predictions of the considered models. We shall focus on the breaking patterns of the non-Abelian discrete flavour and CP symmetries, which enforce the lepton mixing matrix to depend on only one or two real free parameters, concentrating on models with massive Majorana neutrinos. In these cases the six observables of the PMNS matrix, the three mixing angles and three CPV phases, are expressed in terms of one or two continuous real parameters and, in certain models, on one or two discrete parameters taking limited number of fixed values. As a result, some of the lepton mixing angles and CPV phases are strongly correlated with each other. These correlations can be tested experimentally. Besides the solar neutrino mixing angle θ_{12} , we study the predictions for the atmospheric neutrino angle θ_{23} , Dirac CPV phase δ_{CP} and Majorana CPV phases α_{21} and α_{31} , as well as for the CPV rephasing invariant J_{CP} which controls the magnitude of CPV effects in neutrino oscillations [45] and is a leptonic analog of the rephasing invariant introduced by Jarlskog in the quark sector [46]. It is interesting to observe that the JUNO's first result can already strongly disfavor or even exclude some mixing patterns predicted by the breaking of the considered flavour and CP symmetries. For example, the lepton mixing matrix with the second column given by $(\frac{1}{\sqrt{3}}, \frac{1}{\sqrt{3}}, \frac{1}{\sqrt{3}})^T$ is ruled out by JUNO, although it is compatible with NuFIT-v6.0 at 3σ confidence level. Moreover, we see that the high precision measurement of θ_{12} by JUNO after six years of data collection, and the precise measurement of θ_{23} and δ_{CP} by the future long baseline experiments DUNE and T2HK allow to perform exhaustive test of the approach to lepton mixing based on the non-Abelian discrete flavour and CP symmetries. The JUNO's result has been studied in the context of discrete flavour symmetry in the case of when a Z_2 residual symmetry is assumed to be preserved by the neutrino mass term [35, 42]. In this work, we shall perform a comprehensive analysis of possible symmetry breaking patterns in models in which a combination of non-Abelian discrete flavour symmetry and CP symmetry are assumed to hold initially. The potential of testing the non-Abelian discrete symmetry approach to the lepton flavour problem by the prospective data from JUNO, DUNE and T2HK has been investigated in [47], where only models based on the A_4 (T'), S_4 and A_5 symmetries, but not also on the gCP symmetry, were considered. The capability of ESSnuSB to test discriminate between a class of lepton flavor models based on discrete non-Abelian flavor symmetrie was studied in [48]. In the models considered in the present study with discrete flavour and gCP symmetries, one obtains predictions for the Majorana phases α_{21} and α_{31} as well and sharper predictions for the Dirac phase δ_{CP} .

The structure of this paper is organised as follows. In section 2 the framework of determining lepton mixing from non-Abelian discrete flavour and CP symmetry breaking is presented, and we give the master formula of the lepton mixing matrix for different symmetry breaking patterns. The symmetry breaking pattern with $\mathcal{G}_\ell = Z_n$ ($n \geq 3$) or K_4 ,

$\mathcal{G}_\nu = Z_2 \times H_{CP}^\nu$ and the possible lepton mixing matrices are studied in section 3, and expressions of lepton mixing parameters as well as CP invariants for each case are presented. In this scenario, the lepton mixing matrix depends on a single real rotation angle θ , and one column of the lepton mixing matrix is fixed by the residual symmetry. We study the symmetry breaking pattern $\mathcal{G}_\ell = Z_2 \times H_{CP}^\ell$, $\mathcal{G}_\nu = Z_2 \times H_{CP}^\nu$ in section 4, the resulting lepton mixing matrix depends on two free rotation angles θ_ℓ and θ_ν , and only one entry of the lepton mixing matrix is fixed by symmetry consideration. The current neutrino oscillation data can be well accommodated in this scenario, and we make definite predictions for θ_{23} and δ_{CP} . A statistical analysis is performed for both NO and IO neutrino mass spectra in section 5, the best fit values and the 3σ allowed regions of the mixing parameters are listed in tables for both neutrino mass spectra. The χ^2 distributions of $\sin^2 \theta_{12}$, $\sin^2 \theta_{23}$ and δ_{CP} are also plotted. Finally we present our main conclusion in section 6. The details on the flavour groups A_5 , $\Sigma(168)$ and $\Delta(6n^2)$ are given in Appendix A. The allowed regions of the lepton mixing parameters for all the viable one-parameter and two-parameters models are collected in Appendix B. We have explored an alternative symmetry breaking pattern $\mathcal{G}_\ell = Z_2$, $\mathcal{G}_\nu = K_4 \times H_{CP}^\nu$ in Appendix C, for which the resulting lepton mixing matrix also depends on two real free parameters. However, no phenomenologically viable lepton mixing matrix can be obtained in this scenario because the predicted value of the solar neutrino mixing angle θ_{12} lies significantly outside the 3σ region allowed by JUNO.

2 Theoretical approach and master formulas

It is well known that in the non-Abelian discrete symmetry approach to the lepton flavour problem one can predict both lepton mixing angles and CPV phases from the breaking of flavour and gCP symmetries [18, 21, 24]. In this approach, the full flavour and CP symmetry described by the group $G_f \times H_{CP}$ ², valid at some high energy scale, is broken down to $\mathcal{G}_\ell = G_\ell \times H_{CP}^\ell$ and $\mathcal{G}_\nu = G_\nu \times H_{CP}^\nu$ in the charged lepton and neutrino sectors, respectively, where G_ℓ , G_ν , with $G_\ell \neq G_\nu$, and H_{CP}^ℓ , H_{CP}^ν are subgroups of G_f and H_{CP} respectively. The lepton flavour mixing is completely fixed by the group structure of $G_f \times H_{CP}$ and the residual symmetries (see, e.g., [49, 50] and the review articles [16, 18, 21]), with the details of the dynamics of the flavour and CP symmetries breaking being irrelevant. In order to accommodate the large lepton mixing angles, the three generations of left-handed leptons are usually assumed to transform as a faithful irreducible triplet representation $\mathbf{3}$ of G_f .

As is also well known, the residual symmetries significantly constrain the lepton mass matrices and their diagonalization matrices (see, e.g., Refs. [16, 18, 21] for details). In the case of the charged lepton mass matrix m_ℓ , assumed to be given in the right-left (R-L) convention (i.e., $\bar{\psi}_R m_\ell \psi_L$), the residual symmetry $G_\ell \times H_{CP}^\ell$ constrains the hermitian combination $m_\ell^\dagger m_\ell$ as follows³

$$\rho_{\mathbf{3}}^\dagger(g_\ell) m_\ell^\dagger m_\ell \rho_{\mathbf{3}}(g_\ell) = m_\ell^\dagger m_\ell, \quad g_\ell \in G_\ell, \quad (2.2)$$

$$X_{\ell\mathbf{3}}^\dagger m_\ell^\dagger m_\ell X_{\ell\mathbf{3}} = (m_\ell^\dagger m_\ell)^*, \quad X_{\ell\mathbf{3}} \in H_{CP}^\ell. \quad (2.3)$$

²When combining the flavour symmetry with gCP symmetry, a certain consistency condition has to be satisfied and the gCP symmetry corresponds to an automorphism of the flavour symmetry group G_f [22, 23]. The full symmetry group is the semi-direct product of the flavour and gCP symmetry groups G_f and H_{CP} , and it is generically denoted as $G_f \times H_{CP}$ [24].

³The residual flavour and gCP symmetries of the charged leptons satisfy the following consistency condition:

$$X_{\ell r} \rho_r^*(g_\ell) X_{\ell r}^{-1} = \rho_r(g_\ell^{-1}), \quad g_\ell \in G_\ell. \quad (2.1)$$

It follows from Eqs. (2.2) and (2.3) that $X_{\ell\mathbf{3}}$ and $\rho_{\mathbf{3}}(g_\ell)$ are diagonalized by the same unitary matrix U_ℓ :

$$U_\ell^\dagger \rho_{\mathbf{3}}(g_\ell) U_\ell = \widehat{\rho}_{\mathbf{3}}(g_\ell), \quad U_\ell^\dagger X_{\ell\mathbf{3}} U_\ell^* = \widehat{X}_{\ell\mathbf{3}}, \quad (2.4)$$

where $U_\ell^\dagger m_\ell^\dagger m_\ell U_\ell = \text{diag}(m_e^2, m_\mu^2, m_\tau^2)$, and $\widehat{\rho}_{\mathbf{3}}(g_\ell)$, $\widehat{X}_{\ell\mathbf{3}}$ are diagonal phase matrices. Note that if the residual flavour symmetry G_ℓ distinguishes the three families, the inclusion of gCP H_{CP}^ℓ would not add any information as far as lepton mixing is concerned [51, 52]

Similarly, the light neutrino Majorana mass matrix m_ν should be invariant under the action of residual symmetry $G_\nu \times H_{CP}^\nu$ ⁴ This implies (for m_ν written in the R-L convention)⁵:

$$\rho_{\mathbf{3}}^T(g_\nu) m_\nu \rho_{\mathbf{3}}(g_\nu) = m_\nu, \quad g_\nu \in G_\nu, \quad (2.6)$$

$$X_{\nu\mathbf{3}}^T m_\nu X_{\nu\mathbf{3}} = m_\nu^*, \quad X_{\nu\mathbf{3}} \in H_{CP}^\nu, \quad (2.7)$$

As a consequence, the neutrino diagonalization matrix U_ν is strongly constrained by the residual symmetry:

$$U_\nu^\dagger \rho_{\mathbf{3}}(g_\nu) U_\nu = \text{diag}(\pm 1, \pm 1, \pm 1), \quad U_\nu^\dagger X_{\nu\mathbf{3}} U_\nu^* = \text{diag}(\pm 1, \pm 1, \pm 1). \quad (2.8)$$

Once the flavour symmetry group G_f and the residual symmetries $G_\ell \times H_{CP}^\ell$ and $G_\nu \times H_{CP}^\nu$ are specified, U_ℓ and U_ν can be constructed by solving Eqs. (2.4) and (2.8). Subsequently the lepton mixing matrix can be determined as

$$U = U_\ell^\dagger U_\nu. \quad (2.9)$$

In the following, we present several typical choices of the residual symmetries for which the lepton mixing matrix only depends on one to two free parameters⁶. The residual symmetries G_ℓ and G_ν are Abelian subgroups of the non-Abelian discrete symmetry G_f . In the present work, G_ℓ is restricted to Z_n ($n \geq 2$) or $K_4 = Z_2 \times Z_2$, and G_ν is taken to be Z_2 for Majorana neutrinos [21, 49, 50]. When $G_f \times H_{CP}$ is broken down to Z_n ($n \geq 3$) and $K_4 \times H_{CP}^\nu$ in the charged lepton and neutrino sectors, respectively, the resulting lepton mixing matrix takes a constant form determined entirely by these residual symmetries [54–58]. This classification yields 17 sporadic mixing patterns, all of which are now ruled out by experimental data [56, 58]. If instead $G_f \times H_{CP}$ is broken into Z_2 and $K_4 \times H_{CP}^\nu$ in the two sectors, the corresponding lepton mixing matrix depends on two real parameters [59]. However, this breaking pattern is disfavored by the latest global analysis from NuFIT [6], as detailed in Appendix C.

2.1 $\mathcal{G}_\ell = Z_n$ ($n \geq 3$) or K_4 and $\mathcal{G}_\nu = Z_2 \times H_{CP}^\nu$

If the flavour symmetry G_f is finite and the residual symmetries G_l generated by g_ℓ distinguishes the three charged lepton families, then G_l can be taken to be a cyclic group

⁴The restricted consistency condition in the case of neutrino Majorana mass term reads:

$$X_{\nu r} \rho_r^*(g_\nu) X_{\nu r}^{-1} = \rho_r(g_\nu), \quad g_\nu \in G_\nu, \quad X_{\nu r} \in H_{CP}^\nu. \quad (2.5)$$

This implies that the residual flavour and CP symmetries in the neutrino sector are commutable.

⁵For neutrino Dirac mass matrix the invariance under the action of the residual symmetry leads to constraints similar to those for the charged lepton mass matrix discussed above.

⁶In certain cases of A_4 , S_4 and A_5 symmetries one gets predictions either for $\sin^2 \theta_{12}$, or for $\sin^2 \theta_{23}$, or else for the Dirac CPV phase δ_{CP} in the PMNS lepton mixing matrix even when the lepton mixing matrix depends on 3 real constant parameters (see, e.g., [47, 53]). Here we do not consider these cases.

Z_n with $n \geq 3$ (or a Klein K_4 group). In this case, the representation matrix $\rho_{\mathbf{3}}(g_\ell)$ is diagonalized by a unitary matrix Σ_ℓ via

$$\Sigma_\ell^\dagger \rho_{\mathbf{3}}(g_\ell) \Sigma_\ell = \rho_{\mathbf{3}}^{\text{diag}}(g_\ell), \quad (2.10)$$

where the columns of Σ_ℓ correspond to the eigenvectors of $\rho_{\mathbf{3}}(g_\ell)$. The matrix Σ_ℓ is defined up to multiplication by a diagonal unitary matrix Q_ℓ and a permutation matrix P_ℓ . As a consequence of Eq. (2.4), the charged lepton diagonalization matrix can be written as

$$U_\ell = \Sigma_\ell P_\ell Q_\ell. \quad (2.11)$$

It implies that the unitary diagonalization matrix U_ℓ of the charged lepton mass matrix is determined entirely, up to column permutations and phases.

Concerning the neutrino sector, since $X_{\nu\mathbf{3}}$ is a symmetric and unitary matrix, by performing the Takagi factorization $X_{\nu\mathbf{3}}$ can be written as

$$X_{\nu\mathbf{3}} = \Sigma_\nu \Sigma_\nu^T, \quad \text{with} \quad \Sigma_\nu^\dagger \rho_{\mathbf{3}}(g_\nu) \Sigma_\nu = \pm \text{diag}(1, -1, -1). \quad (2.12)$$

The Z_2 symmetry constrains $\rho_{\mathbf{3}}^{\text{diag}}(g_\nu)$ to have two identical eigenvalues which is either +1 or -1. These can be any two of the three eigenvalues of $\rho_{\mathbf{3}}(g_\nu)$. In Eq. (2.12) we have chosen them to be the 2nd and the 3rd ones, but we will account for the other possibilities by adding an appropriate permutation matrix P_ν in the neutrino diagonalization matrix (see below).

The unitary matrix Σ_ν is constructed following the method outlined in Ref. [60]. In accordance with the constraints from Eq. (2.8), the neutrino diagonalization matrix U_ν takes the form [24, 60]:

$$U_\nu = \Sigma_\nu R_{23}(\theta) P_\nu Q_\nu, \quad (2.13)$$

where $R_{23}(\theta)$ denotes a rotation in the 2–3 plane by an angle θ , and P_ν represents an arbitrary permutation matrix. Here Q_ν in Eq. (2.13) is a diagonal matrix with elements equal to ± 1 and $\pm i$. Without loss of generality it can be given as $Q_\nu = \text{diag}(1, i^{k_1}, i^{k_2})$ with $k_{1,2} = 0, 1, 2, 3$. Hence the lepton mixing matrix U is of the form [24, 49, 60]

$$U = U_\ell^\dagger U_\nu = Q_\ell^\dagger P_\ell^T \Sigma_\ell^\dagger \Sigma_\nu R_{23}(\theta) P_\nu Q_\nu, \quad (2.14)$$

where the diagonal phase matrix Q_ℓ can be absorbed through a redefinition of the charged lepton fields, whereas the diagonal phase matrix Q_ν is to shift the Majorana CP phases α_{21} and α_{31} by integer multiples of π . The rotation matrix $R_{23}(\theta)$ in Eq. (2.14) and the rotation matrix $R_{13}(\theta)$ to appear later are defined as

$$R_{13}(\theta) = \begin{pmatrix} \cos \theta & 0 & \sin \theta \\ 0 & 1 & 0 \\ -\sin \theta & 0 & \cos \theta \end{pmatrix}, \quad R_{23}(\theta) = \begin{pmatrix} 1 & 0 & 0 \\ 0 & \cos \theta & \sin \theta \\ 0 & -\sin \theta & \cos \theta \end{pmatrix}. \quad (2.15)$$

Thus the lepton mixing matrix in Eq. (2.14) depends only on a single parameter θ which can be determined from the well measured reactor angle θ_{13} . This allows predictions for the solar and atmospheric mixing angles θ_{12} and θ_{23} , as well as for the CPV phases. Furthermore, since the Z_2 residual flavour symmetry can only distinguish one neutrino family from the other two generations, so that only one column of the lepton mixing matrix is fixed through the choice of residual symmetry, as can be seen from Eq. (2.14). Note that the lepton mixing matrix is determined up to possible permutations of rows and columns, since both neutrino and charged lepton masses are not constrained in this approach. The permutation matrices

P_ℓ and P_ν in Eq. (2.14) can take the following six forms:

$$\begin{aligned} P_{123} &= \begin{pmatrix} 1 & 0 & 0 \\ 0 & 1 & 0 \\ 0 & 0 & 1 \end{pmatrix}, & P_{231} &= \begin{pmatrix} 0 & 1 & 0 \\ 0 & 0 & 1 \\ 1 & 0 & 0 \end{pmatrix}, & P_{312} &= \begin{pmatrix} 0 & 0 & 1 \\ 1 & 0 & 0 \\ 0 & 1 & 0 \end{pmatrix}, \\ P_{132} &= \begin{pmatrix} 1 & 0 & 0 \\ 0 & 0 & 1 \\ 0 & 1 & 0 \end{pmatrix}, & P_{213} &= \begin{pmatrix} 0 & 1 & 0 \\ 1 & 0 & 0 \\ 0 & 0 & 1 \end{pmatrix}, & P_{321} &= \begin{pmatrix} 0 & 0 & 1 \\ 0 & 1 & 0 \\ 1 & 0 & 0 \end{pmatrix}. \end{aligned} \quad (2.16)$$

By comparing with the oscillation data in Ref. [6], one can determine which permutation matrices P_ℓ and P_ν are phenomenologically allowed. If the residual symmetry of neutrino is $\mathcal{G}_\nu = Z_2$ where no residual CP symmetry is preserved, the lepton mixing matrix would be of the form of Eq. (2.14) by replacing $R_{23}(\theta)$ with a unitary rotation in the (23) plane. As a consequence, more free parameters would be involved and the values of Majorana phases can not be predicted.

2.2 $\mathcal{G}_\ell = Z_2 \times H_{CP}^\ell$ and $\mathcal{G}_\nu = Z_2 \times H_{CP}^\nu$

When the residual symmetry in the charged lepton sector is assumed to be $Z_2^{g_\ell} \times H_{CP}^\ell$, the diagonalization matrix U_ℓ of the charged lepton mass matrix is constrained through the Takagi factorization described in the preceding section to take the following form [60]:

$$U_\ell = \Sigma_\ell R_{23}(\theta_\ell) P_\ell Q_\ell, \quad (2.17)$$

where Σ_ℓ is the Takagi factorization of the charged lepton residual CP transformation, $Q_\ell = \text{diag}(e^{i\alpha_e}, e^{i\alpha_\mu}, e^{i\alpha_\tau})$ with arbitrary real parameters $\alpha_e, \alpha_\mu, \alpha_\tau$, and P_ℓ denotes a generic three-dimensional permutation matrix chosen from the possibilities listed in Eq. (2.16). Consequently, the residual symmetry fixes the lepton mixing matrix as

$$U \equiv U_\ell^\dagger U_\nu = Q_\ell^\dagger P_\ell^T R_{23}^T(\theta_\ell) \Sigma R_{23}(\theta_\nu) P_\nu Q_\nu, \quad (2.18)$$

with

$$\Sigma \equiv \Sigma_\ell^\dagger \Sigma_\nu. \quad (2.19)$$

The phase matrix Q_ℓ can be absorbed by the charged lepton fields and the effect of Q_ν is a possible change of the Majorana phases by π . In the model independent framework, where lepton masses are not predicted, the PMNS matrix is determined up to permutations of its rows and columns, indicated by the left multiplication by P_ℓ^T and right multiplication by P_ν . Both permutation matrices P_ℓ and P_ν may take any of the six forms specified in Eq. (2.16). Notably, in this setup, one entry of the PMNS matrix is constrained to a constant value by residual symmetry—specifically, the (11) entry of Σ .

Furthermore, all mixing angles and CPV phases depend exclusively on two free parameters θ_ℓ and θ_ν . The fundamental domain for both parameters is $[0, \pi)$, since the lepton mixing matrix U from Eq. (2.18) satisfies

$$\begin{aligned} U(\theta_\ell + \pi, \theta_\nu) &= P_\ell^T \text{diag}(1, -1, -1) P_\ell U(\theta_\ell, \theta_\nu), \\ U(\theta_\ell, \theta_\nu + \pi) &= U(\theta_\ell, \theta_\nu) P_\nu^T \text{diag}(1, -1, -1) P_\nu, \end{aligned} \quad (2.20)$$

where the diagonal matrices $P_\ell^T \text{diag}(1, -1, -1) P_\ell$ and $P_\nu^T \text{diag}(1, -1, -1) P_\nu$ can be absorbed into Q_ℓ and Q_ν , respectively. In addition, the mixing matrix U exhibits the following symmetry properties:

$$P_\ell^T P_{132} P_\ell U(\theta_\ell, \theta_\nu) = Q_\ell' U(\theta_\ell + \frac{\pi}{2}, \theta_\nu), \quad U(\theta_\ell, \theta_\nu) P_\nu^T P_{132} P_\nu = U(\theta_\ell, \theta_\nu + \frac{\pi}{2}) Q_\nu', \quad (2.21)$$

where Q'_ℓ and Q'_ν are given by

$$Q'_\ell = P_\ell^T P_{132} P_\ell Q_\ell P_\ell^T P_{132}^T \text{diag}(1, -1, 1) P_\ell Q_\ell^\dagger, \quad Q'_\nu = Q_\nu P_\nu^T \text{diag}(1, -1, 1) P_{132}^T P_\nu Q_\nu^\dagger P_\nu^T P_{132} P_\nu. \quad (2.22)$$

Here Q'_ℓ represents an arbitrary phase matrix, while Q'_ν is a diagonal matrix with entries ± 1 and $\pm i$. Both can be absorbed into Q_ℓ and Q_ν , respectively. As a result, Eq. (2.21) implies that applying the row permutation $P_\ell^T P_{132} P_\ell$ and column permutation $P_\nu^T P_{132} P_\nu$ to U does not produce a new mixing pattern for any specific choice of P_ℓ and P_ν . Therefore, among the 36 possible permutations of rows and columns, only nine yield physically independent mixing patterns. This also means that the matrix element fixed by residual symmetry can occupy any one of nine distinct positions in the mixing matrix.

3 Lepton mixing with one free parameter

In this section, we consider the scenario that the flavour and CP symmetry $G_f \rtimes H_{CP}$ is broken down to $\mathcal{G}_\ell = Z_n$ ($n \geq 3$) or K_4 and $\mathcal{G}_\nu = Z_2 \times H_{CP}^\nu$ in the charged lepton and neutrino sectors respectively. The master formula of the lepton mixing matrix is given by Eq. (2.14). It is notable that the lepton mixing matrix and all mixing parameters depend on a single rotation angle θ , and one column of the mixing matrix is fixed by residual symmetry. This type of symmetry breaking pattern has also been studied for many flavour symmetry groups combined with gCP, such as A_4 [24, 52, 61], S_4 [24, 51, 62–65], T' [66], $\Delta(27)$ [67, 68], $\Delta(48)$ [69, 70], A_5 [71–75], $\Delta(96)$ [76] and the infinite group series $\Delta(3n^2) = (Z_n \times Z_n) \rtimes Z_3$ [77, 78], $\Delta(6n^2) = (Z_n \times Z_n) \rtimes S_3$ [77, 79] and $D_{9n,3n}^{(1)} = (Z_{9n} \times Z_{3n}) \rtimes S_3$ [80]. A systematical analysis of the discrete flavour group G_f up to order 2000 was performed in [60] in this scenario. It was found that all viable mixing patterns can be obtained by considering $A_5 \rtimes H_{CP}$, $\Sigma(168) \rtimes H_{CP}$, $\Delta(6n^2) \rtimes H_{CP}$ and $D_{9n,3n}^{(1)} \rtimes H_{CP}$. Since the series group $D_{9n,3n}^{(1)}$ is a subgroup of $\Delta(6(9n)^2)$ group for any positive integer n [80], all breaking patterns originating from $D_{9n,3n}^{(1)} \rtimes H_{CP}$ can be derived from those of $\Delta(6(9n)^2) \rtimes H_{CP}$. Therefore we will not explicitly discuss the flavour symmetry $D_{9n,3n}^{(1)}$ combined with CP.

The possible residual subgroups $\mathcal{G}_\ell = Z_n$ or K_4 and $\mathcal{G}_\nu = Z_2 \times H_{CP}^\nu$ have been studied for the symmetries $A_5 \rtimes H_{CP}$, $\Sigma(168) \rtimes H_{CP}$ and $\Delta(6n^2) \rtimes H_{CP}$ [60], and five possible patterns of lepton mixing matrix are found to be compatible with current experimental data of neutrino oscillation [60]. For phenomenological analysis in the next section, we report the explicit form of the mixing matrix together with the residual symmetry in the following. In addition, we shall give the analytical expressions for mixing angles and CP-violation (CPV) invariants J_{CP} , I_1 and I_2 , associated with the Dirac and two Majorana CPV phases in the PMNS neutrino mixing matrix.

In the present work, we will adopt the standard parametrization of the lepton mixing matrix [3],

$$U = \begin{pmatrix} c_{12}c_{13} & s_{12}c_{13} & s_{13}e^{-i\delta_{CP}} \\ -s_{12}c_{23} - c_{12}s_{13}s_{23}e^{i\delta_{CP}} & c_{12}c_{23} - s_{12}s_{13}s_{23}e^{i\delta_{CP}} & c_{13}s_{23} \\ s_{12}s_{23} - c_{12}s_{13}c_{23}e^{i\delta_{CP}} & -c_{12}s_{23} - s_{12}s_{13}c_{23}e^{i\delta_{CP}} & c_{13}c_{23} \end{pmatrix} \text{diag}(1, e^{i\frac{\alpha_{21}}{2}}, e^{i\frac{\alpha_{31}}{2}}), \quad (3.1)$$

where $c_{ij} \equiv \cos\theta_{ij}$, $s_{ij} \equiv \sin\theta_{ij}$, δ_{CP} is the Dirac CPV phase, and $\alpha_{21,31}$ are Majorana CPV phases. For each independent mixing pattern, we can straightforwardly extract the expressions of the mixing angles $\sin^2\theta_{13}$, $\sin^2\theta_{12}$, $\sin^2\theta_{23}$ and the CP invariants J_{CP} , I_1 , I_2 in the usual way. As regards the CPV, three weak basis invariants J_{CP} [46], I_1 and I_2 [81–85]

associated with the CP phases δ_{CP} , α_{21} and α_{31} respectively can be defined

$$\begin{aligned} J_{CP} &= \Im(U_{11}U_{33}U_{13}^*U_{31}^*) = \frac{1}{8} \sin 2\theta_{12} \sin 2\theta_{13} \sin 2\theta_{23} \cos \theta_{13} \sin \delta_{CP}, \\ I_1 &= \Im(U_{11}^{*2}U_{12}^2) = \frac{1}{4} \sin^2 2\theta_{12} \cos^4 \theta_{13} \sin \alpha_{21}, \\ I_2 &= \Im(U_{11}^{*2}U_{13}^2) = \frac{1}{4} \sin^2 2\theta_{13} \cos^2 \theta_{12} \sin(\alpha_{31} - 2\delta_{CP}). \end{aligned} \quad (3.2)$$

Here the CPV rephasing invariant J_{CP} which controls the magnitude of CPV effects in neutrino oscillations [45], is a leptonic analog of the rephasing invariant introduced by Jarlskog in the quark sector [46]. We note that a given Majorana phase α_{i1} would violate the CP-invariance if both $\text{Im}(U_{11}^{*2}U_{1i}^2) \neq 0$ and $\text{Re}(U_{11}^{*2}U_{1i}^2) \neq 0$, $i = 2, 3$ (see, e.g., [86]).

(I) The lepton mixing matrix compatible with oscillation data is given by

$$U^I = \frac{1}{\sqrt{3}} \begin{pmatrix} \sqrt{2} \sin \varphi_1 & e^{i\varphi_2} & \sqrt{2} \cos \varphi_1 \\ \sqrt{2} \cos(\varphi_1 - \frac{\pi}{6}) & -e^{i\varphi_2} & -\sqrt{2} \sin(\varphi_1 - \frac{\pi}{6}) \\ \sqrt{2} \cos(\varphi_1 + \frac{\pi}{6}) & e^{i\varphi_2} & -\sqrt{2} \sin(\varphi_1 + \frac{\pi}{6}) \end{pmatrix} R_{23}(\theta) Q_\nu, \quad (3.3)$$

where φ_1 and φ_2 are rational angles determined by residual symmetries. The mixing matrix U^I arises from the flavour symmetry groups $\Delta(6n^2)$ combined with gCP symmetry. The group structure of $\Delta(6n^2)$ is detailed in Appendix A.3. It is generated by four generators a , b , c , and d . In our working basis, the matrix representations of these generators are either real symmetric or diagonal across all irreducible representations. As a consequence, the gCP transformation matrices coincide in the same form with the representation matrices of the group generators in this basis.

The symmetry breaking pattern leading to U^I is as follows [79]:

$$\Delta(6n^2) \rtimes H_{CP} \quad : \quad G_\ell = \langle ac^s d^t \rangle, \quad G_\nu = Z_2^{bc^x d^x}, \quad X_{\nu r} = \rho_r(c^\gamma d^{-2x-\gamma}), \quad (3.4)$$

with $s, t, x, \gamma = 0, 1, \dots, n-1$. The parameters φ_1 and φ_2 in the PMNS matrix U^I is then given by:

$$\varphi_1 = \frac{s-x}{n}\pi, \quad \varphi_2 = \frac{2t-s-3(\gamma+x)}{n}\pi, \quad (3.5)$$

which are interdependent of each other, and they can take the discrete values

$$\varphi_1 = 0, \pm \frac{1}{n}\pi, \pm \frac{2}{n}\pi, \dots, \pm \frac{n-1}{n}\pi, \quad \varphi_2 \pmod{2\pi} = 0, \frac{1}{n}\pi, \frac{2}{n}\pi, \dots, \frac{2n-1}{n}\pi, \quad (3.6)$$

In particular, widely studied smaller groups $S_4 \cong [24, 12]$ ($n = 2$) and $\Delta(96) \cong [96, 64]$ ($n = 4$) can admit a reasonably good fit to the experimental data. This is compatible with the known results in the literature [24, 51, 62, 63, 76]. From the PMNS matrix U^I in Eq. (3.3), we can read out the lepton mixing angles as follow

$$\begin{aligned} \sin^2 \theta_{13} &= \frac{1}{3} \left(1 + \cos^2 \theta \cos 2\varphi_1 + \sqrt{2} \sin 2\theta \cos \varphi_1 \cos \varphi_2 \right), \\ \sin^2 \theta_{12} &= \frac{1 + \sin^2 \theta \cos 2\varphi_1 - \sqrt{2} \sin 2\theta \cos \varphi_1 \cos \varphi_2}{2 - \cos^2 \theta \cos 2\varphi_1 - \sqrt{2} \sin 2\theta \cos \varphi_1 \cos \varphi_2} = 1 + \frac{\cos 2\varphi_1 - 1}{3 \cos^2 \theta_{13}}, \\ \sin^2 \theta_{23} &= \frac{1 - \cos^2 \theta \sin(\pi/6 + 2\varphi_1) - \sqrt{2} \sin 2\theta \cos \varphi_2 \sin(\pi/6 - \varphi_1)}{2 - \cos^2 \theta \cos 2\varphi_1 - \sqrt{2} \sin 2\theta \cos \varphi_1 \cos \varphi_2}. \end{aligned} \quad (3.7)$$

A sum rule between the solar and reactor mixing angles is given by the relation

$$3 \cos^2 \theta_{12} \cos^2 \theta_{13} = 2 \sin^2 \varphi_1, \quad (3.8)$$

which leads to the constraint $\cos^2 \theta_{12} \cos^2 \theta_{13} \leq 2/3$. Using the experimentally determined 3σ ranges $0.275 \leq \sin^2 \theta_{12} \leq 0.345$ and $0.02030 \leq \sin^2 \theta_{13} \leq 0.02388$ [6], the allowed values for the parameter φ_1 are found to be

$$\varphi_1/\pi \in [0.4351, 0.5649] \cup [1.4351, 1.5649]. \quad (3.9)$$

This indicates that φ_1 is approximately $\pi/2$ or $3\pi/2$. Additionally, when θ_{13} is restricted to its 3σ experimental bounds, the solar mixing angle θ_{12} must lie within the following interval:

$$0.317 \leq \sin^2 \theta_{12} \leq 0.345. \quad (3.10)$$

This range will be directly tested by the JUNO experiment, which is projected to constrain $\sin^2 \theta_{12}$ to $[0.3022, 0.3118]$ at 3σ after six years of operation [31].

The three CP rephasing invariants J_{CP} , I_1 , and I_2 are expressed as:

$$\begin{aligned} |J_{CP}| &= \frac{1}{6\sqrt{6}} |\sin 2\theta \sin \varphi_2 \sin 3\varphi_1|, \\ |I_1| &= \frac{4}{9} \left| \cos \theta \sin^2 \varphi_1 \sin \varphi_2 \left(\cos \theta \cos \varphi_2 - \sqrt{2} \sin \theta \cos \varphi_1 \right) \right|, \\ |I_2| &= \frac{4}{9} \left| \sin \theta \sin^2 \varphi_1 \sin \varphi_2 \left(\sin \theta \cos \varphi_2 + \sqrt{2} \cos \theta \cos \varphi_1 \right) \right|. \end{aligned} \quad (3.11)$$

The above three CP invariants are conventionally defined in Eq. (3.2). In this work, we shall present the absolute values of J_{CP} , I_1 and I_2 because the signs of I_1 and I_2 depend in the case of CP-invariance on the relative CP parity of the relevant neutrino states, which is encoded in the matrix Q_ν , and the overall signs of all the three CP invariant would be changed if the left-handed lepton doublets are assigned to conjugate triplet $\bar{\mathbf{3}}$ instead of $\mathbf{3}$.

Furthermore, an exact sum rule relating the mixing angles and the Dirac CPV phase can be derived as follows:

$$\begin{aligned} \cos \delta_{CP} &= \frac{\cos 2\theta_{23} (3 \cos 2\theta_{12} - 2 \sin^2 \varphi_1) + \sqrt{3} \sin 2\varphi_1}{3 \sin 2\theta_{12} \sin \theta_{13} \sin 2\theta_{23}} \\ &= \frac{\cos 2\theta_{23} (\cos^2 \theta_{12} \sin^2 \theta_{13} - \sin^2 \theta_{12}) + (2 - 3 \cos^2 \theta_{12} \cos^2 \theta_{13})^{\frac{1}{2}} \cos \theta_{12} \cos \theta_{13}}{\sin 2\theta_{12} \sin \theta_{13} \sin 2\theta_{23}}, \end{aligned} \quad (3.12)$$

where we have used Eq. (3.8) to derive the second expression for $\cos \delta_{CP}$. This relation can alternatively be derived from the identities $|U_{\mu 1}|^2 = 2 \cos^2(\varphi_1 - \pi/6)/3$ and $|U_{\tau 1}|^2 = 2 \cos^2(\varphi_1 + \pi/6)/3$. Because the parameter φ_1 should be around $\pi/2$ or $3\pi/2$ as shown in Eq. (3.9), the sum rule of Eq. (3.12) is approximately

$$\cos \delta_{CP} \simeq \frac{(3 \cos 2\theta_{12} - 2) \cot 2\theta_{23}}{3 \sin 2\theta_{12} \sin \theta_{13}}. \quad (3.13)$$

This implies that δ_{CP} would be nearly maximal if the atmospheric angle θ_{23} takes the maximal value $\theta_{23} = \pi/4$. We allow the three mixing angles to freely vary in the experimentally preferred 3σ ranges [6], then the sum rule Eq. (3.13) leads to

$$-0.3440 \leq \cos \delta_{CP} \leq 0.4526. \quad (3.14)$$

Needless to say, the improved measurement of the mixing angles particularly θ_{12} and θ_{23} could help to make more precise prediction for δ_{CP} in our framework.

Note that taking the fixed column vector $\sqrt{\frac{2}{3}}(\sin\varphi_1, \cos(\varphi_1 - \frac{\pi}{6}), \cos(\varphi_1 + \frac{\pi}{6}))^T$ as the second or third column of the PMNS matrix leads to a prediction incompatible with experimental observations.

(II) The lepton mixing matrix for the second case is

$$U_1^{II} = \frac{1}{\sqrt{3}} \begin{pmatrix} e^{i\varphi_1} & 1 & e^{i\varphi_2} \\ \omega e^{i\varphi_1} & 1 & \omega^2 e^{i\varphi_2} \\ \omega^2 e^{i\varphi_1} & 1 & \omega e^{i\varphi_2} \end{pmatrix} R_{13}(\theta) Q_\nu, \quad U_2^{II} = P_{132} U_1^{II}, \quad (3.15)$$

where $\omega = e^{2\pi i/3}$. These two forms differ only by the exchange of the second and third rows. Such mixing structures can be derived from flavour symmetry based on $\Delta(6n^2)$ flavour symmetry group combined with CP symmetry. The associated residual symmetry is:

$$\Delta(6n^2) \times H_{CP} : G_\ell = \langle ac^s d^t \rangle, \quad G_\nu = Z_2^{c^{n/2}}, \quad X_{\nu r} = \rho_r \langle c^\gamma d^\delta \rangle, \quad (3.16)$$

with n being an even integer. The parameters φ_1 and φ_2 are defined as

$$\varphi_1 = \frac{\gamma + \delta + 2s}{n} \pi, \quad \varphi_2 = \frac{2\delta - \gamma + 2t}{n} \pi. \quad (3.17)$$

They are interdependent of each other and can take the discrete values

$$\varphi_1, \varphi_2 \pmod{2\pi} = 0, \frac{1}{n}\pi, \frac{2}{n}\pi, \dots, \frac{2n-1}{n}\pi, \quad (3.18)$$

The smallest symmetry group capable of reproducing the experimental mixing angles for specific values of θ is S_4 . The second column of U_1^{II} and U_2^{II} are $(1, 1, 1)^T/\sqrt{3}$ which is the second column of tri-bimaximal mixing matrix, and consequently they are the so-called TM2 pattern. We can extract the following results for the lepton mixing angles

$$\begin{aligned} \sin^2 \theta_{13} &= \frac{1}{3} [1 + \sin 2\theta \cos(\varphi_2 - \varphi_1)], & \sin^2 \theta_{12} &= \frac{1}{2 - \sin 2\theta \cos(\varphi_2 - \varphi_1)}, \\ \sin^2 \theta_{23} &= \frac{1 - \sin 2\theta \sin(\varphi_2 - \varphi_1 + \pi/6)}{2 - \sin 2\theta \cos(\varphi_2 - \varphi_1)} & \text{for } U_1^{II}, \\ \sin^2 \theta_{23} &= \frac{1 + \sin 2\theta \sin(\varphi_2 - \varphi_1 - \pi/6)}{2 - \sin 2\theta \cos(\varphi_2 - \varphi_1)} & \text{for } U_2^{II}. \end{aligned} \quad (3.19)$$

Therefore, the solar and reactor mixing angles satisfy the well-known sum rule:

$$3 \cos^2 \theta_{13} \sin^2 \theta_{12} = 1. \quad (3.20)$$

This implies a lower bound on the solar mixing angle $\sin^2 \theta_{12} > 1/3$. Using the 3σ range of $\sin^2 \theta_{13}$ from [6], we obtain $0.3402 \leq \sin^2 \theta_{12} \leq 0.3415$. The JUNO experiment has determined the 3σ range of the solar mixing angle $\sin^2 \theta_{12}$ to be $[0.2831, 0.3353]$ [30], thus this mixing pattern has been ruled out by the JUNO experiment. Not only that, the TM2 mixing matrix has been excluded by the JUNO experiment [34, 39, 40]. Moreover, the reactor mixing angle and the atmospheric mixing angle are related as follow

$$\begin{aligned} \frac{3 \cos^2 \theta_{13} \sin^2 \theta_{23} - 1}{1 - 3 \sin^2 \theta_{13}} &= \frac{1}{2} + \frac{\sqrt{3}}{2} \tan(\varphi_2 - \varphi_1), & \text{for } U_1^{II}, \\ \frac{3 \cos^2 \theta_{13} \sin^2 \theta_{23} - 1}{1 - 3 \sin^2 \theta_{13}} &= \frac{1}{2} - \frac{\sqrt{3}}{2} \tan(\varphi_2 - \varphi_1), & \text{for } U_2^{II}. \end{aligned} \quad (3.21)$$

For both the mixing matrices U_1^{II} and U_2^{II} , the three CP invariants take the form

$$\begin{aligned} |J_{CP}| &= \frac{1}{6\sqrt{3}} |\cos 2\theta|, \\ |I_1| &= \frac{2}{9} |(\cos \theta \cos \varphi_1 - \sin \theta \cos \varphi_2)(\cos \theta \sin \varphi_1 - \sin \theta \sin \varphi_2)|, \\ |I_2| &= \frac{1}{9} |\cos 2\theta \sin(2\varphi_1 - 2\varphi_2)|. \end{aligned} \quad (3.22)$$

The J_{CP} invariant can be expressed in terms of θ_{13} and θ_{23} :

$$|J_{CP}| = \frac{1}{6} |\cos^4 \theta_{13} \sin^2 2\theta_{23} - \cos^2 2\theta_{13}|^{\frac{1}{2}}. \quad (3.23)$$

Furthermore, the mixing angles and Dirac CPV phase fulfill the following sum rule

$$\cos \delta_{CP} = \frac{\cos 2\theta_{13} \cot 2\theta_{23}}{\sqrt{3} \cos^2 \theta_{13} - 1 \sin \theta_{13}}. \quad (3.24)$$

Therefore, the value of δ_{CP} is strongly correlated with the deviation of θ_{23} from maximal mixing. Using the 3σ ranges of $\sin^2 \theta_{13}$ and $\sin^2 \theta_{23}$ from the global fit [6], we find that $\cos \delta_{CP}$ can span nearly the entire interval $[-0.8330, 0.6333]$, indicating that the current sum rule provides only a weak constraint on the Dirac CP phase. Nevertheless, with future neutrino experiments expected to significantly reduce the uncertainty in the atmospheric mixing angle θ_{23} , the sum rule given in Eq. (3.24) could place a stringent bound on the allowed values of δ_{CP} .

The flavour symmetry group $G_f = S_4$ yields the mixing patterns U_1^{II} and U_2^{II} for the parameter values $(\varphi_1, \varphi_2) = (\pi, 0)$. In this configuration, the atmospheric mixing angle θ_{23} and the Dirac CPV phase δ_{CP} are both predicted to be maximal. Furthermore, the Majorana phases are constrained to be either 0 or π . Notably, U_1^{II} and U_2^{II} represent the same physical mixing pattern in this case, as they are connected through a redefinition of the parameter θ and the matrix Q_ν :

$$U_2^{II}(\theta, \varphi_1 = \pi, \varphi_2 = 0) = U_1^{II}\left(\frac{\pi}{2} - \theta, \varphi_1 = \pi, \varphi_2 = 0\right) \text{diag}(1, 1, -1). \quad (3.25)$$

Note that the mixing matrices in Eq. (3.15) can also be obtained from breaking the series symmetry $\Delta(3n^2) \rtimes H_{CP}$ [78]. Here, gCP transformations can be consistently defined within $\Delta(3n^2)$, provided that nontrivial singlet representations are absent from the model. Hence, the minimal group that yields the mixing patterns U_1^{II} and U_2^{II} is A_4 , whose predictions coincide with those of S_4 .

(III) In this case, the lepton mixing matrix is given by

$$U^{III} = \begin{pmatrix} -i\sqrt{\frac{\phi_g}{\sqrt{5}}} & \sqrt{\frac{1}{\sqrt{5}\phi_g}} & 0 \\ i\sqrt{\frac{1}{2\sqrt{5}\phi_g}} & \sqrt{\frac{\phi_g}{2\sqrt{5}}} & -\frac{1}{\sqrt{2}} \\ i\sqrt{\frac{1}{2\sqrt{5}\phi_g}} & \sqrt{\frac{\phi_g}{2\sqrt{5}}} & \frac{1}{\sqrt{2}} \end{pmatrix} R_{13}(\theta) Q_\nu, \quad (3.26)$$

where $\phi_g = (\sqrt{5} + 1)/2$ is the golden ratio. This the mixing matrix can arise from the breaking of the flavour symmetry group $A_5 \rtimes H_{CP}$. In the chosen basis, the consistent gCP transformation matrices coincide structurally with the representation matrices of the flavour

symmetry. Then the mixing matrix U^{III} results from the following symmetry-breaking structure [71–73]:

$$A_5 \times H_{CP} : G_\ell = Z_5^T, \quad G_\nu = Z_2^{T^3 ST^2 ST^3}, \quad X_{\nu r} = \rho_r(S), \quad (3.27)$$

This scenario has previously been identified in studies of A_5 flavour symmetry combined with gCP invariance [71–73], and our results are in full agreement with those earlier findings.

For the mixing matrix U^{III} , the mixing angles read

$$\sin^2 \theta_{13} = \frac{\phi_g}{\sqrt{5}} \sin^2 \theta, \quad \sin^2 \theta_{12} = \frac{4 - 2\phi_g}{5 - 2\phi_g + \cos 2\theta}, \quad \sin^2 \theta_{23} = \frac{1}{2}. \quad (3.28)$$

The solar and reactor mixing angles have the correlation

$$\sin^2 \theta_{12} \cos^2 \theta_{13} = (3 - \phi_g)/5. \quad (3.29)$$

Using the 3σ range of the reactor mixing angle $0.02030 \leq \sin^2 \theta_{13} \leq 0.02388$ [6], we get

$$0.2821 \leq \sin^2 \theta_{12} \leq 0.2832, \quad (3.30)$$

where the theoretical upper limit of $\sin^3 \theta_{12} = 0.2832$ is only slightly larger than the lower limit of 0.2831 provided by the JUNO experiment. Therefore, this mixing pattern will soon be tested by the JUNO experiment. For the CPV phases, we find δ_{CP} is exactly maximal while both Majorana phases α_{21} and α_{31} are trivial with

$$|J_{CP}| = \frac{1}{4} \sqrt{\frac{\phi_g}{5\sqrt{5}}} |\sin 2\theta| = \frac{1}{2\sqrt{5}} \left(\frac{\sqrt{5}-1}{\sqrt{5}+1} \right)^{\frac{1}{2}} \sin \theta_{13} \cot \theta_{12}, \quad \cos \delta_{CP} = 0, \quad I_1 = I_2 = 0. \quad (3.31)$$

where we have used Eq. (3.28) to get the expressions for $|J_{CP}|$ in terms of θ_{13} and θ_{12} .

(IV) The lepton mixing matrices for this case are given by

$$U_1^{IV} = \frac{1}{2} \begin{pmatrix} \phi_g & 1 & \phi_g - 1 \\ \phi_g - 1 & -\phi_g & 1 \\ 1 & 1 - \phi_g & -\phi_g \end{pmatrix} R_{23}(\theta) Q_\nu, \quad U_2^{IV} = P_{132} U_1^{IV}. \quad (3.32)$$

These two mixing matrices are related by an exchange of their second and third rows. Similar to case III, this mixing pattern also originates from the flavour symmetry group A_5 in combination with gCP and they come from the following breaking pattern:

$$A_5 \times H_{CP} : G_\ell = K_4^{(ST^2 ST^3 S, TST^4)}, \quad G_\nu = Z_2^S, \quad X_{\nu r} = \rho_r(T^3 ST^2 ST^3). \quad (3.33)$$

Earlier studies of this mixing pattern in the context of A_5 flavour symmetry and CP can be found in Refs. [71–73]. We can extract the following results for the mixing angles

$$\begin{aligned} \sin^2 \theta_{13} &= \frac{(\cos \theta + \phi_g \sin \theta)^2}{4\phi_g^2}, & \sin^2 \theta_{12} &= \frac{(\phi_g \cos \theta - \sin \theta)^2}{4\phi_g^2 - (\cos \theta + \phi_g \sin \theta)^2}, \\ \sin^2 \theta_{23} &= \frac{\phi_g^2 (\cos \theta - \phi_g \sin \theta)^2}{4\phi_g^2 - (\cos \theta + \phi_g \sin \theta)^2} & \text{for } U_1^{IV}, & \\ \sin^2 \theta_{23} &= \frac{(\sin \theta + \phi_g^2 \cos \theta)^2}{4\phi_g^2 - (\cos \theta + \phi_g \sin \theta)^2} & \text{for } U_2^{IV}. & \end{aligned} \quad (3.34)$$

After some tedious calculations, we find the following relations between the mixing angles

$$\begin{aligned}
4 \cos^2 \theta_{12} \cos^2 \theta_{13} &= 1 + \phi_g, \\
\sin^2 \theta_{23} &= 1 - \left[\frac{\sqrt{5}}{\phi_g} + (1 + 2\phi_g) \tan^2 \theta_{13} + 2\phi_g \tan \theta_{13} \sqrt{\sqrt{5}\phi_g - (2 + 3\phi_g) \tan^2 \theta_{13}} \right] / 5, \text{ for } U_1^{IV} \\
\sin^2 \theta_{23} &= \left[\frac{\sqrt{5}}{\phi_g} + (1 + 2\phi_g) \tan^2 \theta_{13} + 2\phi_g \tan \theta_{13} \sqrt{\sqrt{5}\phi_g - (2 + 3\phi_g) \tan^2 \theta_{13}} \right] / 5, \text{ for } U_2^{IV} \quad (3.35)
\end{aligned}$$

Using the 3σ range of the reactor mixing angle $\sin^2 \theta_{13}$, we have

$$\begin{aligned}
0.3295 &\leq \sin^2 \theta_{12} \leq 0.3319, \\
0.5148 &\leq \sin^2 \theta_{23} \leq 0.5324 \quad \text{for } U_1^{IV}, \\
0.4676 &\leq \sin^2 \theta_{23} \leq 0.4852 \quad \text{for } U_2^{IV}, \quad (3.36)
\end{aligned}$$

for NO. The CP invariants J_{CP} , I_1 and I_2 are found to vanish exactly so that both Dirac and Majorana CP phases take CP conserving values 0 and π .

(V) The lepton mixing matrix is

$$U^V = \frac{1}{2\sqrt{3}} \begin{pmatrix} \sqrt{3} - 1 & 2e^{-i\varphi} & -(\sqrt{3} + 1)e^{\frac{3\pi i}{4}} \\ -\sqrt{3} - 1 & 2e^{-i\varphi} & (\sqrt{3} - 1)e^{\frac{3\pi i}{4}} \\ 2 & 2e^{-i\varphi} & 2e^{\frac{3\pi i}{4}} \end{pmatrix} R_{13}(\theta) Q_\nu, \quad (3.37)$$

where $\varphi = \arctan(2 - \sqrt{7})$. This form of the mixing matrix arises from the breaking of the flavour symmetry group $\Sigma(168) \cong PSL(2, 7) \cong \Gamma_7$ and gCP symmetry. In our basis, the gCP transformation consistent with $\Sigma(168)$ flavour symmetry takes the same form as the flavour symmetry transformation itself. The mixing matrix U^V results from the symmetry breaking pattern

$$\Sigma(168) \times H_{CP} \quad : \quad G_\ell = Z_3^{ST^4 ST^2 S}, \quad G_\nu = Z_2^S, \quad X_{\nu r} = \rho_r(1). \quad (3.38)$$

In this scenario, one column of the PMNS matrix is fixed as $(1, 1, 1)^T / \sqrt{3}$, which must correspond to the second column to match experimental lepton mixing data. Among the six mixing matrices generated by row permutations of U^V , four are compatible with current experimental data:

$$U_1^V = U^V, \quad U_2^V = P_{132} U^V, \quad U_3^V = P_{213} U^V, \quad U_4^V = P_{231} U^V. \quad (3.39)$$

Notably, U_2^V and U_4^V are related to U_1^V and U_3^V by exchange of their second and third rows. Moreover, the four matrices satisfy the following symmetry relations

$$\begin{aligned}
U_3^V(\theta) &= e^{\frac{3\pi i}{4}} \left[U_1^V \left(\frac{\pi}{2} - \theta \right) \right]^* \text{diag}(-1, -ie^{\frac{i}{2} \arctan(\sqrt{7}/3)}, 1), \\
U_4^V(\theta) &= e^{\frac{3\pi i}{4}} \left[U_2^V \left(\frac{\pi}{2} - \theta \right) \right]^* \text{diag}(-1, -ie^{\frac{i}{2} \arctan(\sqrt{7}/3)}, 1). \quad (3.40)
\end{aligned}$$

It implies that the mixing matrices U_3^V (U_4^V) from left-handed leptons assigned to $\bar{\mathbf{3}}$ and U_1^V (U_2^V) from left-handed leptons assigned to $\mathbf{3}$ describe identical physical mixing patterns, up to the Majorana CP phase α_{21} . This equivalence follows from the fact that U_3^V (U_4^V) can be obtained from $(U_1^V)^*$ ($(U_2^V)^*$) by reparameterizing θ up to the diagonal phase Q_ν and an overall phase. Consequently, the predictions for lepton mixing parameters from U_3^V and U_4^V follow directly from those of U_1^V and U_2^V , and are therefore not presented separately.

For U_1^V and U_2^V , the mixing angles and all three CP rephasing invariants are given by

$$\begin{aligned}
\sin^2 \theta_{13} &= \frac{1}{12} \left(4 + 2\sqrt{3} \cos 2\theta + \sqrt{2} \sin 2\theta \right), \\
\sin^2 \theta_{12} &= \frac{4}{8 - 2\sqrt{3} \cos 2\theta - \sqrt{2} \sin 2\theta}, \\
\sin^2 \theta_{23} &= \frac{4 - 2\sqrt{3} \cos 2\theta + \sqrt{2} \sin 2\theta}{8 - 2\sqrt{3} \cos 2\theta - \sqrt{2} \sin 2\theta} \quad \text{for } U_1^V, \\
\sin^2 \theta_{23} &= \frac{4 - 2\sqrt{2} \sin 2\theta}{8 - 2\sqrt{3} \cos 2\theta - \sqrt{2} \sin 2\theta} \quad \text{for } U_2^V, \\
|J_{CP}| &= \frac{1}{6\sqrt{6}} |\sin 2\theta|, \quad |I_2| = \frac{1}{36} \left| \cos 2\theta - \sqrt{6} \sin 2\theta \right|, \\
|I_1| &= \frac{1}{72} \left| 2\sqrt{7} - \sqrt{3} + \left(2 - \sqrt{21} \right) \cos 2\theta - \sqrt{14} \sin 2\theta \right|. \tag{3.41}
\end{aligned}$$

Then we can derive the following sum rules among the mixing angles

$$\begin{aligned}
\sin^2 \theta_{12} \cos^2 \theta_{13} &= \frac{1}{3}, \\
\sin^2 \theta_{23} \cos^2 \theta_{13} &= \frac{1}{42} \left(9 + 15 \cos 2\theta_{13} \pm 2\sqrt{3} \sqrt{12 \cos 2\theta_{13} - 9 \cos 4\theta_{13} - 4} \right) \quad \text{for } U_1^V, \\
\sin^2 \theta_{23} \cos^2 \theta_{13} &= \frac{1}{21} \left(6 + 3 \cos 2\theta_{13} \pm \sqrt{3} \sqrt{12 \cos 2\theta_{13} - 9 \cos 4\theta_{13} - 4} \right) \quad \text{for } U_2^V. \tag{3.42}
\end{aligned}$$

In the U_1^V and U_2^V cases, as it is not difficult to show, the CP invariant $|J_{CP}|$ can be expressed in terms of θ_{23} and θ_{13} :

$$\begin{aligned}
|J_{CP}| &= \frac{1}{6\sqrt{3}} \left| 1 - 3 \cos^2 \theta_{23} \cos^2 \theta_{13} \right|, \quad \text{for } U_1^V, \\
|J_{CP}| &= \frac{1}{6\sqrt{3}} \left| 1 - 3 \sin^2 \theta_{23} \cos^2 \theta_{13} \right|, \quad \text{for } U_2^V. \tag{3.43}
\end{aligned}$$

According to Eq. (3.41), the minimum value of the reactor mixing angle $\sin^2 \theta_{13}$ is found to be 0.02153. Using the 3σ range of the reactor mixing angle $0.02153 \leq \sin^2 \theta_{13} \leq 0.02388$, we have

$$\begin{aligned}
0.3407 &\leq \sin^2 \theta_{12} \leq 0.3415, \\
0.5405 &\leq \sin^2 \theta_{23} \leq 0.5953 \quad \text{for } U_1^V, \\
0.435 &\leq \sin^2 \theta_{23} \leq 0.4595 \quad \text{for } U_2^V, \tag{3.44}
\end{aligned}$$

Obviously the atmospheric mixing angle θ_{23} is non-maximal in this case. Note that The specific value of the solar mixing angle θ_{12} predicted by this mixing model has been ruled out by the latest results from the JUNO experiment [30].

We find the sum rules in Eq. (3.42) and consequently the estimates given in Eq. (3.44) are satisfied as well. Furthermore, the sum rule of Eq. (3.24) among the mixing angles and Dirac CP phase is fulfilled for all the four permutations of the PMNS matrices in Eq. (3.39). Consequently the comments below Eq. (3.24) also hold true here.

4 Lepton mixing with two free parameters

In this section, we shall discuss the breaking patterns in which charged lepton and neutrino sectors preserve $\mathcal{G}_\ell = Z_2^{g_\ell} \times H_{CP}^\ell$ and $\mathcal{G}_\nu = Z_2^{g_\nu} \times H_{CP}^\nu$, respectively. The master

The residual $Z_2 \times CP$ from $A_5 \times H_{CP}$ and the corresponding $\Sigma_\ell(\Sigma_\nu)$		
$Z_2^{g_\ell} (Z_2^{g_\nu})$	$X_{\ell r} (X_{\nu r})$	$\Sigma_\ell (\Sigma_\nu)$
Z_2^S	$\rho_r(1)$	U_{GR}
	$\rho_r(T^3 ST^2 ST^3)$	$U_{GR} \text{diag}(i, 1, i)$
$Z_2^{TST^4}$	$\rho_r(T^2)$	$\text{diag}(1, \omega_5, \omega_5^4) U_{GR}$
	$\rho_r(T^3 ST^2 ST^3 S)$	$\text{diag}(1, \omega_5, \omega_5^4) U_{GR} \text{diag}(-i, -i, 1)$
$Z_2^{T^2 ST^3}$	$\rho_r(T^4)$	$\text{diag}(1, \omega_5^2, \omega_5^3) U_{GR}$
	$\rho_r(ST^2 S)$	$\text{diag}(1, \omega_5^2, \omega_5^3) U_{GR} \text{diag}(i, 1, i)$
$Z_2^{T^4 (ST^2)^2}$	$\rho_r(T^2)$	$\text{diag}(1, \omega_5, \omega_5^4) U_{GR} P_{213}$
	$\rho_r(TST)$	$\text{diag}(1, \omega_5, \omega_5^4) U_{GR} \text{diag}(1, -i, i) P_{213}$
$Z_2^{T^3 ST^2 ST^3}$	$\rho_r(1)$	$U_{GR} P_{213}$
	$\rho_r(S)$	$U_{GR} \text{diag}(1, i, i) P_{213}$
$Z_2^{T^3 ST^2 ST^3 S}$	$\rho_r(1)$	$\frac{1}{\sqrt{2}} \begin{pmatrix} 0 & 0 & \sqrt{2} \\ -1 & 1 & 0 \\ 1 & 1 & 0 \end{pmatrix}$
	$\rho_r(S)$	$U_{GR} \text{diag}(1, i, i) P_{321}$
The independent breaking patterns from $A_5 \times H_{CP}$ and the corresponding Σ matrix		
$(Z_2^{g_\ell}, Z_2^{g_\nu})$	$(X_{\ell r}, X_{\nu r})$	$\Sigma = \Sigma_\ell^\dagger \Sigma_\nu$
$(Z_2^S, Z_2^{TST^4})$	$(\rho_r(1), \rho_r(T^3 ST^2 ST^3 S))$	$\Sigma_1^{VI} = \text{diag}(i, -i, 1) U_{RC} \text{diag}(-1, 1, -1)$
	$(\rho_r(T^3 ST^2 ST^3), \rho_r(T^3 ST^2 ST^3 S))$	$\Sigma_2^{VI} = \text{diag}(i, 1, 1) U_{RC} \text{diag}(1, -1, 1)$
$(Z_2^S, Z_2^{T^2 ST^3})$	$(\rho_r(1), \rho_r(ST^2 S))$	$\Sigma_3^{VI} = \text{diag}(1, -1, -i) P_{312} U_{RC} \text{diag}(i, 1, -1)$
	$(\rho_r(T^3 ST^2 ST^3), \rho_r(ST^2 S))$	$\Sigma_4^{VI} = \text{diag}(i, 1, 1) P_{312} U_{RC} \text{diag}(i, 1, -1)$
$(Z_2^S, Z_2^{T^4 (ST^2)^2})$	$(\rho_r(1), \rho_r(T^3 ST^2 ST^3 S))$	$\Sigma_5^{VI} = \text{diag}(1, -1, -i) U_{RC} P_{213} \text{diag}(i, 1, 1)$
	$(\rho_r(T^3 ST^2 ST^3), \rho_r(T^3 ST^2 ST^3 S))$	$\Sigma_6^{VI} = \text{diag}(i, 1, 1) U_{RC} P_{213} \text{diag}(i, 1, 1)$

Table 1: The possible residual subgroups of the structure $Z_2 \times CP$ and the corresponding Takagi factorization matrices $\Sigma_\ell(\Sigma_\nu)$, and possible six viable breaking patterns and the corresponding $\Sigma = \Sigma_\ell^\dagger \Sigma_\nu$ matrices from breaking the symmetry $A_5 \times H_{CP}$. The matrices U_{GR} is the golden ratio mixing matrix in Eq. (4.3), the matrix U_{RC} is defined in Eq. (4.5), and the permutation matrices P_{213} and P_{321} are given in Eq. (2.16). In each Σ matrix, the (11) entry is fully constrained by combinations of residual symmetries of the charged lepton and neutrino sectors.

formula of the lepton mixing matrix is given by Eq. (2.18). We see that the lepton mixing angles and CP phases in this scenario depend on two real parameters θ_ℓ and θ_ν , with only one element of the PMNS matrix being fixed by symmetry. This breaking pattern has been studied for the flavor symmetry groups S_4 [87], $\Delta(6n^2)$ [88] and the Dihedral groups D_n [89] in combination with gCP. Similar to section 3, we are also concerned with the flavour and CP symmetries $A_5 \times H_{CP}$, $\Sigma(168) \times H_{CP}$ and $\Delta(6n^2) \times H_{CP}$. All independent residual symmetry of the structure $Z_2 \times CP$ would be analyzed for each symmetry group, and the corresponding predictions for lepton flavour mixing will be studied in the following.

4.1 The breaking patterns of $A_5 \times H_{CP}$

We now classify the distinct symmetry breaking patterns that arise from breaking the flavour group $A_5 \times H_{CP}$. If a pair of residual flavour subgroups $\{Z_2^{g'_\ell}, Z_2^{g'_\nu}\}$ is related to

$\{Z_2^{g_\ell}, Z_2^{g_\nu}\}$ by conjugation under some element $h \in A_5$, i.e.

$$Z_2^{g_\ell} = hZ_2^{g_\ell}h^{-1}, \quad Z_2^{g_\nu} = hZ_2^{g_\nu}h^{-1}, \quad (4.1)$$

then these two breaking patterns will yield identical phenomenological predictions for mixing parameters. As all fifteen Z_2 subgroups are conjugate to each other. As a consequence, it is sufficient to only consider the residual symmetries $Z_2^S \times H_{CP}^\ell$ in the charged lepton sector. A systematic analysis of the breaking of $A_5 \rtimes H_{CP}$ shows that the neutrino residual symmetry $Z_2^{g_\nu} \times H_{CP}^\nu$ can be chosen from the following five subgroups of $A_5 \rtimes H_{CP}$:

$$Z_2^{TST^4} \times H_{CP}^\nu, \quad Z_2^{T^2ST^3} \times H_{CP}^\nu, \quad Z_2^{T^4(ST^2)^2} \times H_{CP}^\nu, \quad Z_2^{T^3ST^2T^3} \times H_{CP}^\nu, \quad Z_2^{T^3ST^2T^3S} \times H_{CP}^\nu. \quad (4.2)$$

Following the procedures presented in section 2, the corresponding Takagi factorization for each residual symmetry can be calculated, and all these results are summarized in table 1, where U_{GR} denotes the golden ratio mixing matrix, given by

$$U_{GR} = \begin{pmatrix} -\sqrt{\frac{\phi_g}{\sqrt{5}}} & \sqrt{\frac{1}{\sqrt{5}\phi_g}} & 0 \\ \sqrt{\frac{1}{2\sqrt{5}\phi_g}} & \sqrt{\frac{\phi_g}{2\sqrt{5}}} & -\frac{1}{\sqrt{2}} \\ \sqrt{\frac{1}{2\sqrt{5}\phi_g}} & \sqrt{\frac{\phi_g}{2\sqrt{5}}} & \frac{1}{\sqrt{2}} \end{pmatrix}. \quad (4.3)$$

We compute the absolute of the fixed elements of the PMNS matrices for the five independent breaking patterns (see Eq. (4.2)), yielding the following values, respectively:

$$\frac{\phi_g}{2}, \quad \frac{1}{2}, \quad \frac{1}{2\phi_g}, \quad 0, \quad 0. \quad (4.4)$$

A comparison with current experimental constraints indicates that only the patterns containing $\frac{\phi_g}{2}$, $\frac{1}{2}$, and $\frac{1}{2\phi_g}$ may be phenomenologically acceptable. Moreover, the positions of these elements within the mixing matrix are strongly constrained: $\frac{\phi_g}{2}$ must be the (11) entry, $\frac{1}{2\phi_g}$ must occupy either the (21) or (31) position, and $\frac{1}{2}$ can be assigned to the (21), (22), (31) or (32) entry.

Considering all independent residual CP choices yields twelve distinct breaking patterns; a numerical scan shows that only six of them are compatible with present data. These six viable breakings and their mixing matrices are summarized in table 1. Here we define the matrix

$$U_{RC} = \frac{1}{2} \begin{pmatrix} \phi_g & 1/\phi_g & 1 \\ 1/\phi_g & 1 & -\phi_g \\ 1 & -\phi_g & -1/\phi_g \end{pmatrix}. \quad (4.5)$$

From the six breaking patterns summarized in table 1, we obtained the following 11 viable mixing matrices:

$$\begin{aligned} U_1^{VI} &= R_{23}^T(\theta_\ell)\Sigma_1^{VI}R_{23}(\theta_\nu), & U_2^{VI} &= R_{23}^T(\theta_\ell)\Sigma_2^{VI}R_{23}(\theta_\nu), & U_{3,1}^{VI} &= P_{213}R_{23}^T(\theta_\ell)\Sigma_3R_{23}(\theta_\nu), \\ U_{3,2}^{VI} &= P_{231}R_{23}^T(\theta_\ell)\Sigma_3^{VI}R_{23}(\theta_\nu), & U_{4,1}^{VI} &= P_{213}R_{23}^T(\theta_\ell)\Sigma_4^{VI}R_{23}(\theta_\nu), \\ U_{4,2}^{VI} &= P_{231}R_{23}^T(\theta_\ell)\Sigma_4^{VI}R_{23}(\theta_\nu), & U_{4,3}^{VI} &= P_{213}R_{23}^T(\theta_\ell)\Sigma_4^{VI}R_{23}(\theta_\nu)P_{213}, \\ U_{4,4}^{VI} &= P_{231}R_{23}^T(\theta_\ell)\Sigma_4^{VI}R_{23}(\theta_\nu)P_{213}, & U_5^{VI} &= P_{213}R_{23}^T(\theta_\ell)\Sigma_5^{VI}R_{23}(\theta_\nu), \\ U_{6,1}^{VI} &= P_{213}R_{23}^T(\theta_\ell)\Sigma_6^{VI}R_{23}(\theta_\nu), & U_{6,2}^{VI} &= P_{231}R_{23}^T(\theta_\ell)\Sigma_6^{VI}R_{23}(\theta_\nu), \end{aligned} \quad (4.6)$$

where we have omitted the diagonal phase matrices Q_ℓ and Q_ν here. As Q_ℓ can be absorbed by the charged lepton fields, while Q_ν is a diagonal matrix with entries ± 1 or $\pm i$. Its effect

is to change the Majorana phases by π . Observe that the mixing matrices $U_{3,2}^{VI}$, $U_{4,2}^{VI}$, $U_{4,4}^{VI}$ and $U_{6,2}^{VI}$ are derived from $U_{3,1}^{VI}$, $U_{4,1}^{VI}$, $U_{4,3}^{VI}$ and $U_{6,1}^{VI}$ by interchanging the second and third rows of the PMNS matrix, respectively. As established, such an exchange transforms the atmospheric mixing angle via $\theta_{23} \rightarrow \pi/2 - \theta_{23}$, shifts the Dirac CP phase as $\delta_{CP} \rightarrow \pi + \delta_{CP}$, and leaves all other mixing parameters unchanged. For each independent mixing pattern, the mixing angles $\sin^2 \theta_{13}$, $\sin^2 \theta_{12}$, $\sin^2 \theta_{23}$ and the CP invariants J_{CP} , I_1 , I_2 are computed in the standard manner.

Note that the diagonal phase matrix $\text{diag}(i, 1, 1)$ in Σ_2^{VI} , Σ_4^{VI} , and Σ_6^{VI} commutes with both rotation matrices $R_{23}(\theta_\ell)$ and $R_{23}(\theta_\nu)$, and can therefore be absorbed into the phase matrices Q_ℓ and Q_ν . As a result, the mixing matrices U_2^{VI} , $U_{4,i}^{VI}$ and $U_{6,i}^{VI}$ in Eq. (4.6) are real up to the overall phase matrices Q_ℓ and Q_ν , leading to trivial CP phases.

We see that the mixing parameters depend on the continuous parameters θ_ℓ and θ_ν . As a consequence, sum rules among the mixing angles and the Dirac CP phase δ_{CP} can be found as follows:

$$\begin{aligned}
U_1^{VI}, U_2^{VI} &: \quad \cos^2 \theta_{12} \cos^2 \theta_{13} = \frac{\phi_g^2}{4}, \\
U_{4,1}^{VI} &: \quad 1 = \frac{1 - 4 \sin^2 \theta_{12} \cos^2 \theta_{23} - 4 \sin^2 \theta_{13} \cos^2 \theta_{12} \sin^2 \theta_{23}}{2 \sin 2\theta_{12} \sin \theta_{13} \sin 2\theta_{23}}, \\
U_{4,2}^{VI} &: \quad 1 = \frac{1 - 4 \sin^2 \theta_{12} \sin^2 \theta_{23} - 4 \sin^2 \theta_{13} \cos^2 \theta_{12} \cos^2 \theta_{23}}{2 \sin 2\theta_{12} \sin \theta_{13} \sin 2\theta_{23}}, \\
U_{4,3}^{VI} &: \quad 1 = -\frac{1 - 4 \cos^2 \theta_{12} \cos^2 \theta_{23} - 4 \sin^2 \theta_{13} \sin^2 \theta_{12} \sin^2 \theta_{23}}{2 \sin 2\theta_{12} \sin \theta_{13} \sin 2\theta_{23}}, \\
U_{4,4}^{VI} &: \quad 1 = -\frac{1 - 4 \cos^2 \theta_{12} \sin^2 \theta_{23} - 4 \sin^2 \theta_{13} \sin^2 \theta_{12} \cos^2 \theta_{23}}{2 \sin 2\theta_{12} \sin \theta_{13} \sin 2\theta_{23}}, \\
U_{6,1}^{VI} &: \quad 1 = -\frac{1/\phi_g^2 - 4 \sin^2 \theta_{12} \cos^2 \theta_{23} - 4 \sin^2 \theta_{13} \cos^2 \theta_{12} \sin^2 \theta_{23}}{2 \sin 2\theta_{12} \sin \theta_{13} \sin 2\theta_{23}}, \\
U_{6,2}^{VI} &: \quad 1 = -\frac{1/\phi_g^2 - 4 \sin^2 \theta_{12} \sin^2 \theta_{23} - 4 \sin^2 \theta_{13} \cos^2 \theta_{12} \cos^2 \theta_{23}}{2 \sin 2\theta_{12} \sin \theta_{13} \sin 2\theta_{23}}, \\
U_{3,1}^{VI} &: \quad \cos \delta_{CP} = \frac{1 - 4 \sin^2 \theta_{12} \cos^2 \theta_{23} - 4 \sin^2 \theta_{13} \cos^2 \theta_{12} \sin^2 \theta_{23}}{2 \sin 2\theta_{12} \sin \theta_{13} \sin 2\theta_{23}}, \\
U_{3,2}^{VI} &: \quad \cos \delta_{CP} = -\frac{1 - 4 \sin^2 \theta_{12} \sin^2 \theta_{23} - 4 \sin^2 \theta_{13} \cos^2 \theta_{12} \cos^2 \theta_{23}}{2 \sin 2\theta_{12} \sin \theta_{13} \sin 2\theta_{23}}, \\
U_5^{VI} &: \quad \cos \delta_{CP} = \frac{1/\phi_g^2 - 4 \sin^2 \theta_{12} \cos^2 \theta_{23} - 4 \sin^2 \theta_{13} \cos^2 \theta_{12} \sin^2 \theta_{23}}{2 \sin 2\theta_{12} \sin \theta_{13} \sin 2\theta_{23}}, \quad (4.7)
\end{aligned}$$

Using the 3σ range of θ_{13} as input, we find $\sin^2 \theta_{12} \in [0.3295, 0.3319]$ for mixing matrices U_1^{VI} and U_2^{VI} . This prediction will be directly tested by the JUNO experiment after six years of operation [31]. If all the three mixing angles freely vary within their 3σ intervals, the last three relations lead to $[0.6699, 1]$, $[-1, -0.5853]$ and $[-1, -0.4346]$, respectively.

4.2 The breaking patterns of $\Sigma(168) \times H_{CP}$

Let us systematically analyze the distinct breaking patterns arising from the flavour symmetry group $\Sigma(168) \times H_{CP}$ with $\mathcal{G}_\ell = Z_2^{g_\ell} \times H_{CP}^\ell$ and $\mathcal{G}_\nu = Z_2^{g_\nu} \times H_{CP}^\nu$. The group $\Sigma(168)$ has 21 Z_2 subgroups, and all them are conjugate to each other. Without loss of generality, we consider the residual symmetries $\mathcal{G}_\ell = Z_2^S \times H_{CP}^\ell$ in the charged lepton sector. After performing a comprehensive analysis of lepton mixing patterns which arise from the

breaking of $\Sigma(168) \times H_{CP}$, we find that the residual symmetry $Z_2^{g\nu} \times H_{CP}^\nu$ of neutrino sector can be any one of the following five subgroups:

$$Z_2^{TST^6} \times H_{CP}^\nu, \quad Z_2^{T^2ST^5} \times H_{CP}^\nu, \quad Z_2^{T^4ST^3} \times H_{CP}^\nu, \quad Z_2^{TST^3ST^2} \times H_{CP}^\nu, \quad Z_2^{TST^5ST^5} \times H_{CP}^\nu. \quad (4.8)$$

It is easy to check that the absolute of the fixed elements of the PMNS matrices for the five breaking patterns yielding the following values, respectively:

$$\frac{1}{\sqrt{2}}, \quad \frac{1}{2}, \quad \frac{1}{\sqrt{2}}, \quad 0, \quad 0. \quad (4.9)$$

A comparison with current experimental data on lepton mixing parameters shows that only the pattern with fixed elements $\frac{1}{\sqrt{2}}$ and $\frac{1}{2}$ are potentially viable. Furthermore, the allowed positions of these elements within the mixing matrix are highly constrained: $\frac{1}{\sqrt{2}}$ must be the (23) or (33) entry, and $\frac{1}{2}$ can be assigned to the (21), (22), (31) or (32) entry. A systematic scan of the parameter space for all independent breaking patterns and their mixing matrices shows that only six matrices can accommodate the experimental data. These viable candidates arise from two breaking patterns:

$$\begin{aligned} G_\ell = Z_2^S, \quad G_\nu = Z_2^{T^2ST^5}, \quad X_{lr} = \rho_r(1), \quad X_{\nu r} = \rho_r(T^4), \\ G_\ell = Z_2^S, \quad G_\nu = Z_2^{T^2ST^5}, \quad X_{lr} = \rho_r(T^2ST^5ST^2), \quad X_{\nu r} = \rho_r(T^4ST^5ST^4). \end{aligned} \quad (4.10)$$

Following the procedures presented in section 2, the $\Sigma \equiv \Sigma_\ell^\dagger \Sigma_\nu$ matrices corresponding to the two breaking patterns in Eq. (4.10) can be taken to be

$$\begin{aligned} \Sigma_1^{VII} &= \text{diag}(1, e^{-\frac{\pi i}{4}}, e^{\frac{\pi i}{4}}) \Sigma_2^{VII} \text{diag}(1, e^{\frac{\pi i}{4}}, e^{-\frac{\pi i}{4}}), \\ \Sigma_2^{VII} &= \frac{1}{4} \begin{pmatrix} -2 & \sqrt{2(\sqrt{7}+3)} & \sqrt{2(3-\sqrt{7})} \\ \sqrt{2(\sqrt{7}+3)} & \sqrt{7}-1 & \sqrt{2} \\ \sqrt{2(3-\sqrt{7})} & \sqrt{2} & -\sqrt{7}-1 \end{pmatrix}. \end{aligned} \quad (4.11)$$

Then the six viable mixing matrices corresponding those two viable breaking patterns take the following form:

$$\begin{aligned} U_{1,1}^{VII} &= P_{213} R_{23}^T(\theta_\ell) \Sigma_1^{VII} R_{23}(\theta_\nu) P_{213}, & U_{1,2}^{VII} &= P_{231} R_{23}^T(\theta_\ell) \Sigma_1^{VII} R_{23}(\theta_\nu) P_{213}, \\ U_{2,1}^{VII} &= P_{213} R_{23}^T(\theta_\ell) \Sigma_2^{VII} R_{23}(\theta_\nu), & U_{2,2}^{VII} &= P_{231} R_{23}^T(\theta_\ell) \Sigma_2^{VII} R_{23}(\theta_\nu), \\ U_{2,3}^{VII} &= P_{213} R_{23}^T(\theta_\ell) \Sigma_2^{VII} R_{23}(\theta_\nu) P_{213}, & U_{2,4}^{VII} &= P_{231} R_{23}^T(\theta_\ell) \Sigma_2^{VII} R_{23}(\theta_\nu) P_{213}. \end{aligned} \quad (4.12)$$

Note that the four lepton mixing matrices $U_{2,i}^{VII}$ are real, therefore implying trivial CPV phases. We see that $U_{1,2}^{VII}$, $U_{2,2}^{VII}$ and $U_{2,4}^{VII}$ are related to $U_{1,1}^{VII}$, $U_{2,1}^{VII}$ and $U_{2,3}^{VII}$ through an exchange of the second and third rows, respectively. Consequently, the mixing angles and CP phases predicted by $U_{1,2}^{VII}$, $U_{2,2}^{VII}$ and $U_{2,4}^{VII}$ can be directly inferred from the corresponding results for $U_{1,1}^{VII}$, $U_{2,1}^{VII}$ and $U_{2,3}^{VII}$, respectively. Given that all mixing parameters are functions of the free parameters $\theta_{l,\nu}$, they exhibit strong mutual correlations. In particular, each mixing pattern yields a specific sum rule that connects the mixing angles and the Dirac CP phase

$$\begin{aligned} U_{1,1}^{VII} : \quad \cos \delta_{CP} &= -\frac{1 - 4 \cos^2 \theta_{12} \cos^2 \theta_{23} - 4 \sin^2 \theta_{13} \sin^2 \theta_{12} \sin^2 \theta_{23}}{2 \sin 2\theta_{12} \sin \theta_{13} \sin 2\theta_{23}}, \\ U_{1,2}^{VII} : \quad \cos \delta_{CP} &= \frac{1 - 4 \cos^2 \theta_{12} \sin^2 \theta_{23} - 4 \sin^2 \theta_{13} \sin^2 \theta_{12} \cos^2 \theta_{23}}{2 \sin 2\theta_{12} \sin \theta_{13} \sin 2\theta_{23}}, \end{aligned}$$

$$\begin{aligned}
U_{2,1}^{VII} &: 1 = \frac{1 - 4 \sin^2 \theta_{12} \cos^2 \theta_{23} - 4 \sin^2 \theta_{13} \cos^2 \theta_{12} \sin^2 \theta_{23}}{2 \sin 2\theta_{12} \sin \theta_{13} \sin 2\theta_{23}}, \\
U_{2,2}^{VII} &: 1 = \frac{1 - 4 \sin^2 \theta_{12} \sin^2 \theta_{23} - 4 \sin^2 \theta_{13} \cos^2 \theta_{12} \cos^2 \theta_{23}}{2 \sin 2\theta_{12} \sin \theta_{13} \sin 2\theta_{23}}, \\
U_{2,3}^{VII} &: 1 = -\frac{1 - 4 \cos^2 \theta_{12} \cos^2 \theta_{23} - 4 \sin^2 \theta_{13} \sin^2 \theta_{12} \sin^2 \theta_{23}}{2 \sin 2\theta_{12} \sin \theta_{13} \sin 2\theta_{23}}, \\
U_{2,4}^{VII} &: 1 = -\frac{1 - 4 \cos^2 \theta_{12} \sin^2 \theta_{23} - 4 \sin^2 \theta_{13} \sin^2 \theta_{12} \cos^2 \theta_{23}}{2 \sin 2\theta_{12} \sin \theta_{13} \sin 2\theta_{23}}.
\end{aligned} \tag{4.13}$$

The sum rules for $\cos \delta_{CP}$ in terms of the mixing angles, as presented above, are also obtained in Ref. [65]. This agreement arises because these relations are derived by setting the (22), or (32) entries of the PMNS matrix equal to 1/2, respectively. However, while the lepton mixing matrix in our framework is determined by two free parameters, the model in Ref. [65] involves three. As a result, the correlations among neutrino mixing parameters and their allowed ranges differ between the two approaches. When the three mixing angles are varied freely within their 3σ bounds from Ref. [6], the first two relations yield $\cos \delta_{CP}$ in the intervals $[0.3829, 1]$, and $[-1, -0.5537]$, respectively. Distinct allowed intervals of $\cos \delta_{CP}$ provide a means to discriminate among the two mixing matrices $U_{1,1}^{VII}$ and $U_{1,2}^{VII}$. Should future measurements determine θ_{12} and θ_{23} with significantly improved precision, these sum rules could be used to predict the Dirac CP phase δ_{CP} based on experimentally measured mixing angles. The derived sum rules thus serve as sensitive probes for testing the validity of this class of mixing patterns [90, 91].

4.3 The breaking patterns of $\Delta(6n^2) \rtimes H_{CP}$

Now we shall perform a comprehensive analyze of the lepton mixing patterns arising from the $\Delta(6n^2)$ flavour group and CP symmetries which are broken down to $Z_2 \times CP$ in the neutrino and charged lepton sectors. All possible admissible residual subgroups of the structure $Z_2 \times CP$ would be considered, and the phenomenological predictions for lepton mixing matrix would be discussed. Note that $D_{9n,3n}^{(1)}$ is a subgroup of $\Delta(6(9n)^2)$ group. We shall not consider that the breaking patterns arise from $D_{9n,3n}^{(1)} \rtimes H_{CP}$. After performing a comprehensive analysis of lepton mixing patterns derived from the flavour group $\Delta(6n^2) \rtimes H_{CP}$, we find that only three symmetry breaking patterns are found to be phenomenologically viable, with the residual subgroups given by $\mathcal{G}_\ell = Z_2^{bc^x d^x} \times H_{CP}^\ell$ and \mathcal{G}_ν equal to either $Z_2^{bc^y d^y} \times H_{CP}^\nu$, $Z_2^{abc^y} \times H_{CP}^\nu$ and $Z_2^{n/2} \times H_{CP}^\nu$. These patterns were fully analyzed in Ref. [88]. Here, we present updated predictions for the lepton mixing parameters using the latest experimental data.

Following the framework outlined in section 2, we compute the Takagi factorization for the $Z_2 \times CP$ symmetry in each viable residual symmetry configuration. The results are summarized in table 2. The corresponding lepton mixing matrix for the three phenomenologically allowed breaking patterns are then derived from the symmetry breaking patterns given in Eq. (2.18). For each breaking pattern, the matrix $\Sigma = \Sigma_\ell^\dagger \Sigma_\nu$, which is fixed by the residual symmetry, is explicitly listed in table 2. The fixed element (the (11) entry of each Σ matrix) is uniquely determined by the residual flavour symmetry. It is given by the inner product of the eigenvectors corresponding to non-degenerate eigenvalues of the generators $Z_2^{g_\ell}$ and $Z_2^{g_\nu}$. Then we proceed to study these three cases and their predictions for lepton mixing angles and CPV phases one by one.

$$\text{(VIII)} \quad G_\ell = Z_2^{bc^x d^x}, \quad X_{\ell r} = \rho_r(c^\alpha d^{-2x-\alpha}), \quad G_\nu = Z_2^{bc^y d^y}, \quad X_{\nu r} = \rho_r(c^\beta d^{-2y-\beta})$$

The residual $Z_2 \times CP$ from $\Delta(6n^2) \rtimes H_{CP}$ and the corresponding $\Sigma_\ell(\Sigma_\nu)$		
$Z_2^{g_\ell} (Z_2^{g_\nu})$	$X_{\ell r} (X_{\nu r})$	$\Sigma_\ell (\Sigma_\nu)$
$Z_2^{bc^x d^x}$	$\rho_{\mathbf{r}}(c^\alpha d^{-2x-\alpha})$	$\frac{1}{\sqrt{2}} \begin{pmatrix} -e^{\frac{i\pi\alpha}{n}} & e^{\frac{i\pi\alpha}{n}} & 0 \\ 0 & 0 & -\sqrt{2}e^{-\frac{2i\pi(x+\alpha)}{n}} \\ e^{\frac{i\pi(2x+\alpha)}{n}} & e^{\frac{i\pi(2x+\alpha)}{n}} & 0 \end{pmatrix}$
$Z_2^{abc^x}$	$\rho_{\mathbf{r}}(c^\alpha d^{2x+2\alpha})$	$\frac{1}{\sqrt{2}} \begin{pmatrix} -e^{\frac{i\pi\alpha}{n}} & 0 & e^{\frac{i\pi\alpha}{n}} \\ e^{\frac{i\pi(2x+\alpha)}{n}} & 0 & e^{\frac{i\pi(2x+\alpha)}{n}} \\ 0 & -\sqrt{2}e^{-\frac{2i\pi(x+\alpha)}{n}} & 0 \end{pmatrix}$
$Z_2^{c^{n/2}}$	$c^\alpha d^\beta$	$\begin{pmatrix} 0 & 0 & e^{\frac{i\pi\alpha}{n}} \\ 0 & -e^{-\frac{i\pi(\alpha-\beta)}{n}} & 0 \\ e^{-\frac{i\pi\beta}{n}} & 0 & 0 \end{pmatrix}$
The independent breaking patterns from $\Delta(6n^2) \rtimes H_{CP}$ and the corresponding Σ matrix		
$(Z_2^{g_\ell}, Z_2^{g_\nu})$	$(X_{\ell r}, X_{\nu r})$	$\Sigma = \Sigma_\ell^\dagger \Sigma_\nu$
$(Z_2^{bc^x d^x}, Z_2^{bc^y d^y})$	$(\rho_{\mathbf{r}}(c^\alpha d^{-2x-\alpha}), \rho_{\mathbf{r}}(c^\beta d^{-2y-\beta}))$	$\Sigma^{VIII} = \begin{pmatrix} \cos \varphi_1 & -i \sin \varphi_1 & 0 \\ -i \sin \varphi_1 & \cos \varphi_1 & 0 \\ 0 & 0 & e^{i\varphi_2} \end{pmatrix}$
$(Z_2^{bc^x d^x}, Z_2^{abc^y})$	$(\rho_{\mathbf{r}}(c^\alpha d^{-2x-\alpha}), \rho_{\mathbf{r}}(c^\beta d^{2y+2\beta}))$	$\Sigma^{IX} = \frac{1}{2} \begin{pmatrix} 1 & -\sqrt{2}e^{i\varphi_2} & -1 \\ -1 & -\sqrt{2}e^{i\varphi_2} & 1 \\ -\sqrt{2}e^{i\varphi_1} & 0 & -\sqrt{2}e^{i\varphi_1} \end{pmatrix}$
$(Z_2^{bc^x d^x}, Z_2^{c^{n/2}})$	$(\rho_{\mathbf{r}}(c^\alpha d^{-2x-\alpha}), \rho_{\mathbf{r}}(c^\beta d^\gamma))$	$\Sigma^X = \frac{1}{\sqrt{2}} \begin{pmatrix} e^{i\varphi_2} & 0 & -1 \\ e^{i\varphi_2} & 0 & 1 \\ 0 & \sqrt{2}e^{i\varphi_1} & 0 \end{pmatrix}$

Table 2: Residual subgroups of the structure $Z_2 \times CP$ along with the corresponding Takagi factorization matrices, and the form of $\Sigma = \Sigma_\ell^\dagger \Sigma_\nu$ for the three viable breaking patterns derived from $\Delta(6n^2) \rtimes H_{CP}$. Parameters x, y, α, β and γ take integer values from 0 to $n-1$. The discrete parameters φ_1 and φ_2 that appear in Σ^{VIII} , Σ^{IX} , and Σ^X are determined by the chosen residual symmetries and take the forms $\varphi_1 = \frac{x-y}{n}\pi$, $\varphi_2 = \frac{3(x-y+\alpha-\beta)}{n}\pi$ for Σ^{VIII} , $\varphi_1 = \frac{3\alpha+2(x+y)}{n}\pi$, $\varphi_2 = -\frac{3\beta+2(x+y)}{n}\pi$ for Σ^{IX} , and $\varphi_1 = \frac{2x+3\alpha-2\beta+\gamma}{n}\pi$, $\varphi_2 = -\frac{2x+\beta+\gamma}{n}\pi$ for Σ^X . In each Σ matrix, the (11) entry is fully constrained by combinations of residual symmetries of the charged lepton and neutrino sectors.

For this breaking pattern, the Σ^{VIII} matrix in table 2 gives rise to the lepton mixing matrix

$$U^{VIII} = \begin{pmatrix} \cos \varphi_1 & s_\nu \sin \varphi_1 & -c_\nu \sin \varphi_1 \\ -s_\ell \sin \varphi_1 & c_\ell c_\nu e^{i\varphi_2} + s_\ell s_\nu \cos \varphi_1 & c_\ell s_\nu e^{i\varphi_2} - c_\nu s_\ell \cos \varphi_1 \\ c_\ell \sin \varphi_1 & c_\nu s_\ell e^{i\varphi_2} - c_\ell s_\nu \cos \varphi_1 & s_\ell s_\nu e^{i\varphi_2} + c_\ell c_\nu \cos \varphi_1 \end{pmatrix}, \quad (4.14)$$

up to row and column permutations, and with phase matrices Q_ℓ and Q_ν omitted. Here the parameters are defined as

$$s_\ell \equiv \sin \theta_\ell, \quad c_\ell \equiv \cos \theta_\ell, \quad s_\nu \equiv \sin \theta_\nu, \quad c_\nu \equiv \cos \theta_\nu. \quad (4.15)$$

The independent parameters φ_1 and φ_2 are fixed by the remnant symmetries:

$$\varphi_1 = \frac{x-y}{n}\pi, \quad \varphi_2 = \frac{3(x-y+\alpha-\beta)}{n}\pi. \quad (4.16)$$

They take discrete values:

$$\varphi_1 \pmod{2\pi} = 0, \frac{1}{n}\pi, \frac{2}{n}\pi, \dots, \frac{2n-1}{n}\pi,$$

$$\begin{aligned}
\varphi_2 \pmod{2\pi} &= 0, \frac{3}{n}\pi, \frac{6}{n}\pi, \dots, \frac{2n-3}{n}\pi, \quad 3 \mid n, \\
\varphi_2 \pmod{2\pi} &= 0, \frac{1}{n}\pi, \frac{2}{n}\pi, \dots, \frac{2n-1}{n}\pi, \quad 3 \nmid n.
\end{aligned} \tag{4.17}$$

It is easy to check that the mixing matrix in Eq. (4.14) has the following symmetry properties,

$$\begin{aligned}
U^{VIII}(\pi + \varphi_1, \varphi_2, \theta_\ell, \theta_\nu) &= \text{diag}(-1, 1, -1)U^{VIII}(\varphi_1, \varphi_2, \pi - \theta_\ell, \theta_\nu), \\
U^{VIII}(\pi - \varphi_1, \varphi_2, \theta_\ell, \theta_\nu) &= \text{diag}(-1, 1, 1)U^{VIII}(\varphi_1, \varphi_2, \theta_\ell, \pi - \theta_\nu)\text{diag}(1, 1, -1), \\
U^{VIII}(\varphi_1, \pi + \varphi_2, \theta_\ell, \theta_\nu) &= U^{VIII}(\varphi_1, \varphi_2, \theta_\ell, \pi - \theta_\nu)\text{diag}(1, -1, 1), \\
U^{VIII}(\varphi_1, \pi - \varphi_2, \theta_\ell, \theta_\nu) &= (U^{VIII})^*(\varphi_1, \varphi_2, \theta_\ell, \pi - \theta_\nu)\text{diag}(1, -1, 1).
\end{aligned} \tag{4.18}$$

The diagonal matrices mentioned above can be incorporated into the redefinition of the lepton fields. In general, it is sufficient to consider the allowed values φ_1 and φ_2 within the intervals $0 \leq \varphi_1 \leq \pi/2$ and $0 \leq \varphi_2 \leq \pi/2$. As outlined in section 2, the fixed element $\cos \varphi_1$ may correspond to any of the nine entries of the PMNS mixing matrix. The 36 possible arrangements resulting from permutations of rows and columns generally yield nine distinct mixing patterns, which can be taken as the independent cases for analysis.

$$\begin{aligned}
U_1^{VIII} &= U^{VIII}, & U_2^{VIII} &= U^{VIII}P_{213}, & U_3^{VIII} &= U^{VIII}P_{321}, \\
U_4^{VIII} &= P_{213}U^{VIII}, & U_5^{VIII} &= P_{213}U^{VIII}P_{213}, & U_6^{VIII} &= P_{213}U^{VIII}P_{321}, \\
U_7^{VIII} &= P_{231}U^{VIII}, & U_8^{VIII} &= P_{231}U^{VIII}P_{213}, & U_9^{VIII} &= P_{231}U^{VIII}P_{321}.
\end{aligned} \tag{4.19}$$

It is observed that the mixing matrices U_7^{VIII} , U_8^{VIII} and U_9^{VIII} are derivable from U_4^{VIII} , U_5^{VIII} and U_6^{VIII} by interchanging their second and third rows. Therefore they lead to the same solar mixing angle, reactor mixing angle and Majorana CP phases while atmospheric angle changes from θ_{23} to $\pi/2 - \theta_{23}$ and the Dirac CP phase changes from δ_{CP} to $\pi + \delta_{CP}$. We see that the mixing parameters depend on the continuous parameters θ_ℓ and θ_ν as well as the discrete parameters φ_1 and φ_2 . This leads to the following sum rules connecting the mixing angles and the Dirac CP phase δ_{CP} :

$$\begin{aligned}
U_1^{VIII} : \quad \cos^2 \theta_{12} \cos^2 \theta_{13} &= \cos^2 \varphi_1, & U_2^{VIII} : \quad \sin^2 \theta_{12} \cos^2 \theta_{13} &= \cos^2 \varphi_1, \\
U_6^{VIII} : \quad \sin^2 \theta_{23} \cos^2 \theta_{13} &= \cos^2 \varphi_1, & U_9^{VIII} : \quad \cos^2 \theta_{23} \cos^2 \theta_{13} &= \cos^2 \varphi_1, \\
U_4^{VIII} : \quad \cos \delta_{CP} &= \frac{2(\cos^2 \varphi_1 - \sin^2 \theta_{12} \cos^2 \theta_{23} - \sin^2 \theta_{13} \cos^2 \theta_{12} \sin^2 \theta_{23})}{\sin 2\theta_{12} \sin \theta_{13} \sin 2\theta_{23}}, \\
U_5^{VIII} : \quad \cos \delta_{CP} &= -\frac{2(\cos^2 \varphi_1 - \cos^2 \theta_{12} \cos^2 \theta_{23} - \sin^2 \theta_{13} \sin^2 \theta_{12} \sin^2 \theta_{23})}{\sin 2\theta_{12} \sin \theta_{13} \sin 2\theta_{23}}, \\
U_7^{VIII} : \quad \cos \delta_{CP} &= -\frac{2(\cos^2 \varphi_1 - \sin^2 \theta_{12} \sin^2 \theta_{23} - \sin^2 \theta_{13} \cos^2 \theta_{12} \cos^2 \theta_{23})}{\sin 2\theta_{12} \sin \theta_{13} \sin 2\theta_{23}}, \\
U_8^{VIII} : \quad \cos \delta_{CP} &= \frac{2(\cos^2 \varphi_1 - \cos^2 \theta_{12} \sin^2 \theta_{23} - \sin^2 \theta_{13} \sin^2 \theta_{12} \cos^2 \theta_{23})}{\sin 2\theta_{12} \sin \theta_{13} \sin 2\theta_{23}}.
\end{aligned} \tag{4.20}$$

For a given value of φ_1 , the allowed intervals for $\cos \delta_{CP}$ can be derived from the aforementioned correlations by scanning the mixing angles across their experimentally allowed 3σ intervals [6]. As a result, such sum rules may be tested and potentially differentiated in upcoming neutrino oscillation experiments, provided the Dirac CPV phase δ_{CP} is measured. Under this framework, the choice of residual symmetry fixes one element of the mixing matrix to $\cos \varphi_1$, so that constraints on φ_1 can be inferred by requiring $\cos \varphi_1$ to lie within the experimentally favored 3σ range. Additionally, we conduct a detailed numerical scan of the $\Delta(6n^2)$ group with $n \leq 4$, showing that only the mixing matrices labeled U_4^{VIII} through

U_9^{VIII} are consistent with current mixing angle data for specific choices of the parameters θ_ℓ and θ_ν .

Note that if the left-handed lepton doublets are assigned to a *reducible* three-dimensional representation, given by the direct sum of a singlet and a doublet representation of G_f , the lepton mixing pattern U^{VIII} in Eq. (4.14) can also arise from the breaking of the dihedral group D_n combined with generalized CP symmetry [89]. The relevant group-theoretical properties of D_n are summarized in Appendix A.4. In this scenario, the residual symmetries in the lepton sector can be chosen as

$$G_\ell = Z_2^{SR^{ze}}, \quad X_\ell = \{R^{-z_e+x}, SR^x\}, \quad G_\nu = Z_2^{SR^{z\nu}}, \quad X_\nu = \{R^{-z_\nu+y}, SY^y\}, \quad (4.21)$$

where $z_e, z_\nu = 0, 1, \dots, n-1$, and $x = y = 0$ for odd n , while $x, y = 0, n/2$ for even n . In this case, the explicit expressions of the discrete parameters φ_1 and φ_2 entering the mixing pattern U^{VIII} are rather involved (see [89] for details). Nevertheless, φ_1 and φ_2 are restricted to the following discrete sets of values:

$$\varphi_1 \pmod{2\pi} = 0, \frac{1}{n}\pi, \frac{2}{n}\pi, \dots, \frac{2n-1}{n}\pi, \quad \varphi_2 \pmod{2\pi} = 0, \frac{1}{2}\pi, \pi, \frac{3}{2}\pi, \quad (4.22)$$

Moreover, φ_2 is further constrained to take only the values 0 or π if the group index n of D_n is odd, or if $x = y = 0, n/2$ with even n .

The fixed entry of U^{VIII} is $\cos \varphi_1$, which depends only on φ_1 ; consequently, the phenomenology is directly affected by the value of φ_1 . By comparing Eq. (4.16) with Eq. (4.22), we observe that for the same value of n , the parameter φ_2 can generally take a larger set of discrete values in the case of $\Delta(6n^2)$ than in the case of D_n , while the allowed values of φ_1 remain identical for both groups. It is worth emphasizing, however, that the group order of D_n is $2n$, which is substantially smaller than the order $6n^2$ of $\Delta(6n^2)$. From the perspective of maintaining analytical tractability while avoiding excessively large group orders, the dihedral group D_n can in fact provide a richer and more flexible phenomenology than $\Delta(6n^2)$. For this reason, it is necessary to also consider the realization of the mixing pattern U^{VIII} originating from $D_n \rtimes H_{CP}$ in the following discussion.

(IX) $G_\ell = Z_2^{bc^x d^x}, X_{\ell r} = \rho_r(c^\alpha d^{-2x-\alpha}), G_\nu = Z_2^{abc^y}, X_{\nu r} = \rho_r(c^\beta d^{2y+2\beta})$

Using the Σ^{IX} matrix in table 2, we obtain that the lepton mixing matrix is given by

$$U^{IX} = \frac{1}{2} \begin{pmatrix} 1 & c_\nu + \sqrt{2}e^{i\varphi_2}s_\nu & s_\nu - \sqrt{2}e^{i\varphi_2}c_\nu \\ s_\ell + \sqrt{2}e^{i\varphi_1}c_\ell & s_\ell c_\nu - \sqrt{2}(e^{i\varphi_1}c_\ell c_\nu + e^{i\varphi_2}s_\ell s_\nu) & s_\ell s_\nu - \sqrt{2}(e^{i\varphi_1}c_\ell s_\nu - e^{i\varphi_2}s_\ell c_\nu) \\ c_\ell - \sqrt{2}e^{i\varphi_1}s_\ell & c_\ell c_\nu + \sqrt{2}(e^{i\varphi_1}s_\ell c_\nu - e^{i\varphi_2}c_\ell s_\nu) & c_\ell s_\nu + \sqrt{2}(e^{i\varphi_1}s_\ell s_\nu + e^{i\varphi_2}c_\ell c_\nu) \end{pmatrix}. \quad (4.23)$$

with

$$\varphi_1 = \frac{3\alpha + 2(x+y)}{n}\pi, \quad \varphi_2 = -\frac{3\beta + 2(x+y)}{n}\pi. \quad (4.24)$$

Our analysis reveals that the parameters φ_1 and φ_2 are not entirely independent. Instead, they are restricted to the following discrete sets:

$$\begin{aligned} \varphi_1 \pmod{2\pi} &= 0, \frac{1}{n}\pi, \frac{2}{n}\pi, \dots, \frac{2n-1}{n}\pi, \\ \varphi_1 + \varphi_2 \pmod{2\pi} &= 0, \frac{3}{n}\pi, \frac{6}{n}\pi, \dots, \frac{2n-3}{n}\pi, \quad 3 \mid n, \\ \varphi_1 + \varphi_2 \pmod{2\pi} &= 0, \frac{1}{n}\pi, \frac{2}{n}\pi, \dots, \frac{2n-1}{n}\pi, \quad 3 \nmid n. \end{aligned} \quad (4.25)$$

It is adequate to restrict attention to the fundamental domains $0 \leq \varphi_1 < \pi$ and $0 \leq \varphi_2 < \pi$. According to Eq. (4.23), we see that one element of the PMNS mixing matrix equals $1/2$. To align with experimental observations, this constant entry may correspond to the (21), (22), (31), or (32) elements of the matrix. Consequently, the PMNS matrix can assume four distinct configurations:

$$U_1^{IX} = P_{213}U^{IX}, \quad U_2^{IX} = P_{213}U^{IX}P_{213}, \quad U_3^{IX} = P_{231}U^{IX}, \quad U_4^{IX} = P_{231}U^{IX}P_{213}. \quad (4.26)$$

We see that U_3^{IX} and U_4^{IX} are related to U_1^{IX} and U_2^{IX} through an exchange of the second and third rows of the PMNS mixing matrix, respectively. The strong correlations among the mixing parameters stem from their common dependence on θ_ℓ and θ_ν . For these four mixing matrices, the sum rule takes the form of the last four correlations in Eq. (4.20) with $\cos \varphi_1$ replaced by $1/2$, then we obtain the corresponding $\cos \delta_{CP}$ intervals: $[0.6699, 1]$, $[0.3829, 1]$, $[-1, -0.5853]$ and $[-1, -0.5537]$.

$$(\mathbf{X}) \quad G_\ell = Z_2^{bc^x d^x}, \quad X_{\ell r} = \rho_r(c^\alpha d^{-2x-\alpha}), \quad G_\nu = Z_2^{c^n/2}, \quad X_{\nu r} = \rho_r(c^\beta d^\gamma)$$

We obtain the lepton mixing matrix from the Σ^X matrix in table 2. This matrix can be taken to the form

$$U^X = \frac{1}{\sqrt{2}} \begin{pmatrix} c_\nu & & s_\nu & -e^{i\varphi_2} \\ s_\ell c_\nu + \sqrt{2}e^{i\varphi_1} c_\ell s_\nu & s_\ell s_\nu - \sqrt{2}e^{i\varphi_1} c_\ell c_\nu & e^{i\varphi_2} s_\ell & \\ c_\ell c_\nu - \sqrt{2}e^{i\varphi_1} s_\ell s_\nu & c_\ell s_\nu + \sqrt{2}e^{i\varphi_1} s_\ell c_\nu & e^{i\varphi_2} c_\ell & \end{pmatrix}, \quad (4.27)$$

where the parameters φ_1 and φ_2 are defined as

$$\varphi_5 = \frac{2x + 3\alpha - 2\beta + \gamma}{n}\pi, \quad \varphi_6 = -\frac{2x + \beta + \gamma}{n}\pi, \quad (4.28)$$

where the group index n has to be even number. We see that the discrete values of φ_1 and φ_2 are correlated in the case that n is divisible by 3. To be specific, their values could be

$$\begin{aligned} \varphi_1 \pmod{2\pi} &= 0, \frac{1}{n}\pi, \frac{2}{n}\pi, \dots, \frac{2n-1}{n}\pi, \\ \varphi_1 + \varphi_2 \pmod{2\pi} &= 0, \frac{3}{n}\pi, \frac{6}{n}\pi, \dots, \frac{2n-3}{n}\pi, \quad 3 \mid n \\ \varphi_1 + \varphi_2 \pmod{2\pi} &= 0, \frac{1}{n}\pi, \frac{2}{n}\pi, \dots, \frac{2n-1}{n}\pi, \quad 3 \nmid n. \end{aligned} \quad (4.29)$$

It is easy to check that U^X has the following symmetry properties:

$$\begin{aligned} U^X(\varphi_1 + \pi, \varphi_2, \theta_\ell, \theta_\nu) &= U^X(\varphi_1, \varphi_2, \theta_\ell, \pi - \theta_\nu) \text{diag}(-1, 1, 1), \\ U^X(\varphi_1, \varphi_2 + \pi, \theta_\ell, \theta_\nu) &= U^X(\varphi_1, \varphi_2, \theta_\ell, \theta_\nu) \text{diag}(1, 1, -1), \\ U^X(\varphi_1, \varphi_2 + \frac{\pi}{2}, \theta_\ell, \theta_\nu) &= U^X(\varphi_1, \varphi_2, \theta_\ell, \theta_\nu) \text{diag}(1, 1, i), \\ U^X(\pi - \varphi_1, \pi - \varphi_2, \theta_\ell, \theta_\nu) &= (U^X(\varphi_1, \varphi_2, \theta_\ell, \pi - \theta_\nu))^* \text{diag}(-1, 1, -1). \end{aligned} \quad (4.30)$$

Hence it is sufficient to focus on the fundamental interval of $0 \leq \varphi_1 < \pi/2$ and $0 \leq \varphi_2 \pmod{\pi/2} < \pi/2$ [88]. Furthermore, the impact of φ_2 is confined to the Majorana phase α_{31} . Its effect amounts to a simple mapping $\alpha_{31} \rightarrow \alpha_{31} + 2\varphi_2$ of the $\varphi_2 = 0$ results, leaving all other parameters unaffected. We see the fixed element is $1/\sqrt{2}$ which can only be the (32) or (33) entry in order to achieve agreement with experimental data. As a consequence, we have two phenomenologically viable mixing patterns after the permutations of rows and columns of the mixing matrix U^X are considered,

$$U_1^X = P_{213}U^X, \quad U_2^X = P_{231}U^X. \quad (4.31)$$

Observable	bf $\pm 1\sigma$	3σ range
$\sin^2 \theta_{12}$ (NO & IO)	$0.308_{-0.011}^{+0.012}$	[0.275, 0.345]
$\sin^2 \theta_{13}$ (NO)	$0.02215_{-0.00058}^{+0.00056}$	[0.02030, 0.02388]
$\sin^2 \theta_{13}$ (IO)	$0.02231_{-0.00056}^{+0.00056}$	[0.02060, 0.02409]
$\sin^2 \theta_{23}$ (NO)	$0.470_{-0.013}^{+0.017}$	[0.435, 0.585]
$\sin^2 \theta_{23}$ (IO)	$0.550_{-0.015}^{+0.012}$	[0.440, 0.584]
δ_{CP}/π (NO)	$1.18_{-0.23}^{+0.14}$	[0.69, 2.02]
δ_{CP}/π (IO)	$1.52_{-0.14}^{+0.12}$	[1.12, 1.86]

Table 3: The central values, the 1σ errors and 3σ ranges of the mixing angles and Dirac CPV phase for leptons. We adopt the values of the lepton mixing parameters from NuFIT-v6.0 with Super-Kamiokanda atmospheric data for normal ordering (NO) and inverted ordering (IO) [6].

For the two mixing matrices, all mixing parameters are strongly correlated such that the following sum rules among the mixing angles and Dirac CP phase are found to be satisfied,

$$U_1^X : \quad \cos^2 \theta_{13} \sin^2 \theta_{23} = \frac{1}{2}, \quad U_2^X : \quad \cos^2 \theta_{13} \cos^2 \theta_{23} = \frac{1}{2}, \quad (4.32)$$

Given the measured reactor mixing angle $\sin^2 \theta_{13} \in [0.02030, 0.02388]$ [6], we find the atmospheric mixing angle

$$\sin^2 \theta_{23} \in [0.5104, 0.5122] \text{ for } U_1^X, \quad \sin^2 \theta_{23} \in [0.4878, 0.4896] \text{ for } U_2^X, \quad (4.33)$$

which deviates slightly from maximal mixing. These predictions may be tested at future long-baseline experiments DUNE [92] and T2HK [93], and at the discussed ESS ν SB experiment [94]. A remarkably good fit to experimental data can generally be obtained for any $\Delta(6n^2)$ flavour group with even n in this framework. In the present work, we consider the next group with $n = 4$. Then the allowed values of φ_1 and φ_2 include $(0, 0)$, $(0, \pi/4)$, $(\pi/4, 0)$, $(\pi/4, \pi/4)$, $(\pi/2, 0)$, and $(\pi/2, \pi/4)$ ⁷. From the mixing matrix in Eq. (4.27), for a fixed φ_1 , the cases $\varphi_2 = 0$ and $\varphi_2 = \pi/4$ give identical mixing angles and Dirac CP phase. However, for pattern U_1^X , the Majorana phase α_{21} (or α_{31}) shifts by $\pi/2$. Thus, predictions for $\varphi_2 = \pi/4$ can be directly inferred from those with $\varphi_2 = 0$, and it suffices to analyze only the $\varphi_2 = 0$ cases. When $\varphi_1 = \varphi_2 = 0$, all permutations in Eq. (4.31) can reproduce the measured mixing angles for appropriate choices of θ_ℓ and θ_ν . In this scenario, the mixing matrix is real, so both Dirac and Majorana CP phases are trivial.

5 Numerical analysis

In this section we outline the statistical framework used to test the mixing-parameter predictions of the models discussed above against current neutrino oscillation data, including the latest results from the global analysis NuFIT and the JUNO experiment. The input values of the lepton mixing parameters are taken from the NuFIT-v6.0 with inclusion of the data on atmospheric neutrinos provided by the Super-Kamiokanda and IceCube collaborations [6], and they are summarized in table 3. To quantify the compatibility of each breaking pattern with experimental measurements, we perform a χ^2 analysis for every mixing pattern for both

⁷The pairs $(3\pi/4, 0)$ and $(3\pi/4, \pi/4)$ are also allowed. The resulting mixing matrices are the complex conjugates of those for $(\pi/4, 0)$ and $(\pi/4, \pi/4)$, respectively, up to redefinition of θ_ν and Q_ν , yielding identical mixing angles but reversed overall signs of the CP phases.

NO and IO neutrino mass spectrum. We construct the global test statistic as [47, 95–98]

$$\chi^2(\vec{\sigma}) = \sum_{i=1}^4 \chi_i^2(o_i), \quad \vec{\sigma} = (\sin^2 \theta_{12}, \sin^2 \theta_{13}, \sin^2 \theta_{23}, \delta_{CP}), \quad (5.1)$$

where $\chi_i^2(o_i)$ denotes the one-dimensional projection provided by NuFIT. We remark that the global fit of NuFIT-v6.0 [6] shows an overall preference for normal ordering, with $\chi_{\min, \text{IO}}^2 - \chi_{\min, \text{NO}}^2 = 6.1$ if the Super-Kamiokande data is included. In our analysis, however, we adopt a conservative treatment and consider the two mass orderings on equal footing by setting $\chi_{\min, \text{NO}}^2 = \chi_{\min, \text{IO}}^2 = 0$. For a given mixing pattern, the observables in $\vec{\sigma}$ are not independent but satisfy sum rules since they depend on one or two free real parameters. The best-fit values of these parameters, together with the predicted mixing observables, are obtained by minimizing the global χ^2 . Besides, to determine the one-dimensional profile for a specific observable o_i (e.g. $\sin^2 \theta_{12}$), we minimize the global function while fixing o_i . This defines

$$\chi^2(o_i) = \min \left[\chi^2(\vec{\sigma}) \Big|_{o_i} \right]. \quad (5.2)$$

The corresponding likelihood is then given by

$$L(o_i) = \exp \left[-\chi^2(o_i)/2 \right]. \quad (5.3)$$

In the following, we will first confront the predictions of the one- and two-parameter mixing patterns discussed in sections 3 and 4 with the latest NuFIT results. A given lepton mixing pattern is regarded as phenomenologically viable if its predictions for the mixing parameters at the minimum of the χ^2 function lie within the corresponding 3σ intervals summarized in table 3. After that, we confront the predicted values of $\sin^2 \theta_{12}$ with the most recent 59.1-day JUNO measurement, as well as with the projected precision expected after 6 years of JUNO data taking. We also examine the predictions for $\sin^2 \theta_{23}$ and δ_{CP} in light of the anticipated sensitivity reaches of the future long-baseline experiments DUNE and T2HK. Among the one- and two-parameter mixing patterns, several patterns—namely U^I , U^{II} , U^{VIII} , U^{XI} and U^X —arise from the series of flavour groups $\Delta(6n^2) \rtimes H_{CP}$ (with U^{VIII} also obtainable from $D_n \rtimes H_{CP}$). To keep the analysis tractable and avoid excessively large group orders, we restrict our attention to groups $\Delta(6n^2)$ with $n \leq 4$ and D_n with $n \leq 8$ in what follows.

5.1 Lepton mixing matrix depending on one free parameter

For the one-parameter mixing patterns, U^I , U^{II} , U^{III} , U^{IV} and U^V , the best-fit value of the free parameter θ , the minimum χ_{\min}^2 and the resulting predictions for the lepton mixing angles θ_{12} , θ_{13} , θ_{23} as well as the CPV phases δ_{CP} , α_{21} and α_{31} for both NO and IO neutrino mass spectra are collected in table 4. Note that the entries in the $\sin^2 \theta_{12}$ column highlighted in red indicate predictions that fall within the 3σ interval of the JUNO 59.1-day measurement [99],

$$0.2831 \leq \sin^2 \theta_{12} \leq 0.3353, \quad (5.4)$$

where this interval is obtained by taking the central value and adding/subtracting three times the 1σ uncertainty given in Eq. (1.5). It is worth noting that the quoted 3σ interval of $\sin^2 \theta_{12}$ from JUNO is obtained under the assumption of normal mass ordering. In our comparison, we also apply this interval to the IO case as a working assumption, since the JUNO collaboration concludes in [99] that the results on $\sin^2 \theta_{12}$ and Δm_{21}^2 for the inverted ordering are “fully compatible” with those reported for the normal ordering. The

Order	Case	(φ_1, φ_2)	θ_{bf}/π	χ_{min}^2	$\sin^2 \theta_{12}$	$\sin^2 \theta_{13}$	$\sin^2 \theta_{23}$	δ_{CP}/π	α_{21}/π (mod 1)	α_{31}/π (mod 1)
NO	U^I	$(-\frac{\pi}{2}, \frac{\pi}{2})$	0.9170	5.308	0.318	0.02215	0.5	1.5	0	0
	U_1^{II}	$(0, \pi)$	0.1918	11.862	0.341	0.02208	0.5	1.5	0	0
	U_2^{II}	$(0, \pi)$	0.3083	11.859	0.341	0.02214	0.5	1.5	0	0
	U^{III}	—	0.0560	9.600	0.283	0.02217	0.5	1.5	0	0
	U_1^{IV}	—	0.9053	6.414	0.331	0.02214	0.523	1	0	0
	U_2^{IV}	—	0.9053	11.856	0.331	0.02214	0.477	0	0	0
	U_1^V	—	0.5715	8.921	0.341	0.02212	0.554	1.331*	0.161*	0.559*
	U_2^V	—	0.5746	13.427	0.341	0.02256	0.450	1.652	0.837	0.439
IO	U^I	$(-\frac{\pi}{2}, \frac{\pi}{2})$	0.9166	3.887	0.318	0.02235	0.5	1.5	0	0
	U_1^{II}	$(0, \pi)$	0.1915	10.471	0.341	0.02227	0.5	1.5	0	0
	U_2^{II}	$(0, \pi)$	0.3085	10.471	0.341	0.02227	0.5	1.5	0	0
	U^{III}	—	0.0563	8.188	0.283	0.02236	0.5	1.5	0	0
	U_1^V	—	0.5736	9.012	0.341	0.02241	0.551	1.343*	0.162*	0.561*
	U_2^V	—	0.5758	13.416	0.341	0.02274	0.452	1.646	0.837	0.438

Table 4: The best-fit values of the free parameter and the corresponding lepton mixing observables for all one-parameter mixing patterns in both normal and inverted mass orderings. The discrete parameters (φ_1, φ_2) specify the residual symmetries associated with flavour groups of type $\Delta(6n^2)$ ($n \leq 4$). For each pattern, the global minimum of the test statistic is obtained at $\theta = \theta_{\text{bf}}$, where the χ^2 function reaches χ_{min}^2 . At the best-fit point, we present the predictions for the neutrino mixing angles $\theta_{12}, \theta_{13}, \theta_{23}$, the Dirac CPV phase δ , and the Majorana phases α_{21} and α_{31} . Values of CPV phases marked with a superscript * correspond to scenarios in which the left-handed lepton doublets transform as the conjugate triplet $\bar{\mathbf{3}}$. Entries in the $\sin^2 \theta_{12}$ column highlighted in red color indicate predictions lying within the 3σ interval of the JUNO 59.1-day measurement.

corresponding allowed regions of lepton observables, which are obtained by scanning the parameter space, requiring that three mixing angles and the Dirac CPV phase δ_{CP} fall within their experimentally preferred 3σ ranges given in table 3, are summarized in table 9, in Appendix B.

Confronting the results in table 4 with the NuFIT 3σ allowed regions given in table 3, we find that a total of 8 (6) one-parameter mixing patterns are phenomenologically viable for NO (IO), once all inequivalent row and column permutations of the lepton mixing matrix are taken into account. For the mixing patterns U^I and U^{II} arising from $\Delta(6n^2) \times H_{CP}$, the smallest group that can reproduce the NuFIT data is $\Delta(24) \cong S_4$ with $n = 2$. In case of $(\varphi_1, \varphi_2) = (-\frac{\pi}{2}, \frac{\pi}{2})$, the pattern U^I reduces to the TM1 form [100, 101] with its first column fixed as $(-\frac{2}{\sqrt{6}}, -\frac{1}{\sqrt{6}}, \frac{1}{\sqrt{6}})^T$, as can be seen from Eq. (3.3), and it agrees with the NuFIT limits for both NO and IO. The TM2-type patterns, namely U^{II} with $(\varphi_1, \varphi_2) = (0, \pi)$ and U^V featuring the trimaximal column $(\frac{1}{\sqrt{3}}, \frac{1}{\sqrt{3}}, \frac{1}{\sqrt{3}})^T$ (see Eq. (3.15) and Eq. (3.37)), don't agree with JUNO's latest results at 3σ level, although it is very close to the 3σ upper limit of NuFIT for both NO and IO. Among the one-parameter patterns originating from $A_5 \times H_{CP}$, the GR2 structure U^{III} —which preserves the second column of the Golden Ratio mixing pattern, $(\sqrt{\frac{1}{\sqrt{5}\phi_g}}, \sqrt{\frac{\phi_g}{2\sqrt{5}}}, \sqrt{\frac{\phi_g}{2\sqrt{5}}})^T$ (see Eq. (3.26))—remains compatible with the NuFIT constraints in both NO and IO. By contrast, the real pattern U^{IV} , characterized by the fixed first column $(\frac{\phi_g}{2}, \frac{\phi_g-1}{2}, \frac{1}{2})^T$ (see Eq. (3.32)), is only viable in NO.

We display in figure 1 the best-fit values of the three mixing angles and δ_{CP} for all viable

one-parameter models under both NO and IO neutrino mass spectrum. The dashed lines indicate the central values of the observables from the NuFIT global fit. The light-red band in the $\sin^2 \theta_{12}$ panel corresponds to the 3σ interval derived from the recent JUNO measurement, see Eq. (5.4), while the darker and narrower red band indicates the projected 3σ precision after six years of data taking, assuming the current JUNO central value $\sin^2 \theta_{12} = 0.3092$ and an expected uncertainty of about 0.5% [31]. For NO, three one-parameter mixing patterns — U^I (TM1), U_1^{IV} and U_2^V — yield predictions for $\sin^2 \theta_{12}$ that fall within the current JUNO constraint. In contrast, the patterns U^{II} (TM2), U^{III} (GR2), and U^V (TM2) are disfavored by the JUNO data at the 3σ level. None of the one-parameter patterns, however, would remain compatible with the much better sensitivity expected after six years of operation if the current best fit value would not change significantly. For IO, only the pattern U^I (TM1) lies in the present JUNO 3σ allowed interval, and all patterns would be excluded once the planned future precision is reached. We also observe that the predicted values of $\sin^2 \theta_{13}$ for nearly all patterns lie very close to the NuFIT best-fit line, reflecting the excellent experimental precision already achieved for this observable. Finally, the red bands shown for $\sin^2 \theta_{23}$ and δ_{CP} represent the anticipated future 3σ sensitivities of next-generation long-baseline experiments such as DUNE [92] and T2HK [93]. It is worth noting that the future experimental uncertainties on $\sin^2 \theta_{23}$ and δ_{CP} depend sensitively on their true values. For $\sin^2 \theta_{23}$, as illustrated in Ref. [102], the projected precision of DUNE and T2HK ranges from about 1% when the true value lies near the edges of the current 3σ interval, to roughly 7% around the maximal-mixing point $\sin^2 \theta_{23} = 0.5$. For the present NuFIT best-fit values, $\sin^2 \theta_{23} = 0.47$ (NO) and $\sin^2 \theta_{23} = 0.55$ (IO), the expected uncertainty is approximately 3%, which we adopt as a representative estimate. For δ_{CP} , the projected 1σ precision of DUNE is approximately 6° if the true value is $\delta_{CP} = 0^\circ$, while it degrades to about 16° for $\delta_{CP} = 270^\circ$. In case of T2HK, the corresponding 1σ uncertainties are around 6° for $\delta_{CP} = 0^\circ$ and roughly 20° for $\delta_{CP} = 270^\circ$. Taking these variations into account, we adopt 12° as the expected 1σ precision for δ_{CP} in our analysis for illustration. Combining the numerical results in table 4, we observe that the patterns U^I , U^{II} , and U^{III} predict maximal atmospheric mixing θ_{23} and Dirac CPV phase δ_{CP} . In contrast, the real patterns U_1^{IV} and U_2^V imply CP conservation. Neither maximal nor vanishing δ_{CP} is achievable within U_1^V and U_2^V . Hence precise measurements of θ_{23} and δ_{CP} will therefore play an important role in discriminating among these viable mixing schemes.

To further assess the predictive power of the mixing patterns, we evaluate the likelihood profile defined in Eq. (5.3) for $\sin^2 \theta_{12}$, $\sin^2 \theta_{23}$ and δ_{CP} across all one-parameter patterns with $\chi_{\min}^2 \leq 9$, since models with $\chi_{\min}^2 > 9$ are disfavored at more than 3σ . Under this criterion, only three patterns U^I (TM1), U_1^{IV} and U_1^V satisfy $\chi_{\min}^2 \leq 9$ in the NO case, while for IO only U^I and U^{III} remain viable, as summarized in table 4. Figure 2 displays the corresponding likelihood profiles. The dashed curves denote the likelihoods for $\sin^2 \theta_{12}$, $\sin^2 \theta_{23}$ and δ_{CP} obtained from the NuFIT analysis. In the $\sin^2 \theta_{12}$ panel, the red dashed curve shows the likelihood from the recent JUNO 59.1-day data, while the dotted line indicates the projected 0.5% precision expected after six years of JUNO operation. The dotted curves in the $\sin^2 \theta_{23}$ and δ_{CP} panels correspond to the anticipated sensitivities of DUNE and T2HK. The solid colored lines represent the likelihoods predicted by the individual mixing patterns. The left (right) panels employ the one-dimensional projections $\chi_i^2(o_i)$ for NO (IO).

For $\sin^2 \theta_{12}$, the predicted profiles are exceedingly narrow because $\sin^2 \theta_{12}$ is tightly constrained by the small uncertainties in $\sin^2 \theta_{13}$, as implied by Eqs. (3.8), (3.29), (3.35) and (3.42) for U^I , U^{III} , U_1^{IV} and U_1^V , respectively. In the NO case, the prediction of U_1^V for $\sin^2 \theta_{12}$ is disfavored by the latest JUNO data, whereas U^I and U_1^{IV} remain viable at 3σ . In the IO case, U^{III} is excluded by current JUNO data, while U^I stays consistent. If JUNO achieves the projected 0.5% precision and the current best fit values would not change sig-

nificantly, all these patterns could be tested in both NO and IO cases. These conclusions regarding $\sin^2 \theta_{12}$ for the one-parameter mixing patterns are fully consistent with the earlier analysis based on the best-fit results. For $\sin^2 \theta_{23}$, the patterns U^I and U^{III} predict the fixed value $\sin^2 \theta_{23} = 0.5$, while U_1^{IV} and U_1^V yield sharply peaked predictions with $\sin^2 \theta_{23} > 0.5$, due to correlations with $\sin^2 \theta_{13}$ encoded in Eqs. (3.35) and (3.42). Taking future sensitivities into account, the predicted ranges of U_1^{IV} and U_1^V could be probed in the NO case, while in the IO case both U^I and U^{III} could be tested. Regarding the Dirac phase, U^I and U^{III} predict $\delta_{CP} = 1.5\pi$, while U_1^{IV} predicts $\delta_{CP} = \pi$. i.e., absence of CP-violation in neutrino oscillations. In the NO case, the prediction $\delta_{CP} = 1.5\pi$ lies outside the projected 3σ allowed range of the prospective DUNE and T2HK data, whereas $\delta_{CP} = \pi$ remains within it. In contrast, for the IO case, $\delta_{CP} = 1.5\pi$ falls within the 3σ allowed interval.

In summary, the JUNO 59.1-day data imposes significant restrictions on the landscape of one-parameter mixing patterns. The 3σ interval of $\sin^2 \theta_{12}$ from JUNO excludes several patterns that would otherwise remain compatible with the NuFIT global fit. We have focused on the flavour symmetry groups A_5 , $\Sigma(168)$ and $D(6n^2)$ with $n \leq 4$. For NO, we find that only U^I (TM1), originating from $S_4 \times H_{CP}$, and $U_{1,2}^{IV}$, originating from $A_5 \times H_{CP}$, predict $\sin^2 \theta_{12}$ values consistent with the current JUNO constraint. For IO, the viable space shrinks further, leaving U^I (TM1) as the sole surviving option. Patterns such as U^{II} (TM2), U^{III} (GR2) and U^V (TM2), although acceptable under NuFIT alone, become disfavored once the JUNO likelihood is taken into account. It should be emphasized that, for the mixing pattern U^I , additional phenomenologically viable textures—compatible with the current JUNO data—will emerge other than the TM1 form once higher values of n in the group $\Delta(6n^2)$ are considered. The future precision of $\sin^2 \theta_{12}$, $\sin^2 \theta_{23}$, and δ_{CP} will provide additional discriminatory power among these one-parameter mixing patterns.

5.2 Lepton mixing matrix depending on two free parameters

We now turn to discuss the numerical results for the two-parameter mixing patterns U^{VI} , U^{VII} , U^{VIII} , U^{IX} and U^X . The best-fit values of the two real input parameters (θ_ℓ^{bf} , θ_ν^{bf}), together with the corresponding predictions for the lepton mixing angles and CPV phases, are listed in table 5 for U^{VI} and U^{VII} , in table 6 for U^{VIII} , and in table 7 for U^{IX} and U^X . The resulting allowed regions of the lepton observables are summarized in table 10, table 11, and table 12, in Appendix B. Unlike the one-parameter case, where only 8 (6) patterns are viable for NO (IO), the two-parameter constructions provide substantially greater flexibility: in total, 51 patterns for NO and 24 patterns for IO are compatible with the NuFIT data. We display the best-fit values of the three mixing angles and δ_{CP} for all viable two-parameter models for both NO and IO neutrino mass spectra in figure 3.

For the two-parameter mixing patterns derived from $A_5 \times H_{CP}$, we find 10 and 4 phenomenologically viable realizations of U^{VI} for NO and IO, respectively, as listed in table 5. The patterns U_2^{VI} , $U_{4,1}^{VI}$, $U_{4,2}^{VI}$, $U_{4,3}^{VI}$, $U_{4,4}^{VI}$, $U_{6,1}^{VI}$ and $U_{6,2}^{VI}$ predict CP-conserving Dirac and Majorana phases, consistent with the general argument presented in section 4.1. Consequently, these patterns are compatible with present data in the NO case, while they are disfavored for IO mass spectrum. By contrast, U_1^{VI} , $U_{3,2}^{VI}$ and U_5^{VI} yield nontrivial CPV phases and can accommodate the experimental data for both NO and IO. $U_{3,1}^{VI}$ can provide viable predictions only for the IO scenario. Under the sum rule constraints in Eq. (4.7), the allowed regions of the lepton observables given in table 10 become narrower than the corresponding 3σ intervals in table 3. The likelihood profiles for $\sin^2 \theta_{12}$, $\sin^2 \theta_{23}$ and δ_{CP} are shown in figure 4 for selected viable patterns U^{VI} with $\chi_{\min}^2 \leq 9$. The patterns $U_{4,1}^{VI}$ and $U_{6,2}^{VI}$ for NO, as well as $U_{3,1}^{VI}$, $U_{3,2}^{VI}$ and U_5^{VI} for IO, are not shown in the figure.

For $\sin^2 \theta_{12}$, figure 4 shows that the patterns $U_{4,2}^{VI}$, $U_{4,4}^{VI}$, and $U_{6,1}^{VI}$ are consistent with the

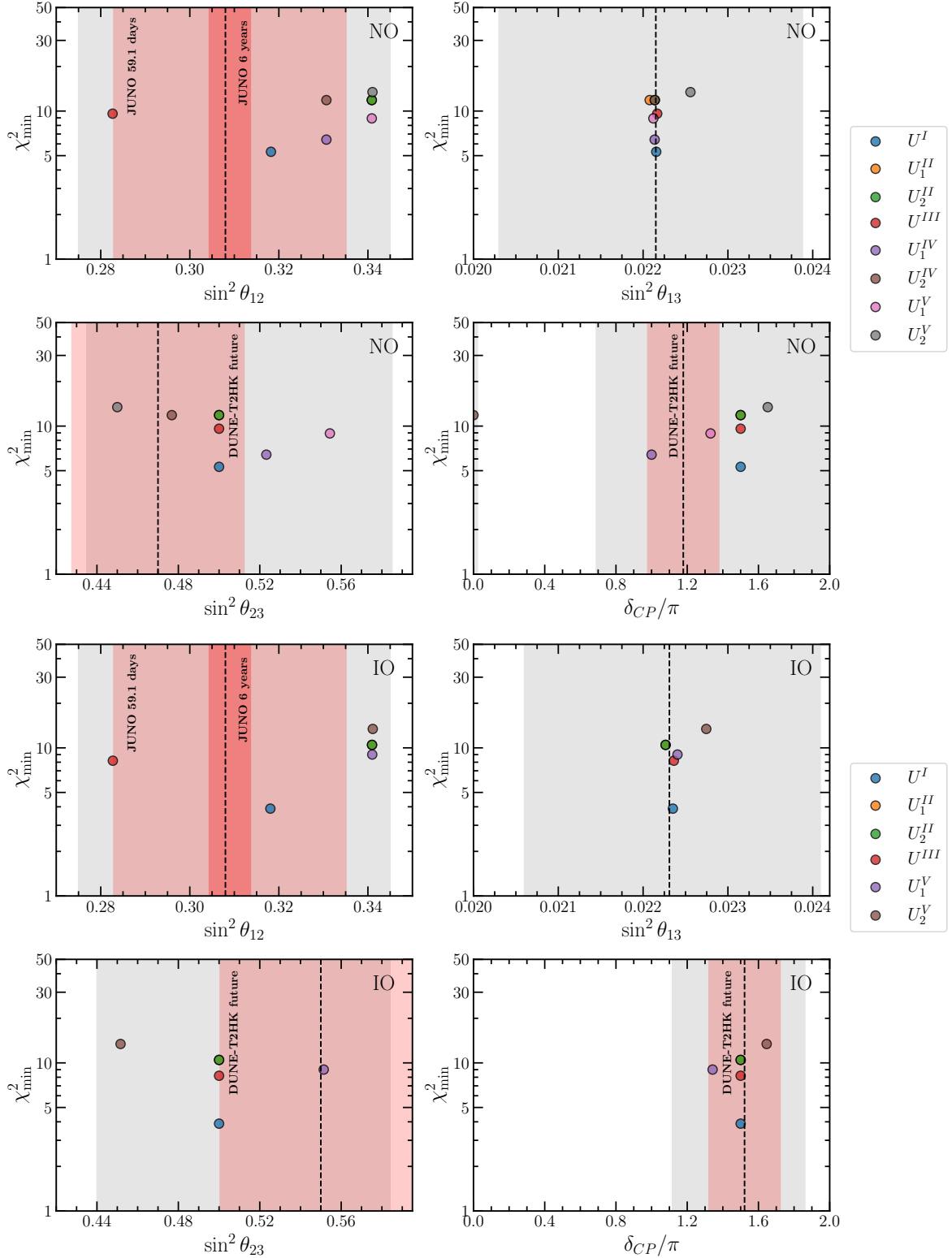


Figure 1: Best-fit predictions of the neutrino mixing angles θ_{12} , θ_{13} , θ_{23} and the Dirac CPV phase δ_{CP} for lepton mixing patterns with one parameter in case of NO and IO neutrino masses spectrum. The gray regions in all plots are the current 3σ ranges of the corresponding observables for NO and IO from [6]. The dashed line is the current best-fit value. The light red and red region for $\sin^2 \theta_{12}$ are the latest 3σ range obtained from the first 59.1 days of JUNE data [30] and the prospective 3σ range of after 6 years of JUNE running with precision of 0.5% [31]. The red regions shown for $\sin^2 \theta_{23}$ and δ_{CP} represent the anticipated future 3σ sensitivities of next-generation long-baseline experiments such as DUNE [92] and T2HK [93], assuming the current NuFit best-fit values together with prospective precisions of about 3% for $\sin^2 \theta_{23}$ and 12° for δ_{CP} .

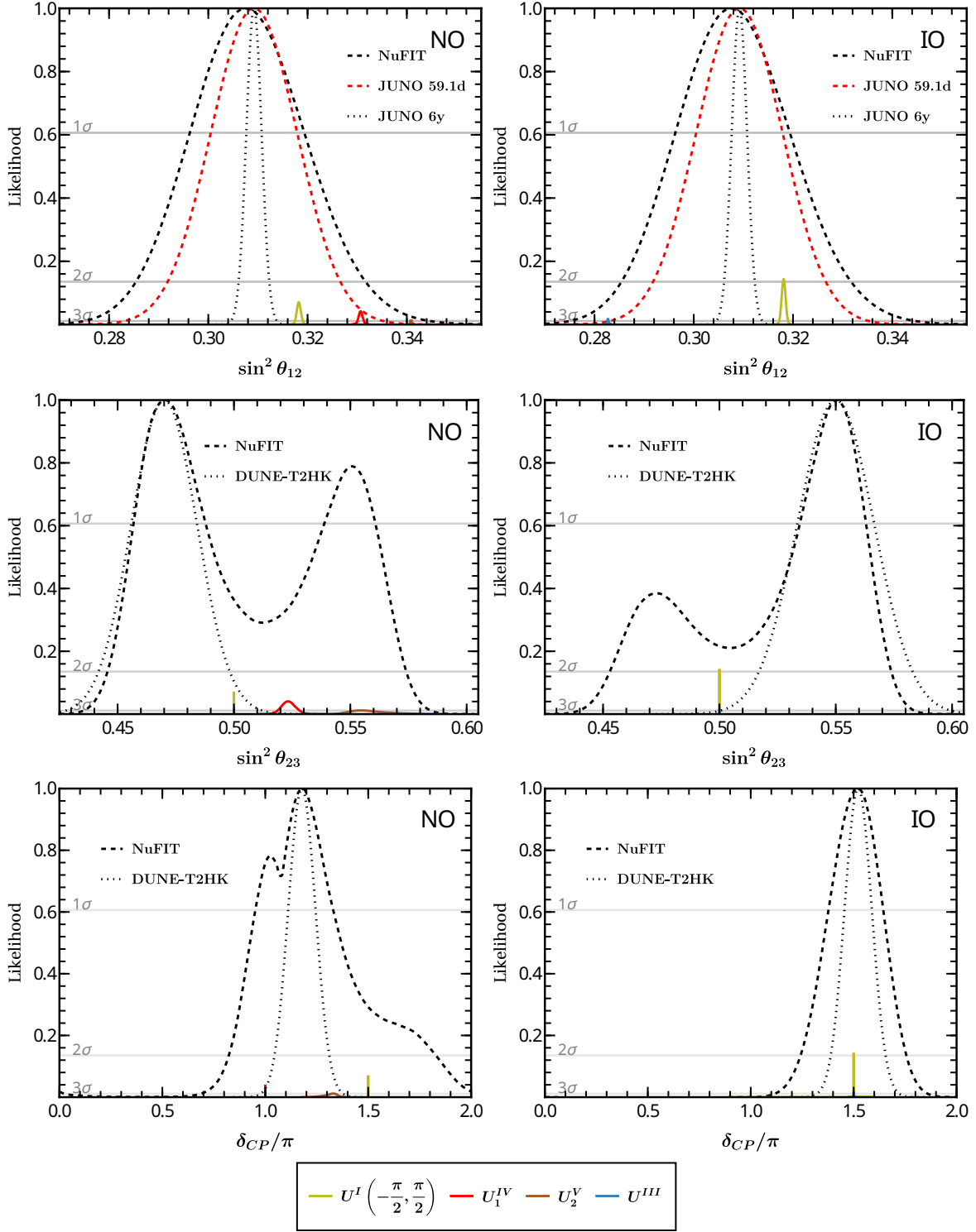


Figure 2: The predictions of likelihood profiles for $\sin^2 \theta_{12}$, $\sin^2 \theta_{23}$ and δ_{CP} obtained using the current global data on the neutrino mixing parameters for lepton mixing patterns with one parameter. The dashed curves denote the likelihoods obtained from the NuFIT [6]. In the $\sin^2 \theta_{12}$ panel, the red dashed curve shows the likelihood from the recent JUNO 59.1-day data [99], while the dotted line indicates the projected 0.5% precision expected after six years of JUNO operation [31]. The dotted curves in the $\sin^2 \theta_{23}$ and δ_{CP} panels correspond to the anticipated sensitivities of DUNE [92] and T2HK [93], assuming the current NuFit best-fit values together with prospective precisions of about 3% for $\sin^2 \theta_{23}$ and 12° for δ_{CP} . The solid colored lines represent the likelihoods predicted by the individual mixing patterns. The left (right) panels employ the one-dimensional projections $\chi_i^2(o_i)$ for NO (IO).

NuFIT data at the 2σ level, whereas U_1^{VI} , U_2^{VI} , $U_{3,2}^{VI}$, $U_{4,3}^{VI}$, and U_5^{VI} remain compatible at 3σ for the NO scenario. In case of IO, only U_1^{VI} is consistent at 2σ . The patterns U_1^{VI} and U_2^{VI} yield very sharp predictions for $\sin^2\theta_{12}$, since $\sin^2\theta_{12}$ is correlated with $\sin^2\theta_{13}$, see Eq. (4.7). The predictions of the patterns U_1^{VI} , U_2^{VI} , $U_{3,2}^{VI}$, and U_5^{VI} partially overlap with the 3σ range of the JUNO 59.1-day measurement, but they are disfavored at the 2σ level and are expected to be excluded once JUNO reaches its projected six-year precision of 0.5%. The remaining four cases $U_{4,2}^{VI}$, $U_{4,3}^{VI}$, $U_{4,4}^{VI}$ and $U_{6,1}^{VI}$ are consistent with both the current and projected JUNO sensitivities for NO and IO.

For $\sin^2\theta_{23}$, the patterns $U_{3,2}^{VI}$, $U_{4,2}^{VI}$, $U_{4,3}^{VI}$ and U_5^{VI} could be excluded by the projected DUNE and T2HK sensitivities in the NO case, as their predicted values of θ_{23} lie in second octant. For IO, the pattern U_1^{VI} remains consistent with the anticipated experimental precision. Moreover, all patterns that predict CP-conserving Dirac phase can be tested by future measurements, whereas those yielding nontrivial δ_{CP} remain viable under the projected sensitivities.

For the two-parameter mixing patterns originating from $\Sigma(168) \times H_{CP}$, we identify 5 viable realizations for NO and 2 for IO, as summarized in table 5. In the NO case, the four patterns $U_{2,i}^{VII}$ with $i = 1, 2, 3, 4$ predict trivial Dirac phase, since $U_{2,i}^{VII}$ is real matrix as follows from Eq. (4.11). The pattern $U_{1,1}^{VII}$ instead yields CP-violating Dirac phase and it remains compatible with global oscillation data for both mass orderings, whereas $U_{1,2}^{VII}$ is viable only for IO. Figure 4 displays the likelihood profiles of 3 cases $U_{2,2}^{VII}$, $U_{2,3}^{VII}$ and $U_{2,4}^{VII}$. All of them predict $\sin^2\theta_{12}$ values lying within both the current JUNO 59.1-day and the projected six-year precision 3σ intervals. Their predictions for $\sin^2\theta_{23}$, however, show different levels of compatibility with future accelerator experiments sensitivities provided the current NuFIT best fit value including the SK data would not change drastically: while the $U_{2,2}^{VII}$ and $U_{2,4}^{VII}$ predictions fall outside the expected DUNE and T2HK ranges, the allowed region of $U_{2,3}^{VII}$ partially overlaps with the projected sensitivities. Since all these patterns exhibit CP-conserving Dirac phase, they will be critically tested once DUNE and T2HK achieve their anticipated precision on δ_{CP} .

There are three distinct two-parameter mixing patterns that can be derived from the group $\Delta(6n^2) \times H_{CP}$, as discussed in section 4.3. We perform a full χ^2 analysis of these three cases for $\Delta(6n^2)$ with $n \leq 4$. For the mixing pattern U^{VIII} , the best-fit values of the two real input parameters and the corresponding predictions for the lepton mixing observables are summarized in table 6, while the resulting allowed regions of these observables are presented in table 11. Taking into account permutations and inequivalent choices of (φ_1, φ_2) , we find 10 and 4 phenomenologically viable realizations for NO and IO, respectively. For NO, the viable patterns include U_i^{VIII} with $i = 4, 5, 6, 7, 8, 9$. In particular, $U_{4,5,7,8}^{VIII}$ arise from $\Delta(54)$ with $(\varphi_1, \varphi_2) = (\frac{\pi}{3}, 0)$, while U_6^{VIII} and U_9^{VIII} arise from $\Delta(96)$ with $(\varphi_1, \varphi_2) = (\frac{\pi}{4}, 0)$, $(\frac{\pi}{4}, \frac{\pi}{4})$, and $(\frac{\pi}{4}, \frac{\pi}{2})$. We note that for $\varphi_2 = 0$, the mixing matrix in Eq. (4.14) becomes real, implying CP-conserving Dirac and Majorana phases. For IO, only U_6^{VIII} and U_9^{VIII} remain viable, both obtained from $\Delta(96)$ with $(\varphi_1, \varphi_2) = (\frac{\pi}{4}, \frac{\pi}{4})$ or $(\frac{\pi}{4}, \frac{\pi}{2})$. Thus the minimal $\Delta(6n^2)$ group that can generate viable mixing pattern U^{VIII} is $\Delta(54)$ with CP-conserving phases, and $\Delta(96)$ with CP-violating phases. Since the mixing pattern U^{VIII} can also originate from $D_n \times H_{CP}$ and the group order of D_n , namely $2n$, is smaller than that of $\Delta(6n^2)$, we further scan the D_n series up to $n \leq 8$. Beyond the viable solutions already found for $\Delta(6n^2)$ with $n = 3, 4$ and $\varphi_2 = 0, \frac{\pi}{2}$ that can also be obtained from D_n , we identify an additional 6 viable cases for NO and 1 for IO, as listed in table 6. The extra viable NO patterns include U_1^{VIII} with $(\varphi_1, \varphi_2) = (\frac{\pi}{5}, 0)$ or $(\frac{\pi}{5}, \frac{\pi}{2})$, U_4^{VIII} and U_7^{VIII} with $(\varphi_1, \varphi_2) = (\frac{2\pi}{5}, 0)$, and U_5^{VIII} and U_8^{VIII} with $(\varphi_1, \varphi_2) = (\frac{2\pi}{7}, 0)$. For IO, the additional viable case is U_1^{VIII} with $(\varphi_1, \varphi_2) = (\frac{2\pi}{5}, \frac{\pi}{2})$. For the case of $D_n \times H_{CP}$, the smallest D_n group capable of producing a viable U^{VIII} mixing pattern is D_3 , which predicts CP-conserving phases, whereas D_4 gives

$A_5 \times H_{CP}$										
Order	Case	$\theta_\ell^{\text{bf}}/\pi$	$\theta_\nu^{\text{bf}}/\pi$	χ_{min}^2	$\sin^2 \theta_{12}$	$\sin^2 \theta_{13}$	$\sin^2 \theta_{23}$	δ_{CP}/π	α_{21}/π (mod 1)	α_{31}/π (mod 1)
NO	U_1^{VI}	0.2623	0.2424	6.076	0.331	0.02209	0.470	1.484	0	0.969
	U_2^{VI}	0.6309	0.2424	4.258	0.331	0.02210	0.471	1	0	0
	$U_{3,2}^{VI}$	0.9717	0.3973	5.998	0.335	0.02213	0.542	1.157	0.082	0.050
	$U_{4,1}^{VI}$	0.0054	0.3986	9.952	0.322	0.02227	0.461	0	0	0
	$U_{4,2}^{VI}$	0.0107	0.3915	1.458	0.314	0.02219	0.556	1	0	0
	$U_{4,3}^{VI}$	0.3984	0.7962	8.575	0.306	0.02212	0.547	0	0	0
	$U_{4,4}^{VI}$	0.8372	0.4333	1.479	0.314	0.02217	0.459	1	0	0
	U_5^{VI}	0.4688	0.1028	5.725	0.335	0.02218	0.546	1.128	0.901	0.927
	$U_{6,1}^{VI}$	0.8407	0.5677	1.287	0.301	0.02217	0.480	1	0	0
	$U_{6,2}^{VI}$	0.5062	0.0872	10.326	0.315	0.02207	0.499	0	0	0
IO	U_1^{VI}	0.2294	0.2418	3.672	0.330	0.02243	0.550	1.526	0	0.052
	$U_{3,1}^{VI}$	0.9714	0.3977	15.911	0.335	0.02245	0.459	1.842*	0.917*	0.950*
	$U_{3,2}^{VI}$	0.0358	0.3921	11.428	0.338	0.02236	0.554	1.205*	0.102*	0.062*
	U_5^{VI}	0.5370	0.1057	12.969	0.336	0.02240	0.555	1.152*	0.882*	0.914*
$\Sigma(168) \times H_{CP}$										
Order	Case	$\theta_\ell^{\text{bf}}/\pi$	$\theta_\nu^{\text{bf}}/\pi$	χ_{min}^2	$\sin^2 \theta_{12}$	$\sin^2 \theta_{13}$	$\sin^2 \theta_{23}$	δ_{CP}/π	α_{21}/π (mod 1)	α_{31}/π (mod 1)
NO	$U_{1,1}^{VII}$	0.7307	0.3390	12.607	0.343	0.02235	0.563	1.700*	0.598*	0.253*
	$U_{2,1}^{VII}$	0.8112	0.2043	9.952	0.322	0.02227	0.461	0	0	0
	$U_{2,2}^{VII}$	0.0275	0.6463	1.460	0.314	0.02222	0.555	1	0	0
	$U_{2,3}^{VII}$	0.6396	0.2418	8.575	0.306	0.02212	0.547	0	0	0
	$U_{2,4}^{VII}$	0.6430	0.2390	1.479	0.314	0.02217	0.459	1	0	0
IO	$U_{1,1}^{VII}$	0.7302	0.3399	11.276	0.342	0.02251	0.565	1.697*	0.596*	0.252*
	$U_{1,2}^{VII}$	0.2682	0.6653	19.115	0.345	0.02261	0.445	1.278*	0.399*	0.744*

Table 5: The best-fit values of the free parameter and the corresponding lepton mixing observables for two-parameter mixing patterns from the $A_5 \times H_{CP}$ and $\Sigma(168) \times H_{CP}$ for both normal and inverted neutrino mass orderings. Here χ_{min}^2 the global minimum of the χ^2 function occurs at $(\theta_\ell, \theta_\nu) = (\theta_\ell^{\text{bf}}, \theta_\nu^{\text{bf}})$. The remaining conventions follow those used in table 4.

rise to nontrivial CPV phases.

We show in figure 5 the likelihood profiles of the lepton observables for all viable U^{VIII} mixing patterns with $\chi_{\text{min}}^2 \leq 9$. Regarding $\sin^2 \theta_{12}$, we find that U_1^{VIII} exhibits a very narrow allowed region. This behaviour originates from the correlation between $\sin^2 \theta_{12}$ and $\sin^2 \theta_{13}$ in Eq. (4.20). For $\varphi_1 = \frac{\pi}{5}$, the value of $\sin^2 \theta_{12}$ is tightly restricted around 0.331. Consequently, the pattern U_1^{VIII} is disfavoured by the current JUNO 59.1-day data at the 2σ level and may be excluded by the projected six-year JUNO precision. In contrast, the predictions for $\sin^2 \theta_{12}$ in the other viable patterns remain compatible with both the present and future JUNO sensitivities.

For U_6^{VIII} and U_9^{VIII} , the value of $\sin^2 \theta_{23}$ is also determined by $\sin^2 \theta_{13}$ via Eq. (4.20), leading to very narrow likelihood profiles. We suppose in the discussion that the current NuFIT best fit values of $\sin^2 \theta_{23}$ would not change visibly. We observe that U_4^{VIII} , U_8^{VIII} and U_9^{VIII} predict $\sin^2 \theta_{23} < 0.5$, which lies within the assumed future 3σ sensitivity of DUNE and T2HK for NO. In contrast, the patterns U_7^{VIII} , U_5^{VIII} and U_6^{VIII} which are obtained from U_4^{VIII} , U_8^{VIII} and U_9^{VIII} by exchanging the second and third rows—predict $\sin^2 \theta_{23} > 0.5$, and could therefore be incompatible with considered future DUNE and T2HK high precision data in the NO case. For IO, the predicted $\sin^2 \theta_{23}$ of U_9^{VIII} can be tested by the future DUNE and T2HK data while that of U_6^{VIII} remains within the projected 3σ ranges.

$\Delta(6n^2) \times H_{CP}$												
Order	Case	φ_1	φ_2	$\theta_\ell^{\text{bf}}/\pi$	$\theta_\nu^{\text{bf}}/\pi$	χ_{min}^2	$\sin^2 \theta_{12}$	$\sin^2 \theta_{13}$	$\sin^2 \theta_{23}$	δ_{CP}/π	α_{21}/π (mod 1)	α_{31}/π (mod 1)
NO	U_4^{VIII}	$\frac{\pi}{3}$	0	0.3893	0.2176	9.952	0.322	0.02227	0.461	0	0	0
	U_5^{VIII}	$\frac{\pi}{3}$	0	0.2178	0.1801	8.575	0.306	0.02212	0.547	0	0	0
	U_6^{VIII}	$\frac{\pi}{4}$	0	0.0676	0.3609	3.040	0.308	0.02223	0.511	1	0	0
		$\frac{\pi}{4}$	$\frac{\pi}{4}$	0.0676	0.3489	2.569	0.308	0.02223	0.511	1.214	0.853	0.891
	U_7^{VIII}	$\frac{\pi}{4}$	$\frac{\pi}{2}$	0.0676	0.6838	4.680	0.307	0.02223	0.511	1.458*	0.791*	0.854*
		$\frac{\pi}{3}$	0	0.6056	0.7756	1.460	0.314	0.02222	0.555	1	0	0
	U_8^{VIII}	$\frac{\pi}{3}$	0	0.7789	0.8171	1.479	0.314	0.02217	0.459	1	0	0
	U_9^{VIII}	$\frac{\pi}{4}$	0	0.9326	0.2648	1.660	0.308	0.02206	0.489	1	0	0
		$\frac{\pi}{4}$	$\frac{\pi}{4}$	0.9326	0.2798	1.564	0.308	0.02206	0.489	1.271	0.146	0.094
U_9^{VIII}	$\frac{\pi}{4}$	$\frac{\pi}{2}$	0.9327	0.3161	3.751	0.307	0.02205	0.489	1.541	0.209	0.146	
	U_6^{VIII}	$\frac{\pi}{4}$	$\frac{\pi}{4}$	0.9324	0.2798	6.045	0.307	0.02224	0.511	1.729*	0.853*	0.905*
$\frac{\pi}{4}$		$\frac{\pi}{2}$	0.9324	0.6840	3.186	0.308	0.02223	0.511	1.458	0.791	0.854	
$\frac{\pi}{4}$		$\frac{\pi}{4}$	0.9324	0.2799	5.740	0.307	0.02221	0.489	1.271	0.147	0.095	
U_9^{VIII}	$\frac{\pi}{4}$	$\frac{\pi}{4}$	0.9324	0.3160	2.602	0.308	0.02221	0.489	1.542	0.209	0.146	
	U_1^{VIII}	$\frac{\pi}{5}$	0	0.1929	0.4186	4.258	0.331	0.02210	0.471	1	0	0
U_1^{VIII}		$\frac{\pi}{5}$	$\frac{\pi}{2}$	0.7398	0.4186	6.204	0.331	0.02210	0.471	1.508*	0*	0.017*
	NO	U_4^{VIII}	$\frac{2\pi}{5}$	0	0.6645	0.7561	1.287	0.301	0.02217	0.480	1	0
U_5^{VIII}		$\frac{2\pi}{7}$	0	0.2467	0.1176	1.271	0.306	0.02219	0.544	1	0	0
U_7^{VIII}		$\frac{2\pi}{5}$	0	0.6702	0.7636	10.328	0.315	0.02209	0.498	0	0	0
U_8^{VIII}		$\frac{2\pi}{7}$	0	0.2499	0.1203	8.719	0.312	0.02212	0.460	0	0	0
IO	U_1^{VIII}	$\frac{\pi}{5}$	$\frac{\pi}{2}$	0.7676	0.4183	3.721	0.331	0.02226	0.550	1.486*	0*	0.971*

$D_n \times H_{CP}$												
Order	Case	φ_1	φ_2	$\theta_\ell^{\text{bf}}/\pi$	$\theta_\nu^{\text{bf}}/\pi$	χ_{min}^2	$\sin^2 \theta_{12}$	$\sin^2 \theta_{13}$	$\sin^2 \theta_{23}$	δ_{CP}/π	α_{21}/π (mod 1)	α_{31}/π (mod 1)
NO	U_1^{VIII}	$\frac{\pi}{5}$	0	0.1929	0.4186	4.258	0.331	0.02210	0.471	1	0	0
		$\frac{\pi}{5}$	$\frac{\pi}{2}$	0.7398	0.4186	6.204	0.331	0.02210	0.471	1.508*	0*	0.017*
	U_4^{VIII}	$\frac{2\pi}{5}$	0	0.6645	0.7561	1.287	0.301	0.02217	0.480	1	0	0
	U_5^{VIII}	$\frac{2\pi}{7}$	0	0.2467	0.1176	1.271	0.306	0.02219	0.544	1	0	0
	U_7^{VIII}	$\frac{2\pi}{5}$	0	0.6702	0.7636	10.328	0.315	0.02209	0.498	0	0	0
U_8^{VIII}	$\frac{2\pi}{7}$	0	0.2499	0.1203	8.719	0.312	0.02212	0.460	0	0	0	
IO	U_1^{VIII}	$\frac{\pi}{5}$	$\frac{\pi}{2}$	0.7676	0.4183	3.721	0.331	0.02226	0.550	1.486*	0*	0.971*

Table 6: The best-fit values of the free parameter and the corresponding lepton mixing observables for two-parameter mixing patterns U^{VIII} originate from $\Delta(6n^2) \times H_{CP}$ with $n \leq 4$ and from $D_n \times H_{CP}$ with $n \leq 8$. The discrete parameters (φ_1, φ_2) specify the residual symmetries associated with flavour groups $\Delta(6n^2)$ and D_n . Here χ_{min}^2 the global minimum of the χ^2 function occurs at $(\theta_\ell, \theta_\nu) = (\theta_\ell^{\text{bf}}, \theta_\nu^{\text{bf}})$. The remaining conventions follow those used in table 4.

The Dirac CPV phase δ_{CP} is strongly constrained in the U^{VIII} patterns. For NO, only U_6^{VIII} and U_9^{VIII} with $(\varphi_1, \varphi_2) = (\frac{\pi}{4}, \frac{\pi}{4})$ might survive the future high precision tests of their predictions for δ_{CP} . For IO, the patterns that could be compatible with the future DUNE and T2HK high precision data on δ_{CP} are U_6^{VIII} and U_9^{VIII} with $(\varphi_1, \varphi_2) = (\frac{\pi}{4}, \frac{\pi}{2})$, as well as U_1^{VIII} with $(\varphi_1, \varphi_2) = (\frac{\pi}{5}, \frac{\pi}{2})$. The preceding discussion should be considered as indicative only since at present it is impossible to foresee the results of the experimental determination of the Dirac CPV phase δ_{CP} .

The second two-parameter mixing pattern obtained from $\Delta(6n^2) \times H_{CP}$ is denoted by U^{IX} . As shown in Eq. (4.26), four distinct realizations arise from different permutations of rows and columns. The χ^2 -minimization results for $U_{1,2,3,4}^{IX}$ are summarized in table 7. There are in total 16 and 11 viable cases for NO and IO respectively. The smallest $\Delta(6n^2)$ group that can reproduce the experimental data is S_4 ($n = 2$). In this case, all four mixing patterns $U_{1,2,3,4}^{IX}$ accommodate the NuFIT results for NO with $(\varphi_1, \varphi_2) = (0, 0)$, and the CPV phases are CP-conserving because the PMNS matrix is real.

The next group capable of explaining the data is $\Delta(96)$ ($n = 4$). For this group, the patterns U_1^{IX} and U_3^{IX} with $(\varphi_1, \varphi_2) = (\frac{\pi}{4}, \frac{\pi}{2})$ are viable for both NO and IO. When $(\varphi_1, \varphi_2) = (0, \frac{\pi}{4})$, the pattern U_3^{IX} is viable for both NO and IO, whereas U_1^{IX} is viable only for NO. For U_2^{IX} and U_4^{IX} , agreement with the NuFIT data can be achieved for both mass orderings when (φ_1, φ_2) takes one of the values $(0, \frac{\pi}{4})$, $(\frac{\pi}{4}, 0)$, $(\frac{\pi}{4}, \frac{\pi}{4})$, or $(\frac{\pi}{4}, \frac{\pi}{2})$. The corresponding allowed regions of the lepton mixing observables are summarized in table 12.

In figure 6, we show the predicted likelihood profile for case U^{IX} with $\chi_{\text{min}}^2 \leq 9$. We find

$\Delta(6n^2) \times H_{CP}$ (Case IX)												
Order	Case	φ_1	φ_2	$\theta_\ell^{\text{bf}}/\pi$	$\theta_\nu^{\text{bf}}/\pi$	χ_{min}^2	$\sin^2 \theta_{12}$	$\sin^2 \theta_{13}$	$\sin^2 \theta_{23}$	δ_{CP}/π	α_{21}/π (mod 1)	α_{31}/π (mod 1)
NO	U_1^{IX}	0	0	0.0852	0.0217	9.952	0.322	0.02227	0.461	0	0	0
		0	$\frac{\pi}{4}$	0.0833	0.0308	8.442	0.325	0.02225	0.460	1.922	0.014	0.507
		$\frac{\pi}{4}$	$\frac{\pi}{2}$	0.1666	0.1461	8.981	0.331	0.02221	0.461	1.876*	0.546*	0.746*
	U_2^{IX}	0	0	0.4782	0.6240	8.576	0.306	0.02212	0.547	0	0	0
		0	$\frac{\pi}{4}$	0.9131	0.9724	5.573	0.305	0.02210	0.553	1.891	0.991	0.491
		$\frac{\pi}{4}$	0	0.4675	0.6258	5.365	0.310	0.02213	0.551	1.882*	0.926*	0.954*
		$\frac{\pi}{4}$	$\frac{\pi}{4}$	0.8892	0.9629	6.028	0.318	0.02221	0.567	1.756*	0.767*	0.358*
		$\frac{\pi}{2}$	$\frac{\pi}{4}$	0.6558	0.6776	4.784	0.312	0.02214	0.557	1.827	0.121	0.395
	U_3^{IX}	0	0	0.3015	0.5797	1.460	0.314	0.02222	0.555	1	0	0
		0	$\frac{\pi}{4}$	0.0873	0.0407	2.062	0.319	0.02224	0.557	1.101*	0.980*	0.489*
		$\frac{\pi}{4}$	$\frac{\pi}{2}$	0.1816	0.1613	4.269	0.331	0.02216	0.549	1.154	0.503	0.287
	U_4^{IX}	0	0	0.4746	0.6210	1.477	0.315	0.02219	0.460	1	0	0
		0	$\frac{\pi}{4}$	0.9182	0.9808	2.014	0.317	0.02217	0.459	1.075*	0.006*	0.506*
		$\frac{\pi}{4}$	0	0.4638	0.6242	2.617	0.317	0.02226	0.453	1.131	0.082	0.050
		$\frac{\pi}{4}$	$\frac{\pi}{4}$	0.8962	0.9688	9.628	0.330	0.02228	0.441	1.247	0.217	0.630
		$\frac{\pi}{2}$	$\frac{\pi}{4}$	0.6469	0.6762	4.438	0.306	0.02221	0.445	1.133*	0.852*	0.588*
IO	U_1^{IX}	$\frac{\pi}{4}$	$\frac{\pi}{2}$	0.1746	0.1537	15.915	0.330	0.02245	0.456	1.859*	0.520*	0.729*
		0	$\frac{\pi}{4}$	0.9112	0.9694	10.878	0.301	0.02222	0.558	1.879	0.990	0.490
	U_2^{IX}	$\frac{\pi}{4}$	0	0.4645	0.6245	10.208	0.315	0.02227	0.548	1.872*	0.920*	0.951*
		$\frac{\pi}{4}$	$\frac{\pi}{4}$	0.8897	0.9635	6.488	0.319	0.02233	0.566	1.756*	0.769*	0.359*
		$\frac{\pi}{2}$	$\frac{\pi}{4}$	0.6676	0.6802	6.548	0.320	0.02231	0.561	1.775	0.085	0.373
	U_3^{IX}	0	$\frac{\pi}{4}$	0.0880	0.0419	10.942	0.318	0.02240	0.559	1.104*	0.980*	0.488*
		$\frac{\pi}{4}$	$\frac{\pi}{2}$	0.1938	0.1722	10.368	0.332	0.02244	0.556	1.185	0.541	0.313
	U_4^{IX}	0	$\frac{\pi}{4}$	0.9160	0.9778	14.432	0.312	0.02234	0.454	1.086*	0.007*	0.507*
		$\frac{\pi}{4}$	0	0.4616	0.6233	12.699	0.321	0.02234	0.455	1.139	0.086	0.053
		$\frac{\pi}{4}$	$\frac{\pi}{4}$	0.8968	0.9695	15.468	0.331	0.02241	0.442	1.247	0.215	0.629
		$\frac{\pi}{2}$	$\frac{\pi}{4}$	0.6572	0.6775	13.819	0.313	0.02241	0.443	1.181*	0.884*	0.607*
	$\Delta(6n^2) \times H_{CP}$ (Case X)											
Order	Case	φ_1	φ_2	$\theta_\ell^{\text{bf}}/\pi$	$\theta_\nu^{\text{bf}}/\pi$	χ_{min}^2	$\sin^2 \theta_{12}$	$\sin^2 \theta_{13}$	$\sin^2 \theta_{23}$	δ_{CP}/π	α_{21}/π (mod 1)	α_{31}/π (mod 1)
NO	U_1^X	0	0	0.0676	0.6391	3.040	0.308	0.02223	0.511	1	0	0
		$\frac{\pi}{4}$	0	0.0676	0.6511	2.569	0.308	0.02223	0.511	1.214	0.853	0.891
	U_2^X	0	0	0.9326	0.7352	1.660	0.308	0.02206	0.489	1	0	0
		$\frac{\pi}{4}$	0	0.9326	0.7202	1.564	0.308	0.02206	0.489	1.271	0.146	0.094
IO	U_1^X	$\frac{\pi}{4}$	0	0.9324	0.7202	6.045	0.307	0.02224	0.511	1.729*	0.853*	0.905*
	U_2^X	$\frac{\pi}{4}$	0	0.9324	0.7201	5.740	0.307	0.02221	0.489	1.271	0.147	0.095

Table 7: The best-fit values of the free parameter and the corresponding lepton mixing observables for two-parameter mixing patterns U^{IX} and U^X originate from $\Delta(6n^2) \times H_{CP}$ with $n \leq 4$. The discrete parameters (φ_1, φ_2) specify the residual symmetries associated with flavour groups $\Delta(6n^2)$. Here χ_{min}^2 the global minimum of the χ^2 function occurs at $(\theta_\ell, \theta_\nu) = (\theta_\ell^{\text{bf}}, \theta_\nu^{\text{bf}})$. The remaining conventions follow those used in table 4.

that all selected viable patterns are compatible with the current JUNO 59.1-day data for both NO and IO. The cases U_1^{IX} and U_3^{IX} with $(\varphi_1, \varphi_2) = (\frac{\pi}{4}, \frac{\pi}{2})$ will be most likely excluded by the projected six-year JUNO precision for NO. From the plots of $\sin^2 \theta_{23}$, we can conclude that cases U_1^{IX} and U_4^{IX} predict $\sin^2 \theta_{23} < 0.5$, while U_2^{IX} and U_3^{IX} predict $\sin^2 \theta_{23} > 0.5$, which means the latter cases can be tested by future DUNE and T2HK results for NO, and vice versa for IO. For δ_{CP} , cases U_1^{IX} and U_2^{IX} may be tested by the assumed prospective future DUNE and T2HK results for both NO and IO.

The numerical analysis for the pattern U^X is summarized in table 7. Unlike U^{IX} , only 4 NO and 2 IO realizations are viable. As in the previous case, the smallest group capable of accommodating the data is S_4 ($n = 2$), where the realizations $U_{1,2}^X$ with $(\varphi_1, \varphi_2) = (0, 0)$ imply CP conservation due to the reality of the PMNS matrix. Moving to the next viable

group, $\Delta(96)$ ($n = 4$), both U_1^X and U_2^X become viable when $(\varphi_1, \varphi_2) = (\frac{\pi}{4}, 0)$. Figure 7 illustrates the corresponding likelihood profiles. Owing to the sum rule in Eq. (4.32), the atmospheric angle in U_1^X and U_2^X is tightly correlated with $\sin^2 \theta_{13}$, yielding sharply peaked distributions for $\sin^2 \theta_{23}$. Anticipated sensitivities from DUNE and T2HK will be sufficient to exclude U_1^X for NO and U_2^X for IO. For the Dirac phase, only the configuration U_1^X with $(\varphi_1, \varphi_2) = (\frac{\pi}{4}, 0)$ remain potentially compatible with the considered prospective future long-baseline data in the NO scenario, while the remaining options in both mass orderings are expected to be disfavored.

Based on the numerical analysis above, we conclude that almost all two-parameter mixing patterns remain compatible with the current oscillation data, even when the JUNO 59.1-day measurement of $\sin^2 \theta_{12}$ is taken into account. The discrimination among these patterns will rely on future long-baseline measurements of $\sin^2 \theta_{23}$ and δ_{CP} . For the mixing patterns originating from $A_5 \rtimes H_{CP}$, the mixing matrix $U_{6,1}^{VI}$, featuring a fixed (21) entry of $\frac{1}{2\phi_g}$, achieves the best fit for NO data but exhibits CP-conserving phases. The pattern U_1^{VI} , with a fixed (11) entry of $\frac{\phi_g}{2}$, provides a good fit to the experimental data for both NO and IO and predicts non-trivial CP-violating Dirac and Majorana phases. For the patterns U^{VII} arising from $\Sigma(168) \rtimes H_{CP}$, the fixed entry is $\frac{1}{2}$, and the minimal χ_{\min}^2 among different permutations is obtained for $U_{2,2}^{VII}$. Regarding the three distinct patterns U^{VIII} , U^{IX} , and U^X , with fixed entries $\cos \varphi_1$, $\frac{1}{2}$ and $\frac{1}{\sqrt{2}}$, respectively, which originate from $\Delta(6n^2) \rtimes H_{CP}$, the minimal viable groups for the case of CP-conserving phases are $\Delta(54)$, S_4 and S_4 , respectively. To accommodate CP-violating δ_{CP} , the group $\Delta(96)$ is required, allowing all three patterns to fit the experimental data. Furthermore, the D_3 and D_4 groups, which are the symmetry groups of equilateral triangle and square respectively, can also be employed to generate CP-conserved and CP-violating viable realizations of U^{VIII} , respectively. It is notable that the group order is drastically reduced with respect to $\Delta(54)$ and $\Delta(96)$. Notice that the flavor group D_5 can generate the viable mixing matrix U_1^{VIII} with the fixed (11) entry $\cos(\pi/5)$, leading to $\sin^2 \theta_{12}$ tightly constrained around 0.331 as dictated by Eq. (4.7). This region is consistent with the current JUNO data, but lies near the upper bound and will be subject to further scrutiny with improved JUNO precision.

6 Summary and conclusion

We have carried out a comprehensive assessment of the phenomenological viability of the discrete lepton flavour groups A_5 , $\Sigma(168)$ and the series $\Delta(6n^2)$ combined with gCP symmetry. The full symmetry groups $A_5 \rtimes H_{CP}$, $\Sigma(168) \rtimes H_{CP}$, and $\Delta(6n^2) \rtimes H_{CP}$ are broken to non-trivial residual subgroups $\mathcal{G}_\ell = G_\ell \rtimes H_{CP}^\ell$ and $\mathcal{G}_\nu = G_\nu \times H_{CP}^\nu$ in the charged lepton and neutrino sectors, respectively. The PMNS matrix is completely determined by these residual symmetries, no assumptions about the underlying dynamical origin of symmetry breaking are required. Note that if the residual flavour symmetry G_ℓ distinguishes the three families, the inclusion of gCP symmetry H_{CP}^ℓ would not add any information as far as lepton mixing is concerned [51, 52].

We classify all viable symmetry-breaking schemes into two categories:

- (i) $\mathcal{G}_\ell = Z_n$ ($n \geq 3$) or K_4 and $\mathcal{G}_\nu = Z_2 \times H_{CP}^\nu$;
- (ii) $\mathcal{G}_\ell = Z_2 \times H_{CP}^\ell$ and $\mathcal{G}_\nu = Z_2 \times H_{CP}^\nu$.

Assuming that the three lepton doublets transform as a faithful triplet of the flavour group, we systematically analyze all possible residual symmetries and the resulting predictions for the lepton mixing matrix. These two classes of breaking patterns lead to qualitatively

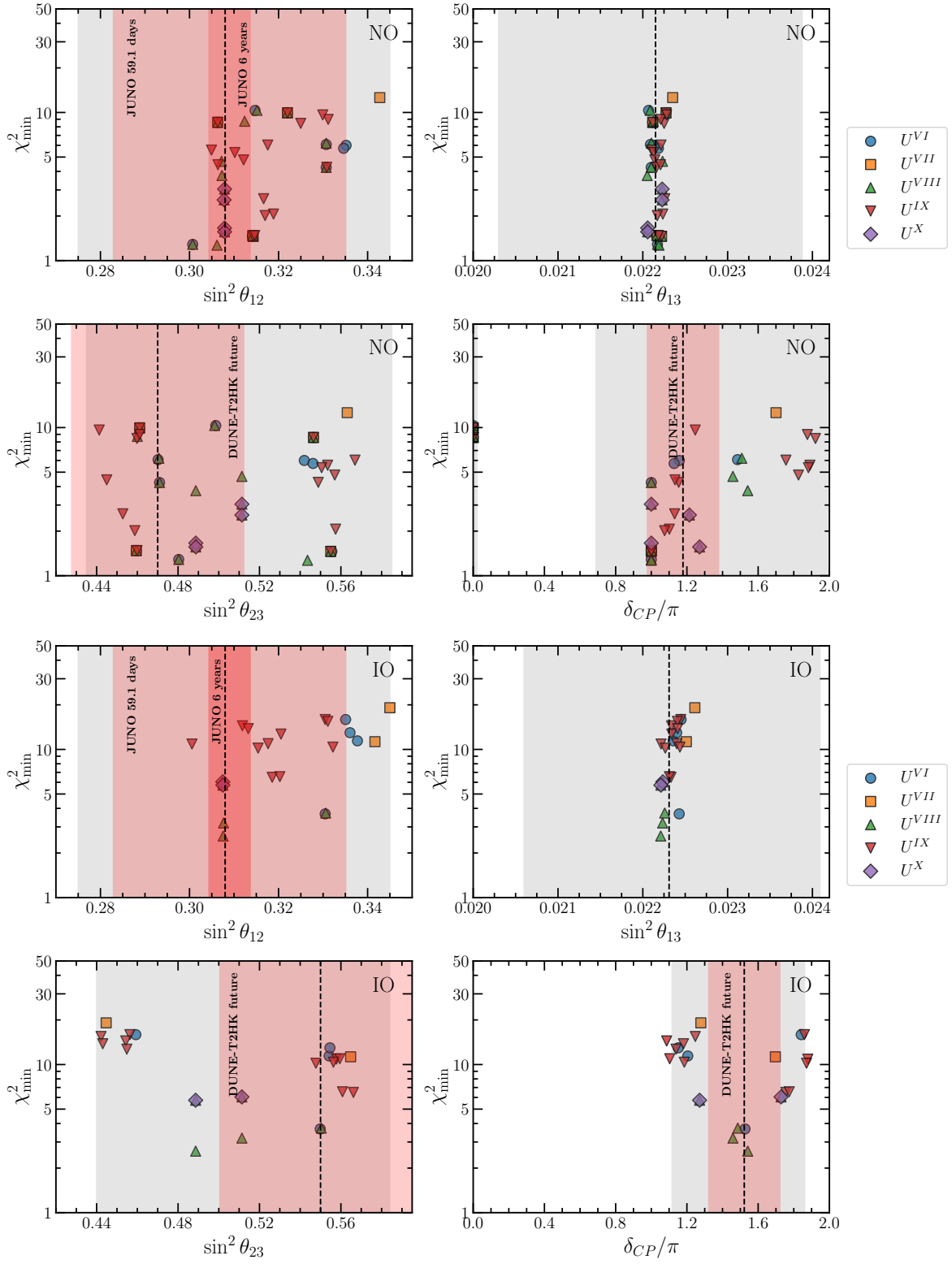


Figure 3: Best-fit predictions of the neutrino mixing angles θ_{12} , θ_{13} , θ_{23} and the Dirac CPV phase δ_{CP} for lepton mixing patterns with two parameter in case of NO and IO neutrino masses spectra. The remaining conventions follow those used in figure 1.

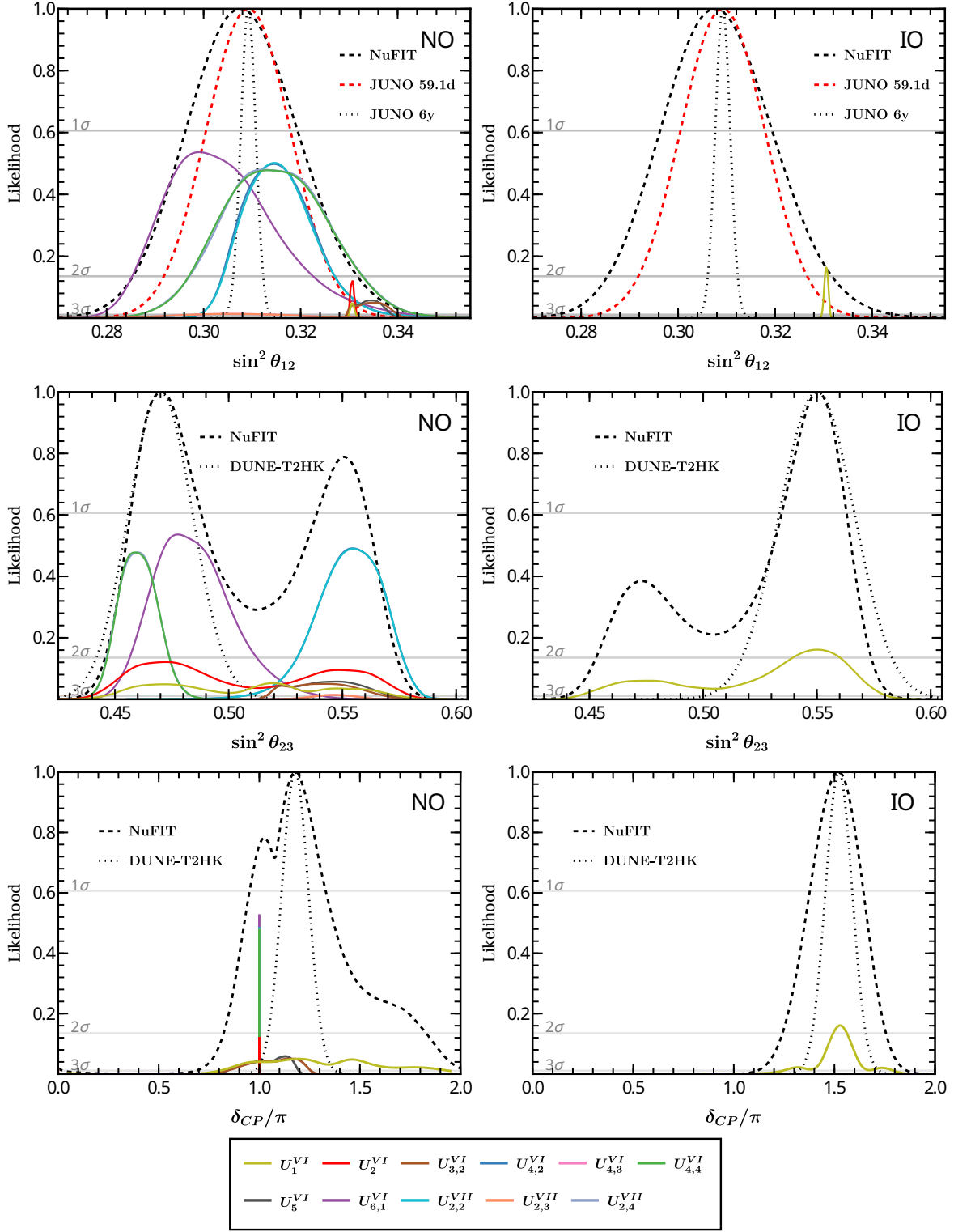


Figure 4: The predictions of likelihood profiles for $\sin^2 \theta_{12}$, $\sin^2 \theta_{23}$ and δ_{CP} obtained using the current global data on the neutrino mixing parameters for two-parameter mixing patterns that originate from $A_5 \times H_{CP}$ and $\Sigma(168) \times H_{CP}$. The remaining conventions follow those used in figure 2.

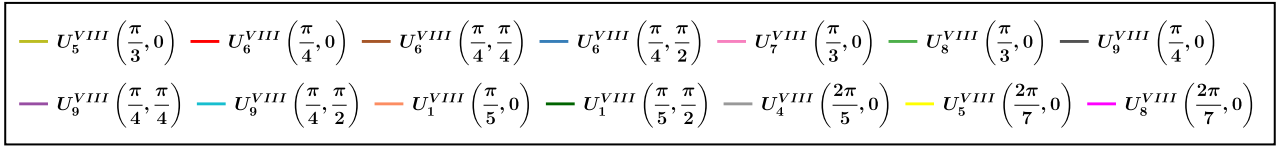
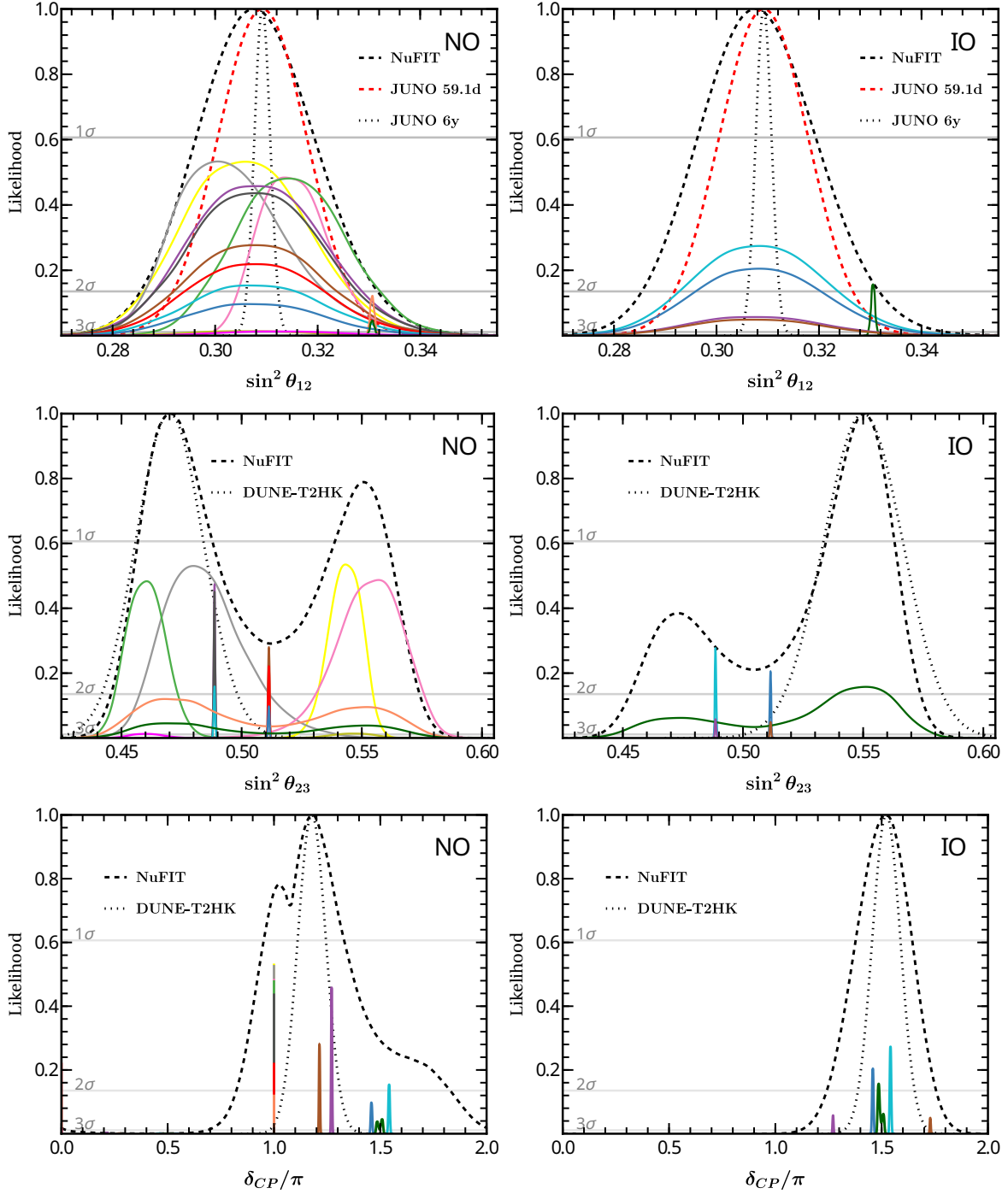


Figure 5: The predictions of likelihood profiles for $\sin^2 \theta_{12}$, $\sin^2 \theta_{23}$ and δ_{CP} obtained using the current global data on the neutrino mixing parameters for two-parameter mixing patterns U^{VIII} that originate from $\Delta(6n^2) \times H_{CP}$ and $D_n \times H_{CP}$. The remaining conventions follow those used in figure 2.

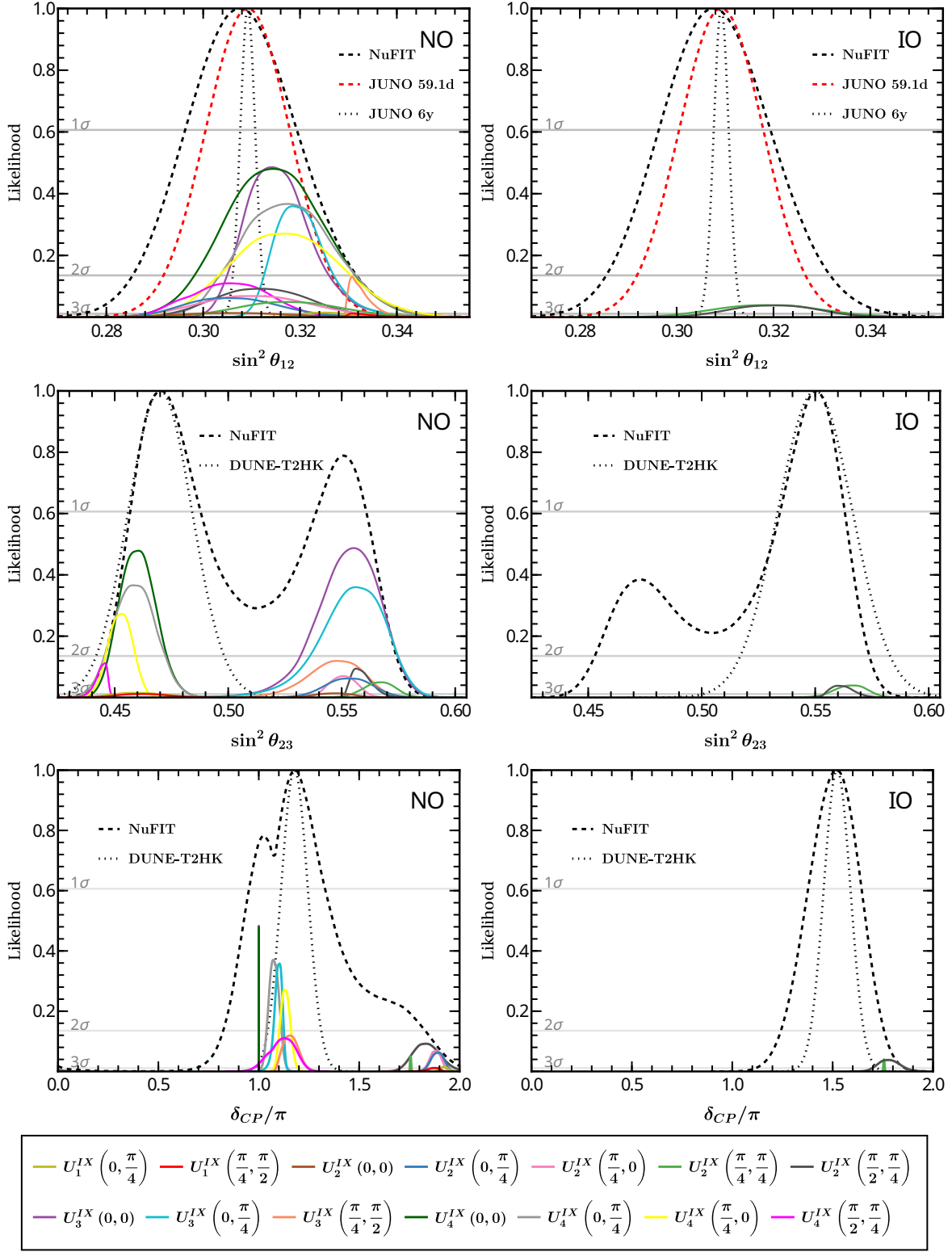


Figure 6: The predictions of likelihood profiles for $\sin^2 \theta_{12}$, $\sin^2 \theta_{23}$ and δ_{CP} obtained using the current global data on the neutrino mixing parameters for two-parameter mixing patterns U^{IX} that originate from $\Delta(6n^2) \times H_{CP}$. The remaining conventions follow those used in figure 2.

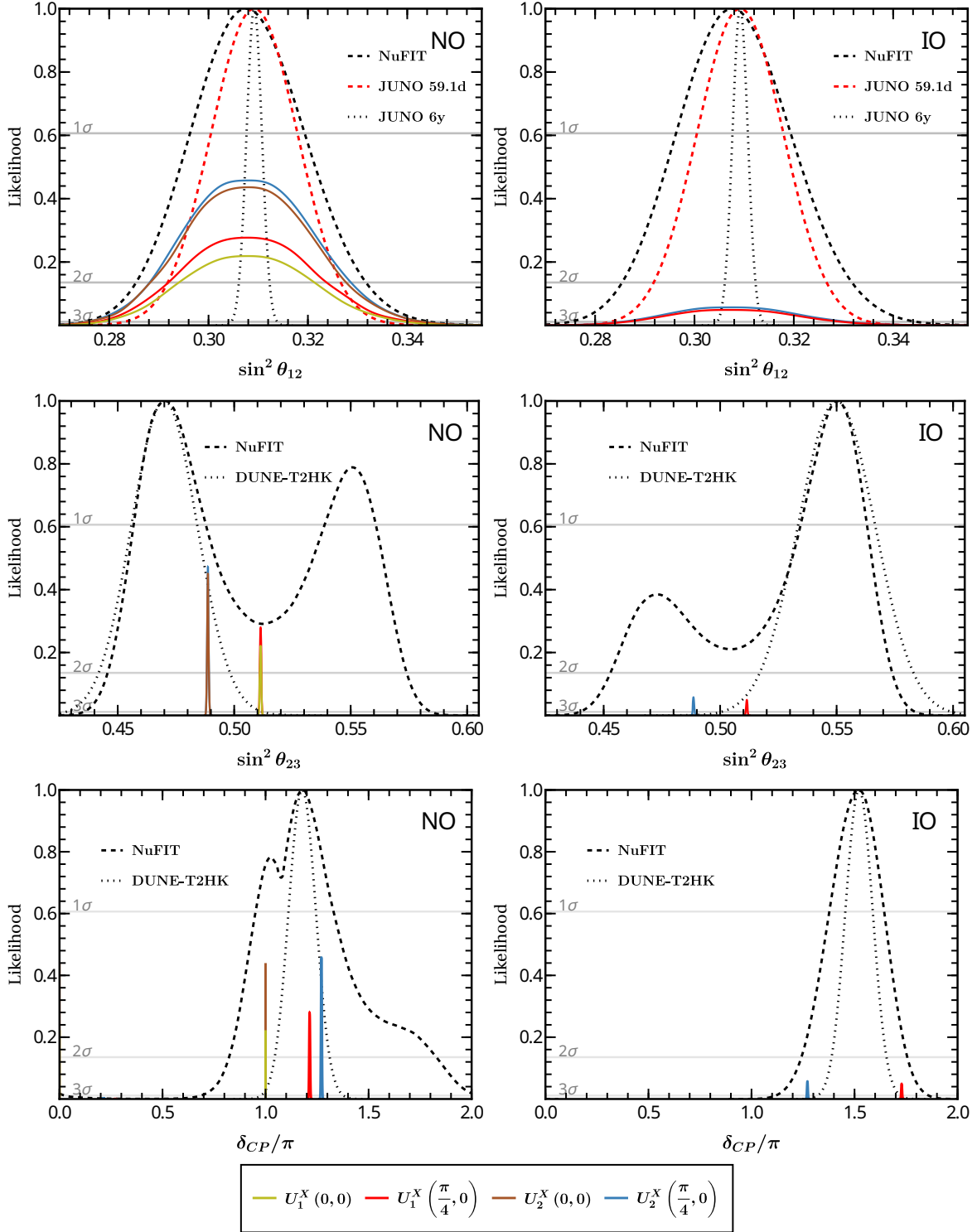


Figure 7: The predictions of likelihood profiles for $\sin^2 \theta_{12}$, $\sin^2 \theta_{23}$ and δ_{CP} obtained using the current global data on the neutrino mixing parameters for two-parameter mixing patterns U^X that originate from $\Delta(6n^2) \times H_{CP}$. The remaining conventions follow those used in figure 2.

different parametric structures of the PMNS matrix. Under pattern (i), the PMNS matrix depends on a single real parameter $\theta \in [0, \pi)$ and one of its columns is completely fixed. Under pattern (ii), the PMNS matrix depends on two real parameters $(\theta_\ell, \theta_\nu)$ in $[0, \pi)$ and one matrix element is fixed. A third possibility, with $\mathcal{G}_\ell = Z_2$ and $\mathcal{G}_\nu = K_4 \times H_{CP}^\nu$, also yields a two-parameter mixing matrix but with one row fixed. This option is incompatible with the NuFIT data and is therefore discarded; see Appendix C.

First of all, we performed a statistical test of the sum-rule predictions among the mixing angles for all patterns obtained in approaches (i) and (ii), using the latest global neutrino oscillation data from NuFIT-v6.0 [6]. Our analysis selects the mixing patterns whose predictions satisfy the following requirement: the three lepton mixing angles $(\theta_{13}, \theta_{12}, \theta_{23})$ and the Dirac CPV phase δ_{CP} must all lie within their experimentally allowed 3σ ranges [6]. In approach (i), all mixing patterns that remain consistent with the measured mixing angles and the δ_{CP} at the 3σ level [6] can be classified into 5 distinct cases, up to permutations of rows and columns. The corresponding mixing matrices are

$$\begin{aligned}
U^I &= \frac{1}{\sqrt{3}} \begin{pmatrix} \sqrt{2} \sin \varphi_1 & e^{i\varphi_2} & \sqrt{2} \cos \varphi_1 \\ \sqrt{2} \cos(\varphi_1 - \frac{\pi}{6}) & -e^{i\varphi_2} & -\sqrt{2} \sin(\varphi_1 - \frac{\pi}{6}) \\ \sqrt{2} \cos(\varphi_1 + \frac{\pi}{6}) & e^{i\varphi_2} & -\sqrt{2} \sin(\varphi_1 + \frac{\pi}{6}) \end{pmatrix} R_{23}(\theta) Q_\nu, \\
U^{II} &= \frac{1}{\sqrt{3}} \begin{pmatrix} e^{i\varphi_1} & 1 & e^{i\varphi_2} \\ \omega e^{i\varphi_1} & 1 & \omega^2 e^{i\varphi_2} \\ \omega^2 e^{i\varphi_1} & 1 & \omega e^{i\varphi_2} \end{pmatrix} R_{13}(\theta) Q_\nu, \\
U^{III} &= \begin{pmatrix} -i\sqrt{\frac{\phi_g}{\sqrt{5}}} & \sqrt{\frac{1}{\sqrt{5}\phi_g}} & 0 \\ i\sqrt{\frac{1}{2\sqrt{5}\phi_g}} & \sqrt{\frac{\phi_g}{2\sqrt{5}}} & -\frac{1}{\sqrt{2}} \\ i\sqrt{\frac{1}{2\sqrt{5}\phi_g}} & \sqrt{\frac{\phi_g}{2\sqrt{5}}} & \frac{1}{\sqrt{2}} \end{pmatrix} R_{13}(\theta) Q_\nu, \\
U^{IV} &= \frac{1}{2} \begin{pmatrix} \phi_g & 1 & \phi_g - 1 \\ \phi_g - 1 & -\phi_g & 1 \\ 1 & 1 - \phi_g & -\phi_g \end{pmatrix} R_{23}(\theta) Q_\nu, \\
U^V &= \frac{1}{2\sqrt{3}} \begin{pmatrix} \sqrt{3} - 1 & 2e^{-i\varphi} & -(\sqrt{3} + 1)e^{\frac{3\pi i}{4}} \\ -\sqrt{3} - 1 & 2e^{-i\varphi} & (\sqrt{3} - 1)e^{\frac{3\pi i}{4}} \\ 2 & 2e^{-i\varphi} & 2e^{\frac{3\pi i}{4}} \end{pmatrix} R_{13}(\theta) Q_\nu. \tag{6.1}
\end{aligned}$$

Notably, U^I and U^{II} arise from the breaking of $\Delta(6n^2)$ flavour symmetries combined with CP. Furthermore, U^{II} can also be realized by breaking $\Delta(3n^2) \times H_{CP}$ [78] if nontrivial singlets are absent from the model. The mixing matrices U^{III} and U^{IV} are minimally realized using the alternating group A_5 combined with CP symmetry, while U^V is reproduced by the flavour symmetry group $\Sigma(168) \times H_{CP}$. In the breaking approach (ii), our statistical analysis identifies 11 viable breaking patterns. Among them, six arise from the breaking of $A_5 \times H_{CP}$, yielding the PMNS matrices U_i^{VI} with $i = 1, \dots, 6$ in Eq. (4.6). Two additional patterns originate from $\Sigma(168) \times H_{CP}$, corresponding to U_1^{VII} and U_2^{VII} in Eq. (4.12). The remaining three patterns stem from $\Delta(6n^2) \times H_{CP}$ and lead to the mixing matrices U^{VIII} , U^{IX} , and U^X , shown in Eq. (4.14), Eq. (4.23), and Eq. (4.27), respectively. Furthermore, when the left-handed lepton doublets transform as a direct sum of a singlet and a doublet, the mixing matrix U^{VIII} in Eq. (4.14) can also be realized through the breaking of the dihedral group D_n combined with generalized CP symmetry. We summarize the fixed columns for the one-parameter mixing patterns U^I , U^{II} , U^{III} , U^{IV} and U^V , and the fixed entries for the two-parameter mixing patterns U^{VI} , U^{VII} , U^{VIII} , U^{IX} and U^X in table 8.

In order to further quantitatively assess how well a viable breaking pattern can describe

Case	Fixed column	Case	Fixed entry
U^I	$\sqrt{\frac{2}{3}} (\sin \varphi_1, \cos(\varphi_1 - \frac{\pi}{6}), \cos(\varphi_1 + \frac{\pi}{6}))^T$	U^{VI}	$\frac{\phi_g}{2}, \frac{1}{2}, \frac{1}{2\phi_g}$
U^{II}	$\frac{1}{\sqrt{3}} (1, 1, 1)^T$	U^{VII}	$\frac{1}{2}$
U^{III}	$\left(\sqrt{\frac{1}{\sqrt{5}\phi_g}}, \sqrt{\frac{\phi_g}{2\sqrt{5}}}, \sqrt{\frac{\phi_g}{2\sqrt{5}}} \right)^T$	U^{VIII}	$\cos \varphi_1$
U^{IV}	$\frac{1}{2} (\phi_g, \phi_g - 1, 1)^T$	U^{IX}	$\frac{1}{2}$
U^V	$\frac{1}{\sqrt{3}} (1, 1, 1)^T$	U^X	$\frac{1}{\sqrt{2}}$

Table 8: The fixed columns for the one-parameter mixing patterns U^I , U^{II} , U^{III} , U^{IV} and U^V , and the fixed entries for the two-parameter mixing patterns U^{VI} , U^{VII} , U^{VIII} , U^{IX} and U^X . Here $\phi_g = (\sqrt{5} + 1)/2$ is the golden ratio, and the parameter φ_1 in U^I and U^{VIII} takes the forms given in Eq. (3.5) and Eq. (4.16), respectively.

the current experiment data (NuFIT and JUNO 59.1-day results), we perform a parameter scan and compute the minimum χ^2 (defined in Eq. (5.1)) value for those one- and two-parameter mixing patterns. This analysis is restricted to mixing patterns arising from $\Delta(6n^2) \rtimes H_{CP}$ with $n \leq 4$ and from $D_n \rtimes H_{CP}$ with $n \leq 8$. The best-fit values of input parameter and mixing parameters for mixing patterns with one input parameter for both NO and IO cases are shown in table 4. The best-fit values of input parameters and mixing parameters for mixing patterns with two input parameters arise from $A_5 \rtimes H_{CP}$, $\Sigma(168) \rtimes H_{CP}$, $\Delta(6n^2) \rtimes H_{CP}$ and $D_n \rtimes H_{CP}$ are shown in tables 5, 6 and 7. We scanned the parameter spaces of each mixing matrix to identify viable ranges consistent with neutrino oscillation data at the 3σ level. This procedure yielded predictions for lepton mixing parameters with the results detailed in tables 9, 10, 11 and 12. Furthermore, we can pin down the minimal value of χ_{\min}^2 for each mixing matrix relevant to the mixing angles and the Dirac CPV phase. The results for mixing patterns with one and two free parameters are shown in figures 1 and 3, respectively. We then assessed the robustness of these predictions under future experimental conditions. This assessment assumed that: (1) the current best-fit values for the mixing angles remain unchanged, and (2) the relative 1σ uncertainties on $\sin^2 \theta_{12}$, $\sin^2 \theta_{23}$ and δ_{CP} are scaled to 0.5%, 3% and 12° of their current best-fit values, respectively. These projected uncertainties, corresponding to 6 years of JUNO [31] data and 15 years of DUNE [92] and T2HK [93] data, are visualized in figures 2, 4, 5, 6 and 7 in which the likelihood profiles for $\sin^2 \theta_{12}$, $\sin^2 \theta_{23}$ and δ_{CP} are displayed for selected viable patterns with $\chi_{\min}^2 \leq 9$.

For the one-parameter mixing patterns, all five candidates are capable of accommodating the current NuFIT data and yield sharply constrained predictions for the lepton mixing parameters in both the NO and IO neutrino mass spectra. The only exceptions are U_1^{IV} and U_2^{IV} , whose predictions imply a CP-conserving Dirac phase δ_{CP} ; these remain compatible with the NuFIT constraints only in the NO case. The smallest $\Delta(6n^2)$ group that can realize the viable patterns U^I and U^{II} is $\Delta(24) \cong S_4$ with $n = 2$. We note that the minimal group capable of generating U^{II} is A_4 if the nontrivial singlet representations are absent from the model [61]. For $n = 2$, the choice $(\varphi_1, \varphi_2) = (-\frac{\pi}{2}, \frac{\pi}{2})$ reduces U^I to the well-known TM1 mixing form. The recent JUNO 59.1-day results further sharpen these constraints. At the 3σ level, the viable parameter space of one-parameter patterns is significantly reduced. In the NO case, only TM1 mixing (U^I) and the patterns U_1^{IV} (U_2^{IV}), which feature fixed columns $(\phi_g, \phi_g - 1, 1)^T/2$ ($(\phi_g, 1, \phi_g - 1)^T/2$), remain compatible after incorporating the JUNO likelihood, as shown in figure 2. For the IO spectrum, U^I (TM1) is the sole surviving option. Mixing patterns such as U^{II} (TM2), U^{III} (GR2), and U^V (TM2) are disfavored once the current JUNO constraint on $\sin^2 \theta_{12}$ is taken into account. We note that, for the mixing pattern U^I , higher values of n in $\Delta(6n^2)$ admit additional viable textures—beyond

the TM1 form—that are consistent with current JUNO data. Looking into the future, the full set of one-parameter patterns is expected to come under decisive scrutiny: the projected precision of JUNO on $\sin^2 \theta_{12}$, together with forthcoming measurements of $\sin^2 \theta_{23}$ and δ_{CP} from DUNE and T2HK, will provide a definitive test of these scenarios.

Nearly all two-parameter neutrino mixing patterns remain consistent with current NuFIT data and JUNO 59.1-day measurement of $\sin^2 \theta_{12}$. Moreover, future high-precision JUNO results are unlikely to exclude the majority of these two-parameter scenarios. Distinguishing among these patterns will require improved long-baseline measurements of $\sin^2 \theta_{23}$ and δ_{CP} . For mixing patterns from $A_5 \rtimes H_{CP}$, those with fixed elements $\frac{\phi_g}{2}$, $\frac{1}{2}$ and $\frac{1}{2\phi_g}$ are viable. The best experimental agreement is furnished by the $U_{6,1}^{VI}$ pattern, which has $\frac{1}{2\phi_g}$ fixed at the (21) entry and gives the best fit for NO data, but conserves the CP-symmetry. In contrast, U_1^{VI} , with the fixed element $\frac{\phi_g}{2}$ at the (11) entry, offers a good fit to both NO and IO and predicts nontrivial CP violation. For the mixing patterns derived from $\Sigma(168) \rtimes H_{CP}$, the fixed entry is $\frac{1}{2}$. The smallest χ_{\min}^2 among permutations occurs for $U_{2,2}^{VII}$, with the fixed (31) entry. Among the three mixing patterns U^{VIII} , U^{IX} and U^X obtained from $\Delta(6n^2) \rtimes H_{CP}$ —with fixed entries $\cos \varphi_1$, $\frac{1}{2}$ and $\frac{1}{\sqrt{2}}$, respectively—the minimal flavour groups realizing these patterns with conserved CP phases are $\Delta(54)$ for U^{VIII} and S_4 for both U^{IX} and U^X . Allowing for CP violation requires extending the symmetry to $\Delta(96)$, and then U_9^{VIII} for $\varphi_1 = \varphi_2 = \frac{\pi}{4}$ and U_2^X for $(\varphi_1, \varphi_2) = (\frac{\pi}{4}, 0)$ give rise to $\frac{1}{\sqrt{2}}$ at (33) entry, yielding the smallest χ_{\min}^2 . It is remarkable that the dihedral groups D_3 and D_4 can also give rise to the viable mixing pattern U^{VIII} with CP-conserving and CP-violating phases, respectively.

In summary, we have shown that the discrete flavour symmetries $A_5 \rtimes H_{CP}$, $\Sigma(168) \rtimes H_{CP}$, $\Delta(6n^2) \rtimes H_{CP}$ and $D_n \rtimes H_{CP}$, when broken to suitable residual symmetries in the charged lepton and neutrino sectors, give rise to a well defined set of viable neutrino mixing scenarios characterized by one or two real parameters. These constructions lead to sharp, testable predictions for the mixing angles θ_{12} , θ_{23} and the Dirac phase δ_{CP} . We find that the smallest flavour group capable of generating phenomenologically viable one-parameter mixing patterns is S_4 (of order 24). For two-parameter mixing patterns, the minimal realizations arise from the dihedral groups D_4 (order 8) or D_3 (order 6), the latter giving rise to CP-conserving Dirac and Majorana phases. The recent JUNO 59.1-day dataset has reduced the 3σ region of $\sin^2 \theta_{12}$ with respect to that of NuFIT by a factor of roughly 1.3, exerting a particularly strong impact on one-parameter scenarios, while the constraints on two-parameter patterns remain comparatively mild. A decisive discrimination among the surviving mixing patterns will require the next generation of precision measurements. In particular, the full JUNO dataset, together with the upcoming long-baseline experiments DUNE and T2HK, will be essential for thoroughly testing and potentially ruling out, or providing evidence for, the residual symmetry-based frameworks, originating from the non-Abelian discrete symmetry approach to the lepton mixing problem in particle physics.

Acknowledgements

CCL is supported by Natural Science Basic Research Program of Shaanxi (Program No. 2024JC-YBQN-0004), and the National Natural Science Foundation of China under Grant No. 12247103. JNL is supported by the Grant No. NSFC-12505133. GJD is supported by the National Natural Science Foundation of China under Grant Nos. 12375104 and Guizhou Provincial Major Scientific and Technological Program XKBF (2025)010. The work of S. T. P. was supported in part by the European Union’s Horizon Europe research and innovation programme under the Marie Skłodowska-Curie Staff Exchange grant agreement No

Appendix

A Group theory of A_5 , $\Sigma(168)$ and $\Delta(6n^2)$

A.1 The group A_5

A_5 is the group of even permutations of five objects. It can be generated by the two generators S and T which satisfy the multiplication rules [103]:

$$S^2 = T^5 = (ST)^3 = 1. \quad (\text{A.1})$$

The A_5 group has five irreducible representations: one singlet representation $\mathbf{1}$, two three-dimensional representations $\mathbf{3}$ and $\mathbf{3}'$, one four-dimensional representation $\mathbf{4}$ and one five-dimensional representation $\mathbf{5}$. In the present work, our analysis uses the basis of Refs. [71, 103–105]. The explicit forms of the generators S and T in the five irreducible representations are as follows:

$$\begin{aligned}
 \mathbf{1}: \quad S &= 1, & T &= 1, \\
 \mathbf{3}: \quad S &= \frac{1}{\sqrt{5}} \begin{pmatrix} 1 & -\sqrt{2} & -\sqrt{2} \\ -\sqrt{2} & -\phi_g & \phi_g - 1 \\ -\sqrt{2} & \phi_g - 1 & -\phi_g \end{pmatrix}, & T &= \text{diag}(1, \omega_5, \omega_5^4), \\
 \mathbf{3}': \quad S &= \frac{1}{\sqrt{5}} \begin{pmatrix} -1 & \sqrt{2} & \sqrt{2} \\ \sqrt{2} & 1 - \phi_g & \phi_g \\ \sqrt{2} & \phi_g & 1 - \phi_g \end{pmatrix}, & T &= \text{diag}(1, \omega_5^2, \omega_5^3), \\
 \mathbf{4}: \quad S &= \frac{1}{\sqrt{5}} \begin{pmatrix} 1 & \phi_g - 1 & \phi_g & -1 \\ \phi_g - 1 & -1 & 1 & \phi_g \\ \phi_g & 1 & -1 & \phi_g - 1 \\ -1 & \phi_g & \phi_g - 1 & 1 \end{pmatrix}, & T &= \text{diag}(\omega_5, \omega_5^2, \omega_5^3, \omega_5^4), \\
 \mathbf{5}: \quad S &= \frac{1}{5} \begin{pmatrix} -1 & \sqrt{6} & \sqrt{6} & \sqrt{6} & \sqrt{6} \\ \sqrt{6} & (\phi_g - 1)^2 & -2\phi_g & 2(\phi_g - 1) & \phi_g^2 \\ \sqrt{6} & -2\phi_g & \phi_g^2 & (\phi_g - 1)^2 & 2(\phi_g - 1) \\ \sqrt{6} & 2(\phi_g - 1) & (\phi_g - 1)^2 & \phi_g^2 & -2\phi_g \\ \sqrt{6} & \phi_g^2 & 2(\phi_g - 1) & -2\phi_g & (\phi_g - 1)^2 \end{pmatrix}, & T &= \text{diag}(1, \omega_5, \omega_5^2, \omega_5^3, \omega_5^4),
 \end{aligned} \quad (\text{A.2})$$

where $\omega_5 = e^{2\pi i/5}$ denotes the quintic root of unit and $\phi_g = (1 + \sqrt{5})/2$ is the golden ratio. In our working basis, the generator T represented by a diagonal matrix and S by a real symmetric matrix in all irreducible representations. As a result, the consistent gCP transformation matrices X_r coincide in form with the family group transformation matrices $\rho_r(g)$ with $g \in A_5$.

A.2 The group $\Sigma(168)$

The group $\Sigma(168) \cong PSL(2, Z_7)$ is a non-Abelian finite subgroup of $SU(3)$ of order 168. $\Sigma(168)$ group can be generated by two generators S and T which satisfy the multiplication

rules:

$$S^2 = (ST)^3 = T^7 = (ST^3)^4 = 1. \quad (\text{A.3})$$

The Γ_7 group has six irreducible representations: one singlet representation **1**, two three-dimensional representations **3** and $\bar{\mathbf{3}}$, one six-dimensional representation **6**, one seven-dimensional representation **7** and one eight-dimensional representation **8**. The explicit forms of the generators S and T in the five irreducible representations are chosen as follows [106]:

$$\begin{aligned}
\mathbf{1}: S &= 1, & T &= 1, \\
\mathbf{3}: S &= \frac{2}{\sqrt{7}} \begin{pmatrix} -s_2 & -s_1 & s_3 \\ -s_1 & s_3 & -s_2 \\ s_3 & -s_2 & -s_1 \end{pmatrix}, & \bar{\mathbf{3}}: S &= \frac{2}{\sqrt{7}} \begin{pmatrix} -s_2 & -s_1 & s_3 \\ -s_1 & s_3 & -s_2 \\ s_3 & -s_2 & -s_1 \end{pmatrix}, \\
\mathbf{6}: S &= \frac{2\sqrt{2}}{7} \begin{pmatrix} \frac{1-c_2}{\sqrt{2}} & \frac{1-c_1}{\sqrt{2}} & c_2 - c_1 & \frac{1-c_3}{\sqrt{2}} & c_3 - c_2 & c_1 - c_3 \\ \frac{1-c_1}{\sqrt{2}} & \frac{1-c_3}{\sqrt{2}} & c_1 - c_3 & \frac{1-c_2}{\sqrt{2}} & c_2 - c_1 & c_3 - c_2 \\ c_2 - c_1 & c_1 - c_3 & \frac{1-c_1}{\sqrt{2}} & c_3 - c_2 & \frac{1-c_2}{\sqrt{2}} & \frac{1-c_3}{\sqrt{2}} \\ \frac{1-c_3}{\sqrt{2}} & \frac{1-c_2}{\sqrt{2}} & c_3 - c_2 & \frac{1-c_1}{\sqrt{2}} & c_1 - c_3 & c_2 - c_1 \\ c_3 - c_2 & c_2 - c_1 & \frac{1-c_2}{\sqrt{2}} & c_1 - c_3 & \frac{1-c_3}{\sqrt{2}} & \frac{1-c_1}{\sqrt{2}} \\ c_1 - c_3 & c_3 - c_2 & \frac{1-c_3}{\sqrt{2}} & c_2 - c_1 & \frac{1-c_1}{\sqrt{2}} & \frac{1-c_2}{\sqrt{2}} \end{pmatrix}, \\
\mathbf{7}: S &= \frac{2}{7} \begin{pmatrix} -\frac{1}{\sqrt{2}} & \sqrt{2} \\ \sqrt{2} & \frac{s_2+4s_3}{\sqrt{7}} & \frac{s_1-4s_2}{\sqrt{7}} & \frac{2s_1-2s_2-4s_3}{\sqrt{7}} & \frac{-4s_1-s_3}{\sqrt{7}} & \frac{4s_1+2s_2+2s_3}{\sqrt{7}} & \frac{-2s_1+4s_2-2s_3}{\sqrt{7}} \\ \sqrt{2} & \frac{s_1-4s_2}{\sqrt{7}} & \frac{-4s_1-s_3}{\sqrt{7}} & \frac{-2s_1+4s_2-2s_3}{\sqrt{7}} & \frac{s_2+4s_3}{\sqrt{7}} & \frac{2s_1-2s_2-4s_3}{\sqrt{7}} & \frac{4s_1+2s_2+2s_3}{\sqrt{7}} \\ \sqrt{2} & \frac{2s_1-2s_2-4s_3}{\sqrt{7}} & \frac{-2s_1+4s_2-2s_3}{\sqrt{7}} & \frac{s_1-4s_2}{\sqrt{7}} & \frac{4s_1+2s_2+2s_3}{\sqrt{7}} & \frac{s_2+4s_3}{\sqrt{7}} & \frac{-4s_1-s_3}{\sqrt{7}} \\ \sqrt{2} & \frac{-4s_1-s_3}{\sqrt{7}} & \frac{s_2+4s_3}{\sqrt{7}} & \frac{4s_1+2s_2+2s_3}{\sqrt{7}} & \frac{s_1-4s_2}{\sqrt{7}} & \frac{-2s_1+4s_2-2s_3}{\sqrt{7}} & \frac{2s_1-2s_2-4s_3}{\sqrt{7}} \\ \sqrt{2} & \frac{4s_1+2s_2+2s_3}{\sqrt{7}} & \frac{2s_1-2s_2-4s_3}{\sqrt{7}} & \frac{s_2+4s_3}{\sqrt{7}} & \frac{-2s_1+4s_2-2s_3}{\sqrt{7}} & \frac{-4s_1-s_3}{\sqrt{7}} & \frac{s_1-4s_2}{\sqrt{7}} \\ \sqrt{2} & \frac{-2s_1+4s_2-2s_3}{\sqrt{7}} & \frac{4s_1+2s_2+2s_3}{\sqrt{7}} & \frac{-4s_1-s_3}{\sqrt{7}} & \frac{2s_1-2s_2-4s_3}{\sqrt{7}} & \frac{s_1-4s_2}{\sqrt{7}} & \frac{s_2+4s_3}{\sqrt{7}} \end{pmatrix}, \\
\mathbf{8}: S &= \frac{2\sqrt{6}}{7} \begin{pmatrix} \frac{2c_2-c_1-c_3}{2\sqrt{6}} & \frac{c_1-c_3}{2\sqrt{2}} & \frac{c_1+c_2-2c_3}{2\sqrt{3}} & \frac{c_1-2c_2+c_3}{2\sqrt{3}} & \frac{c_2+c_3-2c_1}{2\sqrt{3}} & \frac{2c_1-c_2-c_3}{2\sqrt{3}} & \frac{2c_2-c_1-c_3}{2\sqrt{3}} & \frac{2c_3-c_1-c_2}{2\sqrt{3}} \\ \frac{c_1-c_3}{2\sqrt{2}} & \frac{c_1-2c_2+c_3}{2} & \frac{c_1-c_2}{\sqrt{6}} & \frac{c_3-c_1}{\sqrt{6}} & \frac{c_2-c_3}{\sqrt{6}} & \frac{c_3-c_2}{\sqrt{6}} & \frac{c_1-c_3}{\sqrt{6}} & \frac{c_2-c_1}{\sqrt{6}} \\ \frac{c_1+c_2-2c_3}{2\sqrt{3}} & \frac{c_1-c_2}{2} & \frac{c_2-c_1}{\sqrt{6}} & \frac{c_1-c_3}{\sqrt{6}} & \frac{1-c_3}{\sqrt{6}} & \frac{c_2-c_3}{\sqrt{6}} & \frac{c_1-1}{\sqrt{6}} & \frac{c_2-1}{\sqrt{6}} \\ \frac{c_1-2c_2+c_3}{2\sqrt{3}} & \frac{c_3-c_1}{2} & \frac{c_1-c_3}{\sqrt{6}} & \frac{c_3-c_2}{\sqrt{6}} & \frac{1-c_2}{\sqrt{6}} & \frac{c_1-c_2}{\sqrt{6}} & \frac{c_3-1}{\sqrt{6}} & \frac{c_1-1}{\sqrt{6}} \\ \frac{c_2+c_3-2c_1}{2\sqrt{3}} & \frac{c_2-c_3}{2} & \frac{1-c_3}{\sqrt{6}} & \frac{1-c_2}{\sqrt{6}} & \frac{c_1-c_3}{\sqrt{6}} & \frac{c_1-1}{\sqrt{6}} & \frac{c_1-c_2}{\sqrt{6}} & \frac{c_2-c_3}{\sqrt{6}} \\ \frac{2c_1-c_2-c_3}{2\sqrt{3}} & \frac{c_3-c_2}{2} & \frac{c_2-c_3}{\sqrt{6}} & \frac{c_1-c_2}{\sqrt{6}} & \frac{c_1-1}{\sqrt{6}} & \frac{c_1-c_3}{\sqrt{6}} & \frac{1-c_2}{\sqrt{6}} & \frac{1-c_3}{\sqrt{6}} \\ \frac{2c_2-c_1-c_3}{2\sqrt{3}} & \frac{c_1-c_3}{2} & \frac{c_1-1}{\sqrt{6}} & \frac{c_3-1}{\sqrt{6}} & \frac{c_1-c_2}{\sqrt{6}} & \frac{1-c_2}{\sqrt{6}} & \frac{c_3-c_2}{\sqrt{6}} & \frac{c_1-c_3}{\sqrt{6}} \\ \frac{2c_3-c_1-c_2}{2\sqrt{3}} & \frac{c_2-c_1}{2} & \frac{c_2-1}{\sqrt{6}} & \frac{c_1-1}{\sqrt{6}} & \frac{c_2-c_3}{\sqrt{6}} & \frac{1-c_3}{\sqrt{6}} & \frac{c_1-c_3}{\sqrt{6}} & \frac{c_2-c_1}{\sqrt{6}} \end{pmatrix}, \\
\mathbf{3}: T &= \text{diag}(\omega_7, \omega_7^2, \omega_7^4), & \bar{\mathbf{3}}: T &= \text{diag}(\omega_7^6, \omega_7^5, \omega_7^3), \\
\mathbf{6}: T &= \text{diag}(\omega_7^1, \omega_7^2, \omega_7^3, \omega_7^4, \omega_7^5, \omega_7^6), & \mathbf{7}: T &= \text{diag}(1, \omega_7, \omega_7^2, \omega_7^3, \omega_7^4, \omega_7^5, \omega_7^6), \\
\mathbf{8}: T &= \text{diag}(1, 1, \omega_7, \omega_7^2, \omega_7^3, \omega_7^4, \omega_7^5, \omega_7^6),
\end{aligned} \quad (\text{A.4})$$

where the parameter ω_7 is the seventh unit root $\omega_7 = e^{2\pi i/7}$, $s_n = \sin \frac{2n\pi}{7}$ and $c_n = \cos \frac{2n\pi}{7}$ with $n = 1, 2, 3$. One see that T is represented by diagonal matrices in different $\Sigma(168)$ irreducible representations, and the representation matrices of S real and symmetric. As a result, the gCP transformation compatible with $\Sigma(168)$ shares an identical structure with the family group transformation in our chosen basis.

A.3 The series group $\Delta(6n^2)$

$\Delta(6n^2)$ is a non-abelian finite subgroup of $SU(3)$ and it is isomorphic to $(Z_n \times Z_n) \rtimes S_3$ for an arbitrary positive integer n . Its use as a flavour symmetry and the corresponding

implications for lepton mixing have been extensively studied in the literature [59, 77, 79, 88, 107–109]. In this work we follow the conventions of Ref. [79]. The group is generated by four elements a , b , c and d obeying [79, 110]

$$\begin{aligned} a^3 = b^2 = (ab)^2 = 1, \quad c^n = d^n = 1, \quad cd = dc, \\ aca^{-1} = c^{-1}d^{-1}, \quad ada^{-1} = c, \quad bcb^{-1} = d^{-1}, \quad bdb^{-1} = c^{-1}, \end{aligned} \quad (\text{A.5})$$

The $\Delta(6n^2)$ group has $6n^2$ elements which can be expressed as

$$g = a^\alpha b^\beta c^\gamma d^\delta, \quad \alpha = 0, 1, 2, \quad \beta = 0, 1, \quad \gamma, \delta = 0, 1, \dots, n-1. \quad (\text{A.6})$$

The group $\Delta(6n^2)$ has one-dimensional, two-dimensional, three-dimensional and six-dimensional irreducible representations [79, 110]. In particular, there are $2(n-1)$ three-dimensional irreducible representations, denoted $\mathbf{3}_k^l$, whose generators take the form [79]

$$a = \begin{pmatrix} 0 & 1 & 0 \\ 0 & 0 & 1 \\ 1 & 0 & 0 \end{pmatrix}, \quad b = (-1)^k \begin{pmatrix} 0 & 0 & 1 \\ 0 & 1 & 0 \\ 1 & 0 & 0 \end{pmatrix}, \quad c = \begin{pmatrix} \eta^l & 0 & 0 \\ 0 & \eta^{-l} & 0 \\ 0 & 0 & 1 \end{pmatrix}, \quad d = \begin{pmatrix} 1 & 0 & 0 \\ 0 & \eta^l & 0 \\ 0 & 0 & \eta^{-l} \end{pmatrix}, \quad (\text{A.7})$$

where $\eta = e^{2\pi i/n}$, $k = 0, 1$ and $l = 1, 2, \dots, n-1$. We shall restrict ourselves to working with only faithful irreducible representations of $\Delta(6n^2)$. Only triplets with l not dividing n are faithful and unfaithful ones are discarded in our analysis. The two representations $\mathbf{3}_0^l$ and $\mathbf{3}_1^l$ differ only by an overall sign in the generator b . The generator a is the same for all l and the identities $\rho_{\mathbf{3}_k^l}(c) = [\rho_{\mathbf{3}_k^1}(c)]^l$, $\rho_{\mathbf{3}_k^l}(d) = [\rho_{\mathbf{3}_k^1}(d)]^l$ are fulfilled. It is clear that each power of the c and d generators will appear in every faithful three-dimensional irreducible representation. Without loss of generality, we embed the three left-handed lepton fields into the faithful representation $\mathbf{3}_0^1$ which is denoted as $\mathbf{3}$.

It has been demonstrated that CP symmetry can be consistently formulated within $\Delta(6n^2)$ flavour symmetry, provided n is not a multiple of 3. Even when n is divisible by 3, physically well-defined CP transformations may still be realized in a model, as long as no fields transform under the $\Delta(6n^2)$ doublet representations $\mathbf{2}_2$, $\mathbf{2}_3$, or $\mathbf{2}_4$ [79]. As has been shown in Ref. [79], the most general CP transformation consistent with the $\Delta(6n^2)$ flavour symmetry is of the same form as the flavour symmetry transformation in the basis of Eq. (A.7), i.e.

$$X_{\mathbf{r}} = \rho_{\mathbf{r}}(g), \quad g \in \Delta(6n^2), \quad (\text{A.8})$$

where $\rho_{\mathbf{r}}(g)$ denotes the representation matrix of the element g in the irreducible representation \mathbf{r} of the $\Delta(6n^2)$ group.

A.4 The series group D_n

The dihedral group D_n is the symmetry group of a regular n -gon for $n > 1$. A regular n -gon admits n rotations and n reflections, so D_n has $2n$ elements. For $n > 2$ the group is non-abelian, while $D_1 \simeq Z_2$ and $D_2 \simeq Z_2 \times Z_2$. It can be written as the semidirect product $Z_n \rtimes Z_2$. A convenient presentation is given in terms of two generators R and S satisfying

$$R^n = S^2 = (RS)^2 = 1, \quad (\text{A.9})$$

where R represents a rotation and S a reflection. Every group element can be written as

$$g = S^\alpha R^\beta, \quad \alpha = 0, 1, \quad \beta = 0, 1, \dots, n-1. \quad (\text{A.10})$$

The group D_n admits only real one- and two-dimensional irreducible representations. The representation content depends on whether n is odd or even. For odd n , there are two singlets $\mathbf{1}_{1,2}$ and $(n-1)/2$ doublets $\mathbf{2}_j$:

$$\mathbf{1}_1 : R = S = 1, \quad \mathbf{1}_2 : R = 1, S = -1, \quad (\text{A.11})$$

$$\mathbf{2}_j : R = \begin{pmatrix} e^{2\pi ij/n} & 0 \\ 0 & e^{-2\pi ij/n} \end{pmatrix}, \quad S = \begin{pmatrix} 0 & 1 \\ 1 & 0 \end{pmatrix}, \quad j = 1, \dots, \frac{n-1}{2}. \quad (\text{A.12})$$

For even n , the group has four singlets $\mathbf{1}_{1,2,3,4}$ and $(n/2-1)$ doublets $\mathbf{2}_j$:

$$\begin{aligned} \mathbf{1}_1 : R = S = 1, & & \mathbf{1}_2 : R = 1, S = -1, \\ \mathbf{1}_3 : R = -1, S = 1, & & \mathbf{1}_4 : R = S = -1, \\ \mathbf{2}_j : R = \begin{pmatrix} e^{2\pi ij/n} & 0 \\ 0 & e^{-2\pi ij/n} \end{pmatrix}, & & S = \begin{pmatrix} 0 & 1 \\ 1 & 0 \end{pmatrix}, \quad j = 1, \dots, \frac{n}{2} - 1. \end{aligned} \quad (\text{A.13})$$

As shown in Ref. [89], the generalized CP transformations compatible with D_n take the form

$$X_{\mathbf{r}} = \rho_{\mathbf{r}}(g), \quad g \in D_n. \quad (\text{A.14})$$

Thus in the adopted basis, all admissible CP transformations coincide with flavour transformations of D_n .

B Allowed ranges of lepton mixing observables for viable one- and two-parameter patterns

In this section, we summarize the allowed ranges of the lepton mixing angles θ_{12} , θ_{13} , θ_{23} and the CPV phases δ_{CP} , α_{21} , and α_{31} for all viable one- and two-parameter mixing patterns discussed in section 5.1 and section 5.2. The allowed regions are obtained by scanning the full parameter space and imposing the requirement that the three mixing angles and the Dirac CPV phase δ_{CP} lie within their experimentally preferred 3σ intervals from NuFIT v6.0, as summarized in table 3. The resulting allowed ranges of the lepton mixing observables for the viable patterns listed in table 4, table 5, table 6, and table 7 are presented in table 9, table 10, table 11, and table 12, respectively.

C The symmetry breaking pattern $\mathcal{G}_\ell = Z_2$, $\mathcal{G}_\nu = K_4 \times H_{CP}^\nu$ and lepton flavour mixing

This section examines a flavour symmetry breaking pattern where $G_f \times H_{CP}$ is broken to $K_4 \times H_{CP}^\nu$ in the neutrino sector and to Z_2 in the charged lepton sector. The resulting lepton mixing matrix would depend on only two real free parameters. Under this configuration, the residual symmetry $K_4 \times H_{CP}^\nu$ of neutrino sector imposes strong constraints on the neutrino diagonalization matrix U_ν as specified by the consistency conditions:

$$U_\nu^\dagger \rho_{\mathbf{3}}(g_{\nu_i}) U_\nu = \text{diag}(\pm 1, \pm 1, \pm 1), \quad U_\nu^\dagger X_{\nu\mathbf{3}} U_\nu^* = \text{diag}(\pm 1, \pm 1, \pm 1). \quad (\text{C.1})$$

where g_{ν_i} denote the generators of the residual K_4 group and $X_{\nu\mathbf{3}}$ is the corresponding residual CP transformation. Consequently, in this framework, U_ν is determined uniquely up to column permutations P_ν and a diagonal phase matrix $Q_\nu = \text{diag}(\pm i, \pm i, \pm i)$ which can shift the Majorana phases α_{21} and α_{31} by π .

Order	Case	(φ_1, φ_2)	$\sin^2 \theta_{12}$	$\sin^2 \theta_{13}$	$\sin^2 \theta_{23}$	δ_{CP}/π	$\alpha_{21}/\pi(\text{mod } 1)$	$\alpha_{31}/\pi(\text{mod } 1)$
NO	U^I	$(-\frac{\pi}{2}, \frac{\pi}{2})$	[0.3171, 0.3195]	[0.02030, 0.02381]	0.5	1.5	0	0
	U_1^{II}	$(0, \pi)$	[0.3403, 0.3415]	[0.02033, 0.02379]	0.5	1.5	0	0
	U_2^{II}	$(0, \pi)$	[0.3402, 0.3415]	[0.02030, 0.02379]	0.5	1.5	0	0
	U^{III}	—	[0.2821, 0.2831]	[0.02034, 0.02386]	0.5	1.5	0	0
	U_1^{IV}	—	[0.3295, 0.3319]	[0.02031, 0.02383]	[0.515, 0.532]	1	0	0
	U_2^{IV}	—	[0.3295, 0.3319]	[0.02031, 0.02383]	[0.468, 0.485]	0	0	0
	U_1^V	—	[0.3407, 0.3415]	[0.02153, 0.02385]	[0.541, 0.585]	[1.210, 1.382]*	[0.153, 0.165]*	[0.544, 0.565]*
	U_2^V	—	[0.3407, 0.3415]	[0.02157, 0.02385]	[0.435, 0.459]	[1.618, 1.710]	[0.835, 0.841]	[0.435, 0.446]
IO	U^I	$(-\frac{\pi}{2}, \frac{\pi}{2})$	[0.3169, 0.3193]	[0.02062, 0.02408]	0.5	1.5	0	0
	U_1^{II}	$(0, \pi)$	[0.3403, 0.3416]	[0.02060, 0.02409]	0.5	1.5	0	0
	U_2^{II}	$(0, \pi)$	[0.3404, 0.3415]	[0.02066, 0.02405]	0.5	1.5	0	0
	U^{III}	—	[0.2822, 0.2832]	[0.02063, 0.02406]	0.5	1.5	0	0
	U_1^V	—	[0.3407, 0.3416]	[0.02153, 0.02406]	[0.539, 0.584]	[1.214, 1.386]*	[0.154, 0.165]*	[0.545, 0.566]*
	U_2^V	—	[0.3407, 0.3416]	[0.02175, 0.02406]	[0.440, 0.461]	[1.614, 1.690]	[0.835, 0.840]	[0.434, 0.443]

Table 9: The allowed regions of lepton mixing observables for viable one-parameter mixing patterns given in table 4.

$A_5 \times H_{CP}$								
Order	Case	$\sin^2 \theta_{12}$	$\sin^2 \theta_{13}$	$\sin^2 \theta_{23}$	δ_{CP}/π	$\alpha_{21}/\pi(\text{mod } 1)$	$\alpha_{31}/\pi(\text{mod } 1)$	
NO	U_1^{VI}	[0.330, 0.332]	[0.02052, 0.02371]	[0.435, 0.585]	$[0, 0.021] \cup [0.689, 2]$	0	[0, 1]	
	U_2^{VI}	[0.330, 0.332]	[0.02044, 0.02382]	[0.435, 0.585]	1	0	0	
	$U_{3,2}^{VI}$	[0.330, 0.343]	[0.02030, 0.02388]	[0.515, 0.585]	[0.703, 1.297]	$[0, 0.134] \cup [0.867, 1]$	$[0, 0.083] \cup [0.917, 1]$	
	$U_{4,1}^{VI}$	[0.305, 0.345]	[0.02030, 0.02388]	[0.435, 0.511]	0	0	0	
	$U_{4,2}^{VI}$	[0.297, 0.345]	[0.02030, 0.02388]	[0.489, 0.585]	1	0	0	
	$U_{4,3}^{VI}$	[0.275, 0.345]	[0.02030, 0.02388]	[0.513, 0.572]	0	0	0	
	$U_{4,4}^{VI}$	[0.277, 0.345]	[0.02030, 0.02388]	[0.435, 0.486]	1	0	0	
	U_5^{VI}	[0.330, 0.341]	[0.02030, 0.02388]	[0.515, 0.585]	[0.780, 1.220]	$[0, 0.175] \cup [0.826, 1]$	$[0, 0.126] \cup [0.874, 1]$	
	$U_{6,1}^{VI}$	[0.275, 0.345]	[0.02030, 0.02388]	[0.435, 0.549]	1	0	0	
	$U_{6,2}^{VI}$	[0.275, 0.345]	[0.02030, 0.02388]	[0.452, 0.568]	0	0	0	
IO	U^{VI}	[0.329, 0.332]	[0.02061, 0.02408]	[0.440, 0.584]	[1.122, 1.860]	0	[0.001, 0.999]	
	$U_{3,1}^{VI}$	[0.333, 0.339]	[0.02060, 0.02408]	[0.440, 0.471]	[1.760, 1.861]*	[0.881, 0.930]*	[0.927, 0.957]*	
	$U_{3,2}^{VI}$	[0.332, 0.343]	[0.02060, 0.02409]	[0.525, 0.584]	[1.117, 1.298]*	[0.060, 0.135]*	[0.036, 0.083]*	
	U_5^{VI}	[0.333, 0.341]	[0.02060, 0.02409]	[0.535, 0.584]	[1.117, 1.220]*	[0.824, 0.912]*	[0.873, 0.936]*	
$\Sigma(168) \times H_{CP}$								
Order	Case	$\sin^2 \theta_{12}$	$\sin^2 \theta_{13}$	$\sin^2 \theta_{23}$	δ_{CP}/π	$\alpha_{21}/\pi(\text{mod } 1)$	$\alpha_{31}/\pi(\text{mod } 1)$	
NO	$U_{1,1}^{VII}$	[0.332, 0.345]	[0.02052, 0.02388]	[0.549, 0.585]	[1.627, 1.742]*	[0.584, 0.602]*	[0.242, 0.257]*	
	$U_{2,1}^{VII}$	[0.305, 0.345]	[0.02030, 0.02387]	[0.435, 0.511]	0	0	0	
	$U_{2,2}^{VII}$	[0.297, 0.345]	[0.02030, 0.02388]	[0.489, 0.585]	1	0	0	
	$U_{2,3}^{VII}$	[0.275, 0.345]	[0.02030, 0.02388]	[0.513, 0.572]	0	0	0	
	$U_{2,4}^{VII}$	[0.277, 0.345]	[0.02030, 0.02388]	[0.435, 0.486]	1	0	0	
IO	$U_{1,1}^{VII}$	[0.332, 0.345]	[0.02064, 0.02409]	[0.547, 0.584]	[1.632, 1.747]*	[0.584, 0.602]*	[0.242, 0.257]*	
	$U_{1,2}^{VII}$	[0.339, 0.345]	[0.02209, 0.02408]	[0.440, 0.453]	[1.254, 1.291]*	[0.398, 0.405]*	[0.743, 0.748]*	

Table 10: The allowed regions of lepton mixing observables for viable two-parameter mixing patterns given in table 5.

For the charged leptons, the residual symmetry Z_2 is labeled as $Z_2^{g_\ell}$, with generator g_ℓ satisfying $g_\ell^2 = 1$. Under the assumption that the charged lepton sector preserves this $Z_2^{g_\ell}$ symmetry, the unitary matrix U_ℓ is restricted to the form [59]:

$$U_\ell = \Sigma_\ell U_{23}^\dagger(\theta_\ell, \delta_\ell) P_\ell^T Q_\ell^\dagger, \quad (\text{C.2})$$

where Σ_ℓ diagonalizes the representation matrix $\rho_3(g_\ell)$ such that

$$\Sigma_\ell^\dagger \rho_3(g_\ell) \Sigma_\ell = \text{diag}(1, -1, -1). \quad (\text{C.3})$$

$\Delta(6n^2) \times H_{CP}$									
Order	Case	φ_1	φ_2	$\sin^2 \theta_{12}$	$\sin^2 \theta_{13}$	$\sin^2 \theta_{23}$	δ_{CP}/π	$\alpha_{21}/\pi(\text{mod } 1)$	$\alpha_{31}/\pi(\text{mod } 1)$
NO	U_4^{VIII}	$\frac{\pi}{3}$	0	[0.305, 0.345]	[0.02030, 0.02387]	[0.435, 0.511]	0	0	0
	U_5^{VIII}	$\frac{\pi}{3}$	0	[0.275, 0.345]	[0.02030, 0.02388]	[0.513, 0.572]	0	0	0
	U_6^{VIII}	$\frac{\pi}{4}$	0	[0.275, 0.345]	[0.02041, 0.02370]	[0.510, 0.512]	0 \cup 1	0	0
		$\frac{\pi}{4}$	$\frac{\pi}{4}$	[0.275, 0.345]	[0.02041, 0.02370]	[0.510, 0.512]	[1.206, 1.222]	[0.843, 0.864]	[0.878, 0.904]
	U_7^{VIII}	$\frac{\pi}{4}$	0	[0.275, 0.345]	[0.02041, 0.02370]	[0.510, 0.512]	[1.448, 1.469]*	[0.776, 0.806]*	[0.836, 0.872]*
	U_8^{VIII}	$\frac{\pi}{3}$	0	[0.277, 0.345]	[0.02030, 0.02388]	[0.489, 0.585]	1	0	0
	U_9^{VIII}	$\frac{\pi}{3}$	0	[0.275, 0.345]	[0.02030, 0.02388]	[0.435, 0.486]	1	0	0
		$\frac{\pi}{4}$	0	[0.275, 0.345]	[0.02044, 0.02373]	[0.488, 0.490]	0 \cup 1	0	0
		$\frac{\pi}{4}$	$\frac{\pi}{4}$	[0.275, 0.345]	[0.02044, 0.02373]	[0.488, 0.490]	[1.265, 1.278]	[0.136, 0.157]	[0.083, 0.106]
IO	U_6^{VIII}	$\frac{\pi}{4}$	$\frac{\pi}{4}$	[0.275, 0.345]	[0.02061, 0.02392]	[0.511, 0.512]	[1.722, 1.735]*	[0.843, 0.863]*	[0.893, 0.917]*
		$\frac{\pi}{4}$	$\frac{\pi}{2}$	[0.275, 0.345]	[0.02061, 0.02392]	[0.511, 0.512]	[1.448, 1.469]	[0.775, 0.805]	[0.835, 0.871]
	U_9^{VIII}	$\frac{\pi}{4}$	$\frac{\pi}{4}$	[0.275, 0.345]	[0.02079, 0.02389]	[0.488, 0.489]	[1.265, 1.278]	[0.138, 0.157]	[0.084, 0.106]
		$\frac{\pi}{4}$	$\frac{\pi}{2}$	[0.275, 0.345]	[0.02079, 0.02389]	[0.488, 0.489]	[1.531, 1.552]	[0.196, 0.225]	[0.130, 0.165]
$D_n \times H_{CP}$									
Order	Case	φ_1	φ_2	$\sin^2 \theta_{12}$	$\sin^2 \theta_{13}$	$\sin^2 \theta_{23}$	δ_{CP}/π	$\alpha_{21}/\pi(\text{mod } 1)$	$\alpha_{31}/\pi(\text{mod } 1)$
NO	U_1^{VIII}	$\frac{\pi}{5}$	0	[0.330, 0.332]	[0.02044, 0.02382]	[0.435, 0.585]	0 \cup 1	0	0
		$\frac{\pi}{5}$	$\frac{\pi}{2}$	[0.330, 0.332]	[0.02044, 0.02383]	[0.435, 0.585]	[1.475, 1.519]*	0*	[0, 0.038]* \cup [0.949, 1]*
	U_4^{VIII}	$\frac{2\pi}{5}$	0	[0.275, 0.345]	[0.02031, 0.02388]	[0.435, 0.548]	1	0	0
	U_5^{VIII}	$\frac{2\pi}{7}$	0	[0.275, 0.345]	[0.02030, 0.02388]	[0.516, 0.563]	1	0	0
	U_7^{VIII}	$\frac{2\pi}{5}$	0	[0.275, 0.345]	[0.02030, 0.02388]	[0.452, 0.568]	0	0	0
U_8^{VIII}	$\frac{2\pi}{7}$	0	[0.275, 0.345]	[0.02030, 0.02388]	[0.437, 0.484]	0	0	0	
IO	U_1^{VIII}	$\frac{\pi}{5}$	$\frac{\pi}{2}$	[0.329, 0.332]	[0.02075, 0.02399]	[0.440, 0.584]	[1.475, 1.518]*	0*	[0, 0.036]* \cup [0.950, 1]*

Table 11: The allowed regions of lepton mixing observables for viable two-parameter mixing patterns given in table 6.

$\Delta(6n^2) \times H_{CP}$ (Case IX)										
Order	Case	φ_1	φ_2	$\sin^2 \theta_{12}$	$\sin^2 \theta_{13}$	$\sin^2 \theta_{23}$	δ_{CP}/π	$\alpha_{21}/\pi(\text{mod } 1)$	$\alpha_{31}/\pi(\text{mod } 1)$	
NO	U_1^{IX}	0	0	[0.305, 0.345]	[0.02030, 0.02387]	[0.435, 0.511]	0	0	0	
		0	$\frac{\pi}{4}$	[0.312, 0.345]	[0.02030, 0.02388]	[0.435, 0.511]	[1.883, 1.998]	[0, 0.023]	[0.500, 0.514]	
		$\frac{\pi}{4}$	0	[0.329, 0.345]	[0.02030, 0.02388]	[0.435, 0.494]	[1.764, 1.925]*	[0.408, 0.692]*	[0.652, 0.836]*	
	U_2^{IX}	0	0	[0.275, 0.345]	[0.02030, 0.02388]	[0.513, 0.572]	0	0	0	
		0	$\frac{\pi}{4}$	[0.275, 0.345]	[0.02030, 0.02388]	[0.513, 0.585]	[1.773, 1.998]	[0.982, 1]	[0.482, 0.500]	
		$\frac{\pi}{4}$	0	[0.275, 0.345]	[0.02031, 0.02388]	[0.532, 0.585]	[1.623, 1.959]*	[0.786, 0.972]*	[0.867, 0.982]*	
		$\frac{\pi}{4}$	$\frac{\pi}{4}$	[0.287, 0.345]	[0.02030, 0.02388]	[0.547, 0.585]	[1.749, 1.766]*	[0.725, 0.802]*	[0.326, 0.384]*	
	U_3^{IX}	$\frac{\pi}{4}$	$\frac{\pi}{4}$	[0.289, 0.345]	[0.02030, 0.02388]	[0.552, 0.582]	[0, 0.022] \cup [1.636, 2]	[0.001, 0.246] \cup [0.983, 1]	[0.307, 0.473]	
		0	0	[0.297, 0.345]	[0.02030, 0.02388]	[0.489, 0.585]	1	0	0	
		0	$\frac{\pi}{4}$	[0.306, 0.345]	[0.02030, 0.02388]	[0.489, 0.585]	[1.002, 1.145]*	[0.970, 1]*	[0.479, 0.500]*	
	U_4^{IX}	$\frac{\pi}{4}$	$\frac{\pi}{2}$	[0.330, 0.345]	[0.02030, 0.02388]	[0.506, 0.585]	[0.722, 0.767] \cup [1.075, 1.291]	[0.307, 0.646]	[0.164, 0.387]	
		0	0	[0.277, 0.345]	[0.02030, 0.02388]	[0.435, 0.487]	1	0	0	
		0	$\frac{\pi}{4}$	[0.290, 0.345]	[0.02030, 0.02388]	[0.435, 0.487]	[1.002, 1.152]*	[0, 0.012]*	[0.500, 0.513]*	
		$\frac{\pi}{4}$	0	[0.278, 0.345]	[0.02030, 0.02388]	[0.435, 0.469]	[1.047, 1.201]	[0.032, 0.115]	[0.021, 0.068]	
	IO	U_1^{IX}	$\frac{\pi}{4}$	$\frac{\pi}{4}$	[0.318, 0.345]	[0.02030, 0.02388]	[0.435, 0.453]	[1.243, 1.251]	[0.197, 0.233]	[0.616, 0.641]
			$\frac{\pi}{4}$	$\frac{\pi}{4}$	[0.283, 0.330]	[0.02030, 0.02388]	[0.435, 0.448]	[0.902, 1.280]*	[0.717, 0.954]*	[0.503, 0.650]*
0			$\frac{\pi}{2}$	[0.329, 0.334]	[0.02060, 0.02409]	[0.440, 0.464]	[1.781, 1.861]*	[0.428, 0.543]*	[0.666, 0.744]*	
U_2^{IX}		0	$\frac{\pi}{4}$	[0.275, 0.303]	[0.02060, 0.02409]	[0.561, 0.584]	[1.780, 1.861]	[0.982, 0.989]	[0.482, 0.489]	
		$\frac{\pi}{4}$	0	[0.318, 0.345]	[0.02060, 0.02409]	[0.531, 0.584]	[1.626, 1.861]*	[0.785, 0.915]*	[0.866, 0.948]*	
		$\frac{\pi}{4}$	$\frac{\pi}{4}$	[0.288, 0.345]	[0.02060, 0.02409]	[0.547, 0.584]	[1.749, 1.765]*	[0.726, 0.802]*	[0.327, 0.384]*	
U_3^{IX}		$\frac{\pi}{4}$	$\frac{\pi}{4}$	[0.307, 0.345]	[0.02060, 0.02409]	[0.552, 0.582]	[1.636, 1.861]	[0.001, 0.148] \cup [0.983, 1]	[0.308, 0.412]	
		0	$\frac{\pi}{4}$	[0.306, 0.345]	[0.02061, 0.02409]	[0.566, 0.584]	[1.117, 1.281]*	[0.504, 0.511]* \cup [0.970, 0.979]*	[0.480, 0.487]* \cup [0.928, 0.930]*	
		$\frac{\pi}{4}$	$\frac{\pi}{2}$	[0.329, 0.345]	[0.02060, 0.02409]	[0.507, 0.581]	[1.117, 1.292]	[0.315, 0.647]	[0.168, 0.388]	
U_4^{IX}		0	0	[0.293, 0.309]	[0.02061, 0.02406]	[0.440, 0.446]	[1.117, 1.135]*	[0.009, 0.011]*	[0.509, 0.511]*	
	$\frac{\pi}{4}$	0	[0.308, 0.345]	[0.02061, 0.02408]	[0.445, 0.469]	[1.117, 1.199]	[0.072, 0.114]	[0.045, 0.068]		
	$\frac{\pi}{4}$	$\frac{\pi}{4}$	[0.326, 0.345]	[0.02062, 0.02408]	[0.440, 0.453]	[1.245, 1.252]	[0.198, 0.223]	[0.616, 0.634]		
	$\frac{\pi}{4}$	$\frac{\pi}{2}$	[0.304, 0.323]	[0.02061, 0.02409]	[0.440, 0.448]	[1.117, 1.241]*	[0.838, 0.924]*	[0.579, 0.632]*		
$\Delta(6n^2) \times H_{CP}$ (Case X)										
Order	Case	φ_1	φ_2	$\sin^2 \theta_{12}$	$\sin^2 \theta_{13}$	$\sin^2 \theta_{23}$	δ_{CP}/π	$\alpha_{21}/\pi(\text{mod } 1)$	$\alpha_{31}/\pi(\text{mod } 1)$	
NO	U_1^X	0	0	[0.275, 0.345]	[0.02041, 0.02370]	[0.510, 0.512]	0 \cup 1	0	0	
		$\frac{\pi}{4}$	0	[0.275, 0.345]	[0.02041, 0.02370]	[0.510, 0.512]	[1.206, 1.222]	[0.843, 0.864]	[0.878, 0.904]	
IO	U_2^X	0	0	[0.275, 0.345]	[0.02044, 0.02373]	[0.488, 0.490]	0 \cup 1	0	0	
		$\frac{\pi}{4}$	0	[0.275, 0.345]	[0.02044, 0.02373]	[0.488, 0.490]	[1.265, 1.278]	[0.136, 0.157]	[0.083, 0.106]	

Table 12: The allowed regions of lepton mixing observables for viable two-parameter mixing patterns given in table 7.

The matrix $U_{23}(\theta_\ell, \delta_\ell)$ is a unitary rotation in the 2–3 sector, and Q_ℓ is a diagonal phase matrix, i.e.

$$U_{23}(\theta_\ell, \delta_\ell) = \begin{pmatrix} 1 & 0 & 0 \\ 0 & \cos \theta_\ell & \sin \theta_\ell \\ 0 & -\sin \theta_\ell & \cos \theta_\ell \end{pmatrix} \begin{pmatrix} 1 & 0 & 0 \\ 0 & e^{i\delta_\ell} & 0 \\ 0 & 0 & e^{-i\delta_\ell} \end{pmatrix}, \quad Q_\ell = \begin{pmatrix} e^{-i\gamma_1} & 0 & 0 \\ 0 & e^{-i\gamma_2} & 0 \\ 0 & 0 & e^{-i\gamma_3} \end{pmatrix}, \quad (\text{C.4})$$

in which θ_ℓ , δ_ℓ and $\gamma_{1,2,3}$ are unconstrained real parameters. Hence the residual symmetry $\mathcal{G}_\ell = Z_2$, $\mathcal{G}_\nu = K_4 \times H_{CP}^\nu$ constrains the lepton mixing matrix to be of the following form,

$$U = Q_\ell P_\ell U_{23}(\theta_\ell, \delta_\ell) \Sigma_\ell^\dagger U_\nu P_\nu Q_\nu, \quad (\text{C.5})$$

where the diagonal phase matrix Q_ℓ can be absorbed into charged lepton field redefinitions, and Q_ν only affects possible π shifts in the Majorana phases. The resulting mixing matrix in Eq. (C.5) thus depends on only two free parameters θ_ℓ and δ_ℓ , and one row of the mixing matrix is fixed by residual symmetry. Furthermore, the PMNS matrix in Eq. (C.5) exhibits the following symmetry properties:

$$\begin{aligned} U(\theta_\ell + \pi, \delta_\ell, \theta_\nu) &= P_\ell \text{diag}(1, -1, -1) P_\ell^T U(\theta_\ell, \delta_\ell, \theta_\nu) \\ U(\pi - \theta_\ell, \delta_\ell, \theta_\nu) &= P_\ell \text{diag}(1, -i, i) P_\ell^T U(\theta_\ell, \delta_\ell - \pi/2, \theta_\nu) \\ U(\theta_\ell, \delta_\ell + \pi, \theta_\nu) &= P_\ell \text{diag}(1, -1, -1) P_\ell^T U(\theta_\ell, \delta_\ell, \theta_\nu) \end{aligned} \quad (\text{C.6})$$

Since the diagonal matrices $P_\ell \text{diag}(1, -1, -1) P_\ell^T$ and $P_\ell \text{diag}(1, -i, i) P_\ell^T$ can be absorbed into Q_ℓ , the fundamental domains for the parameters are restricted to $\theta_\ell \in [0, \pi/2]$ and $\delta_\ell \in [0, \pi)$.

When $A_5 \times H_{CP}$ is broken down to the residual symmetries Z_2 and $K_4 \times H_{CP}^\nu$ in the charged lepton and neutrino sectors respectively, there are two independent such kind of residual symmetries and accordingly the absolute values of the fixed row is found to be

$$\begin{aligned} \mathcal{G}_\ell = Z_2^S, \quad \mathcal{G}_\nu = K_4^{(ST^2 ST^3 S, TST^4)} \times H_{CP}^\nu &: \left(\frac{\phi_g}{2}, \frac{1}{2}, \frac{\phi_g - 1}{2} \right), \\ \mathcal{G}_\ell = Z_2^{TST^4}, \quad \mathcal{G}_\nu = K_4^{(ST^2 ST^3 S, TST^4)} \times H_{CP}^\nu &: (1, 0, 0), \end{aligned} \quad (\text{C.7})$$

with $\rho_r(T^2) \in H_{CP}^\nu$. The two predicted columns are both outside the 3σ ranges of the magnitude of the elements of the lepton mixing matrix [6].

When the residual symmetries originate from $\Sigma(168) \times H_{CP}$, the only independent breaking pattern that yields a fixed row with no zero elements is $G_\ell = Z_2^S$ and $G_\nu = K_4^{(T^2 ST^5, ST^3 ST^4 S)}$, and the corresponding unitary matrices Σ_ℓ and U_ν are

$$\Sigma_\ell = \frac{1}{2\sqrt{2}} \begin{pmatrix} \frac{1}{s_2} & \frac{2s_2-1}{s_2\sqrt{4c_2(c_2+s_3)+1}} & \frac{-2s_2-1}{s_2\sqrt{4c_2(c_2-s_3)+1}} \\ -\frac{1}{s_3} & \frac{2c_2+2s_3+1}{s_2\sqrt{4c_2(c_2+s_3)+1}} & \frac{2c_2-2s_3+1}{s_2\sqrt{4c_2(c_2-s_3)+1}} \\ \frac{1}{s_1} & \frac{-2c_3}{s_2\sqrt{4c_2(c_2+s_3)+1}} & \frac{-2c_3}{s_2\sqrt{4c_2(c_2-s_3)+1}} \end{pmatrix}, \quad U_\nu = \frac{1}{2\sqrt{2}} \begin{pmatrix} \frac{(-1)^{4/7}}{s_2} & \frac{(-1)^{5/7}}{s_3} & \frac{1}{s_1} \\ \frac{(-1)^{1/7}}{s_1} & -\frac{(-1)^{3/7}}{s_2} & \frac{1}{s_2} \\ \frac{(-1)^{2/7}}{s_1} & \frac{(-1)^{6/7}}{s_2} & -\frac{1}{s_3} \end{pmatrix}, \quad (\text{C.8})$$

where the parameters $s_n = \sin \frac{2n\pi}{7}$ and $c_n = \cos \frac{2n\pi}{7}$ with $n = 1, 2, 3$. Then it is easy to check that the breaking pattern leads to a fixed row $(1, 1, \sqrt{2})/2$ in the PMNS matrix. The full lepton mixing matrix can then be constructed using Eq. (C.5) with $P_\ell = P_{231}$ and $P_\nu = P_{132}$. The three lepton mixing angles depend on two free parameters θ_ℓ and δ_ℓ and we can straightforwardly extract them as follows

$$\sin^2 \theta_{13} = \frac{1}{4} \left[1 + \sin 2\theta_\ell \sin \left(2\delta_\ell - \frac{\pi}{4} \right) \right], \quad \sin^2 \theta_{23} = \frac{1 - \sin 2\theta_\ell \sin \left(2\delta_\ell - \frac{\pi}{4} \right)}{3 - \sin 2\theta_\ell \sin \left(2\delta_\ell - \frac{\pi}{4} \right)},$$

$$\sin^2 \theta_{12} = \frac{3 - \sqrt{7} \cos 2\theta_\ell + \sqrt{2} \cos 2\delta_\ell \sin 2\theta_\ell}{6 - 2 \sin 2\theta_\ell \sin (2\delta_\ell - \frac{\pi}{4})}. \quad (\text{C.9})$$

It is easy to check that the atmospheric and reactor mixing angles have the correlation

$$\cos^2 \theta_{13} \cos^2 \theta_{23} = \frac{1}{2}. \quad (\text{C.10})$$

Using the 3σ range of the reactor mixing angle $0.02030 \leq \sin^2 \theta_{13} \leq 0.02388$ [6], we have $\sin^2 \theta_{23} \in [0.4878, 0.4896]$. Comprehensively scanning over the values of θ_ℓ and δ_ℓ , while requiring θ_{13} in its experimentally favored 3σ region, we identify

$$0.3455 \leq \sin^2 \theta_{12} \leq 0.6545, \quad (\text{C.11})$$

which lies above the 3σ upper limit of $\sin^2 \theta_{12}$ by JUNO [30]. Hence this mixing pattern is ruled out.

When the residual symmetries originate from $\Delta(6n^2) \rtimes H_{CP}$, the only independent breaking pattern that gives a fixed row without zero elements is $G_\ell = Z_2^{bc^x d^x}$, $G_\nu = K_4^{(c^{n/2}, abc^y)}$ and $X_{\nu r} = \rho_r (c^\delta d^{2y+2\gamma})$. The corresponding lepton mixing matrices are given by

$$\begin{aligned} U^{XI(a)} &= \frac{1}{2} R_{13}(\theta_\ell) \text{diag}(e^{i\delta_\ell}, 1, e^{-i\delta_\ell}) \begin{pmatrix} \sqrt{2}e^{i\varphi_1} & -\sqrt{2}e^{i\varphi_1} & 0 \\ 1 & 1 & -\sqrt{2}e^{i\varphi_2} \\ 1 & 1 & \sqrt{2}e^{i\varphi_2} \end{pmatrix} Q_\nu^\dagger, \\ &= \text{diag}(e^{i\delta_\ell}, 1, e^{-i\delta_\ell}) R_{13}(\theta_\ell) \begin{pmatrix} \sqrt{2}e^{i(\varphi_1+2\delta_\ell)} & -\sqrt{2}e^{i(\varphi_1+2\delta_\ell)} & 0 \\ 1 & 1 & -\sqrt{2}e^{i\varphi_2} \\ 1 & 1 & \sqrt{2}e^{i\varphi_2} \end{pmatrix} Q_\nu^\dagger, \\ U^{XI(b)} &= P_{132} U_{PMNS}^{VIII(a)}, \end{aligned} \quad (\text{C.12})$$

where the parameters φ_1 and φ_2 are determined as

$$\Delta(6n^2) : \quad \varphi_1 = \frac{3\delta + 2x + 2y}{n}\pi, \quad \varphi_2 = -\frac{3\gamma + 2x + 2y}{n}\pi, \quad (\text{C.13})$$

These two parameters φ_1 and φ_2 are interdependent of each other, and they can take the discrete values

$$\Delta(6n^2) : \quad \varphi_1, \varphi_2 \pmod{2\pi} = 0, \frac{1}{n}\pi, \frac{2}{n}\pi, \dots, \frac{2n-1}{n}\pi, \quad (\text{C.14})$$

Obvious $U_{PMNS}^{XI(b)}$ is obtained from $U_{PMNS}^{XI(a)}$ by exchanging the second and third rows. In this case, the row fixed by residual symmetry is $(1, 1, -\sqrt{2}e^{i\varphi_2})/2$, and it could be the second or the third row of the PMNS mixing matrix. The sum rule among the reactor and solar mixing angles is given by [60]

$$\sin^2 \theta_{12} = \frac{1}{2} \pm \tan \theta_{13} \sqrt{1 - \tan^2 \theta_{13}} \cos(\varphi_1 + 2\delta_\ell), \quad (\text{C.15})$$

where the “+” and “−” signs are valid $0 < \theta_\ell < \pi/2$ and $\pi/2 < \theta_\ell < \pi$ respectively. Freely varying the phase δ_ℓ and limiting θ_{13} in its 3σ region [6], we find that the solar angle can vary in the range $0.3455 \leq \sin^2 \theta_{12} \leq 0.6545$ which is identical with that of Eq. (C.11) and ruled out by JUNO.

In summary, the breaking pattern with $\mathcal{G}_\ell = Z_2$ and $\mathcal{G}_\nu = K_4 \times H_{CP}'$ is not viable, since the experimental data of solar mixing angle θ_{12} can not be accommodated.

References

- [1] A. B. McDonald, “Nobel Lecture: The Sudbury Neutrino Observatory: Observation of flavor change for solar neutrinos,” *Rev. Mod. Phys.* **88** no. 3, (2016) 030502.
- [2] T. Kajita, “Nobel Lecture: Discovery of atmospheric neutrino oscillations,” *Rev. Mod. Phys.* **88** no. 3, (2016) 030501.
- [3] **Particle Data Group** Collaboration, S. Navas *et al.*, “Review of particle physics,” *Phys. Rev. D* **110** no. 3, (2024) 030001.
- [4] **Particle Data Group** Collaboration, M. Tanabashi *et al.*, “Review of Particle Physics,” *Phys. Rev. D* **98** no. 3, (2018) 030001.
- [5] S. M. Bilenky, J. Hosek, and S. T. Petcov, “On Oscillations of Neutrinos with Dirac and Majorana Masses,” *Phys. Lett. B* **94** (1980) 495–498.
- [6] I. Esteban, M. C. Gonzalez-Garcia, M. Maltoni, I. Martinez-Soler, J. P. Pinheiro, and T. Schwetz, “NuFit-6.0: updated global analysis of three-flavor neutrino oscillations,” *JHEP* **12** (2024) 216, [arXiv:2410.05380 \[hep-ph\]](#).
- [7] P. F. de Salas, D. V. Forero, S. Gariazzo, P. Martínez-Miravé, O. Mena, C. A. Ternes, M. Tórtola, and J. W. F. Valle, “2020 global reassessment of the neutrino oscillation picture,” *JHEP* **02** (2021) 071, [arXiv:2006.11237 \[hep-ph\]](#).
- [8] F. Capozzi, W. Giarè, E. Lisi, A. Marrone, A. Melchiorri, and A. Palazzo, “Neutrino masses and mixing: Entering the era of subpercent precision,” *Phys. Rev. D* **111** no. 9, (2025) 093006, [arXiv:2503.07752 \[hep-ph\]](#).
- [9] F. Capozzi, E. Lisi, F. Marcone, A. Marrone, and A. Palazzo, “Updated bounds on the (1,2) neutrino oscillation parameters after first JUNO results,” [arXiv:2511.21650 \[hep-ph\]](#).
- [10] F. Feruglio, “Pieces of the Flavour Puzzle,” *Eur. Phys. J. C* **75** no. 8, (2015) 373, [arXiv:1503.04071 \[hep-ph\]](#).
- [11] G. Altarelli and F. Feruglio, “Discrete Flavor Symmetries and Models of Neutrino Mixing,” *Rev. Mod. Phys.* **82** (2010) 2701–2729, [arXiv:1002.0211 \[hep-ph\]](#).
- [12] H. Ishimori, T. Kobayashi, H. Ohki, Y. Shimizu, H. Okada, and M. Tanimoto, “Non-Abelian Discrete Symmetries in Particle Physics,” *Prog. Theor. Phys. Suppl.* **183** (2010) 1–163, [arXiv:1003.3552 \[hep-th\]](#).
- [13] S. F. King and C. Luhn, “Neutrino Mass and Mixing with Discrete Symmetry,” *Rept. Prog. Phys.* **76** (2013) 056201, [arXiv:1301.1340 \[hep-ph\]](#).
- [14] S. F. King, A. Merle, S. Morisi, Y. Shimizu, and M. Tanimoto, “Neutrino Mass and Mixing: from Theory to Experiment,” *New J. Phys.* **16** (2014) 045018, [arXiv:1402.4271 \[hep-ph\]](#).
- [15] S. F. King, “Unified Models of Neutrinos, Flavour and CP Violation,” *Prog. Part. Nucl. Phys.* **94** (2017) 217–256, [arXiv:1701.04413 \[hep-ph\]](#).
- [16] S. T. Petcov, “Discrete Flavour Symmetries, Neutrino Mixing and Leptonic CP Violation,” *Eur. Phys. J. C* **78** no. 9, (2018) 709, [arXiv:1711.10806 \[hep-ph\]](#).

- [17] Z.-z. Xing, “Flavor structures of charged fermions and massive neutrinos,” *Phys. Rept.* **854** (2020) 1–147, [arXiv:1909.09610 \[hep-ph\]](#).
- [18] F. Feruglio and A. Romanino, “Lepton flavor symmetries,” *Rev. Mod. Phys.* **93** no. 1, (2021) 015007, [arXiv:1912.06028 \[hep-ph\]](#).
- [19] Y. Almumin, M.-C. Chen, M. Cheng, V. Knapp-Perez, Y. Li, A. Mondol, S. Ramos-Sanchez, M. Ratz, and S. Shukla, “Neutrino Flavor Model Building and the Origins of Flavor and CP Violation,” *Universe* **9** no. 12, (2023) 512, [arXiv:2204.08668 \[hep-ph\]](#).
- [20] G.-J. Ding and S. F. King, “Neutrino mass and mixing with modular symmetry,” *Rept. Prog. Phys.* **87** no. 8, (2024) 084201, [arXiv:2311.09282 \[hep-ph\]](#).
- [21] G.-J. Ding and J. W. Valle, “The symmetry approach to quark and lepton masses and mixing,” *Phys.Rept.* **1109** (2025) 2372, [arXiv:2402.16963 \[hep-ph\]](#).
- [22] M. Holthausen, M. Lindner, and M. A. Schmidt, “CP and Discrete Flavour Symmetries,” *JHEP* **04** (2013) 122, [arXiv:1211.6953 \[hep-ph\]](#).
- [23] M.-C. Chen, M. Fallbacher, K. T. Mahanthappa, M. Ratz, and A. Trautner, “CP Violation from Finite Groups,” *Nucl. Phys. B* **883** (2014) 267–305, [arXiv:1402.0507 \[hep-ph\]](#).
- [24] F. Feruglio, C. Hagedorn, and R. Ziegler, “Lepton Mixing Parameters from Discrete and CP Symmetries,” *JHEP* **07** (2013) 027, [arXiv:1211.5560 \[hep-ph\]](#).
- [25] **JUNO** Collaboration, A. Abusleme *et al.*, “Initial performance results of the JUNO detector,” [arXiv:2511.14590 \[hep-ex\]](#).
- [26] S. T. Petcov and M. Piai, “The LMA MSW solution of the solar neutrino problem, inverted neutrino mass hierarchy and reactor neutrino experiments,” *Phys. Lett. B* **533** (2002) 94–106, [arXiv:hep-ph/0112074](#).
- [27] S. Choubey, S. T. Petcov, and M. Piai, “Precision neutrino oscillation physics with an intermediate baseline reactor neutrino experiment,” *Phys. Rev. D* **68** (2003) 113006, [arXiv:hep-ph/0306017](#).
- [28] J. Learned, S. T. Dye, S. Pakvasa, and R. C. Svoboda, “Determination of neutrino mass hierarchy and $\theta(13)$ with a remote detector of reactor antineutrinos,” *Phys. Rev. D* **78** (2008) 071302, [arXiv:hep-ex/0612022](#).
- [29] Y.-F. Li, J. Cao, Y. Wang, and L. Zhan, “Unambiguous Determination of the Neutrino Mass Hierarchy Using Reactor Neutrinos,” *Phys. Rev. D* **88** (2013) 013008, [arXiv:1303.6733 \[hep-ex\]](#).
- [30] **JUNO** Collaboration, A. Abusleme *et al.*, “First measurement of reactor neutrino oscillations at JUNO,” [arXiv:2511.14593 \[hep-ex\]](#).
- [31] **JUNO** Collaboration, A. Abusleme *et al.*, “Sub-percent precision measurement of neutrino oscillation parameters with JUNO,” *Chin. Phys. C* **46** no. 12, (2022) 123001, [arXiv:2204.13249 \[hep-ex\]](#).
- [32] W. Chao, “Quantum field theory approach to neutrino oscillations in dark matter and implications at JUNO,” [arXiv:2511.15494 \[hep-ph\]](#).

- [33] Y.-F. Li, A. Wang, Y. Xu, and J.-y. Zhu, “Terrestrial Matter Effects on Reactor Antineutrino Oscillations: Constant vs. Fluctuated Density Profiles,” [arXiv:2511.15702 \[hep-ph\]](#).
- [34] D. Zhang, “Trimaximal Mixing Patterns Meet the First JUNO Result,” [arXiv:2511.15654 \[hep-ph\]](#).
- [35] S.-F. Ge, C.-F. Kong, and J. P. Pinheiro, “CP Prediction from Residual \mathbb{Z}_2^s and $\overline{\mathbb{Z}}_2^s$ Symmetries with JUNO First Data,” [arXiv:2511.15442 \[hep-ph\]](#).
- [36] J. Huang and S. Zhou, “Probing unitarity violation of lepton flavor mixing matrix with reactor antineutrinos at JUNO and TAO,” [arXiv:2511.15525 \[hep-ph\]](#).
- [37] Z.-z. Xing, “Divergence in tracing the flavors of astrophysical neutrinos: can JUNO help IceCube?,” [arXiv:2511.15127 \[hep-ph\]](#).
- [38] Z.-Q. Chen, G.-X. Fang, and Y.-L. Zhou, “Probing quark-lepton correlation in GUTs with high-precision neutrino measurements,” [arXiv:2511.16196 \[hep-ph\]](#).
- [39] W.-H. Jiang, R. Ouyang, and Y.-L. Zhou, “Modular TM_1 mixing in light of precision measurement in JUNO,” [arXiv:2511.16348 \[hep-ph\]](#).
- [40] X.-G. He, “Modified Tri-bimaximal neutrino mixing confront with JUNO θ_{12} measurement,” [arXiv:2511.15978 \[hep-ph\]](#).
- [41] S. Luo, “Rescaled Leptonic Unitary Triangles and Rephasing Invariants,” [arXiv:2511.16942 \[hep-ph\]](#).
- [42] S. T. Petcov and A. V. Titov, “Viability of A_4 , S_4 and A_5 Flavour Symmetries in Light of the First JUNO Result,” [arXiv:2511.19408 \[hep-ph\]](#).
- [43] G.-J. Ding, R. Kumar, N. Nath, R. Srivastava, and J. W. F. Valle, “Zooming in on ‘bi-large’ neutrino mixing with the first JUNO results,” [arXiv:2511.22689 \[hep-ph\]](#).
- [44] S. Goswami, A. Gupta, U. Rahman, and S. K. Raut, “Enhancing the sensitivity to neutrino oscillation parameters using synergy between T2K, NO ν A and JUNO,” [arXiv:2512.00172 \[hep-ph\]](#).
- [45] P. I. Krastev and S. T. Petcov, “Resonance Amplification and μ Violation Effects in Three Neutrino Oscillations in the Earth,” *Phys. Lett. B* **205** (1988) 84–92.
- [46] C. Jarlskog, “Commutator of the Quark Mass Matrices in the Standard Electroweak Model and a Measure of Maximal CP Nonconservation,” *Phys.Rev.Lett.* **55** (1985) 1039.
- [47] S. T. Petcov and A. V. Titov, “Assessing the Viability of A_4 , S_4 and A_5 Flavour Symmetries for Description of Neutrino Mixing,” *Phys. Rev. D* **97** no. 11, (2018) 115045, [arXiv:1804.00182 \[hep-ph\]](#).
- [48] M. Blennow, M. Ghosh, T. Ohlsson, and A. Titov, “Testing Lepton Flavor Models at ESSnuSB,” *JHEP* **07** (2020) 014, [arXiv:2004.00017 \[hep-ph\]](#).
- [49] P. Chen, C.-C. Li, and G.-J. Ding, “Lepton Flavor Mixing and CP Symmetry,” *Phys.Rev.D* **91** (2015) 033003, [arXiv:1412.8352 \[hep-ph\]](#).

- [50] P. Chen, C.-Y. Yao, and G.-J. Ding, “Neutrino Mixing from CP Symmetry,” *Phys.Rev.D* **92** no. 7, (2015) 073002, [arXiv:1507.03419 \[hep-ph\]](#).
- [51] C.-C. Li and G.-J. Ding, “Deviation from bimaximal mixing and leptonic CP phases in S_4 family symmetry and generalized CP,” *JHEP* **08** (2015) 017, [arXiv:1408.0785 \[hep-ph\]](#).
- [52] G.-J. Ding, S. F. King, and A. J. Stuart, “Generalised CP and A_4 Family Symmetry,” *JHEP* **12** (2013) 006, [arXiv:1307.4212 \[hep-ph\]](#).
- [53] I. Girardi, S. T. Petcov, A. J. Stuart, and A. V. Titov, “Leptonic Dirac CP Violation Predictions from Residual Discrete Symmetries,” *Nucl. Phys. B* **902** (2016) 1–57, [arXiv:1509.02502 \[hep-ph\]](#).
- [54] R. de Adelhart Toorop, F. Feruglio, and C. Hagedorn, “Finite Modular Groups and Lepton Mixing,” *Nucl. Phys. B* **858** (2012) 437–467, [arXiv:1112.1340 \[hep-ph\]](#).
- [55] M. Holthausen, K. S. Lim, and M. Lindner, “Lepton Mixing Patterns from a Scan of Finite Discrete Groups,” *Phys. Lett. B* **721** (2013) 61–67, [arXiv:1212.2411 \[hep-ph\]](#).
- [56] R. M. Fonseca and W. Grimus, “Classification of lepton mixing matrices from finite residual symmetries,” *JHEP* **09** (2014) 033, [arXiv:1405.3678 \[hep-ph\]](#).
- [57] J. Talbert, “[Re]constructing Finite Flavour Groups: Horizontal Symmetry Scans from the Bottom-Up,” *JHEP* **12** (2014) 058, [arXiv:1409.7310 \[hep-ph\]](#).
- [58] C.-Y. Yao and G.-J. Ding, “Lepton and Quark Mixing Patterns from Finite Flavor Symmetries,” *Phys. Rev. D* **92** no. 9, (2015) 096010, [arXiv:1505.03798 \[hep-ph\]](#).
- [59] J.-N. Lu and G.-J. Ding, “Quark and lepton mixing patterns from a common discrete flavor symmetry with a generalized CP symmetry,” *Phys. Rev. D* **98** no. 5, (2018) 055011, [arXiv:1806.02301 \[hep-ph\]](#).
- [60] C.-Y. Yao and G.-J. Ding, “CP Symmetry and Lepton Mixing from a Scan of Finite Discrete Groups,” *Phys.Rev.D* **94** no. 7, (2016) 073006, [arXiv:1606.05610 \[hep-ph\]](#).
- [61] C.-C. Li, J.-N. Lu, and G.-J. Ding, “ A_4 and CP symmetry and a model with maximal CP violation,” *Nucl.Phys.B* **913** (2016) 110–131, [arXiv:1608.01860 \[hep-ph\]](#).
- [62] C.-C. Li and G.-J. Ding, “Generalised CP and trimaximal TM_1 lepton mixing in S_4 family symmetry,” *Nucl.Phys.B* **881** (2014) 206–232, [arXiv:1312.4401 \[hep-ph\]](#).
- [63] G.-J. Ding, S. F. King, C. Luhn, and A. J. Stuart, “Spontaneous CP violation from vacuum alignment in S_4 models of leptons,” *JHEP* **05** (2013) 084, [arXiv:1303.6180 \[hep-ph\]](#).
- [64] F. Feruglio, C. Hagedorn, and R. Ziegler, “A realistic pattern of lepton mixing and masses from S_4 and CP,” *Eur.Phys.J.C* **74** (2014) 2753, [arXiv:1303.7178 \[hep-ph\]](#).
- [65] J. Penedo, S. Petcov, and A. Titov, “Neutrino mixing and leptonic CP violation from S_4 flavour and generalised CP symmetries,” *JHEP* **12** (2017) 022, [arXiv:1705.00309 \[hep-ph\]](#).

- [66] I. Girardi, A. Meroni, S. T. Petcov, and M. Spinrath, “Generalised geometrical CP violation in a T’ lepton flavour model,” *JHEP* **02** (2014) 050, [arXiv:1312.1966 \[hep-ph\]](#).
- [67] G. C. Branco, I. de Medeiros Varzielas, and S. F. King, “Invariant approach to CP in family symmetry models,” *Phys.Rev.D* **92** no. 3, (2015) 036007, [arXiv:1502.03105 \[hep-ph\]](#).
- [68] G. C. Branco, I. de Medeiros Varzielas, and S. F. King, “Invariant approach to CP in unbroken $\Delta(27)$,” *Nucl.Phys.B* **899** (2015) 14–36, [arXiv:1505.06165 \[hep-ph\]](#).
- [69] G.-J. Ding and Y.-L. Zhou, “Predicting lepton flavor mixing from $\Delta(48)$ and generalized CP symmetries,” *Chin.Phys.C* **39** no. 2, (2015) 021001, [arXiv:1312.5222 \[hep-ph\]](#).
- [70] G.-J. Ding and Y.-L. Zhou, “Lepton mixing parameters from $\Delta(48)$ family symmetry and generalised CP,” *JHEP* **06** (2014) 023, [arXiv:1404.0592 \[hep-ph\]](#).
- [71] C.-C. Li and G.-J. Ding, “Lepton Mixing in A_5 Family Symmetry and Generalized CP,” *JHEP* **05** (2015) 100, [arXiv:1503.03711 \[hep-ph\]](#).
- [72] A. Di Iura, C. Hagedorn, and D. Meloni, “Lepton mixing from the interplay of the alternating group A_5 and CP,” *JHEP* **08** (2015) 037, [arXiv:1503.04140 \[hep-ph\]](#).
- [73] P. Ballett, S. Pascoli, and J. Turner, “Mixing angle and phase correlations from A_5 with generalized CP and their prospects for discovery,” *Phys.Rev.D* **92** no. 9, (2015) 093008, [arXiv:1503.07543 \[hep-ph\]](#).
- [74] J. Turner, “Predictions for leptonic mixing angle correlations and nontrivial Dirac CP violation from A_5 with generalized CP symmetry,” *Phys.Rev.D* **92** no. 11, (2015) 116007, [arXiv:1507.06224 \[hep-ph\]](#).
- [75] A. Di Iura, M. López-Ibañez, and D. Meloni, “Neutrino masses and lepton mixing from $A_5 \times CP$,” *Nucl.Phys.B* **949** (2019) 114794, [arXiv:1811.09662 \[hep-ph\]](#).
- [76] G.-J. Ding and S. F. King, “Generalized CP and $\Delta(96)$ family symmetry,” *Phys.Rev.D* **89** no. 9, (2014) 093020, [arXiv:1403.5846 \[hep-ph\]](#).
- [77] C. Hagedorn, A. Meroni, and E. Molinaro, “Lepton mixing from $\Delta(3n^2)$ and $\Delta(6n^2)$ and CP,” *Nucl.Phys.B* **891** (2015) 499–557, [arXiv:1408.7118 \[hep-ph\]](#).
- [78] G.-J. Ding and S. F. King, “Generalized CP and $\Delta(3n^2)$ Family Symmetry for Semi-Direct Predictions of the PMNS Matrix,” *Phys.Rev.D* **93** (2016) 025013, [arXiv:1510.03188 \[hep-ph\]](#).
- [79] G.-J. Ding, S. F. King, and T. Neder, “Generalised CP and $\Delta(6n^2)$ family symmetry in semi-direct models of leptons,” *JHEP* **12** (2014) 007, [arXiv:1409.8005 \[hep-ph\]](#).
- [80] C.-C. Li, C.-Y. Yao, and G.-J. Ding, “Lepton Mixing Predictions from Infinite Group Series $D_{9n,3n}^{(1)}$ with Generalized CP,” *JHEP* **05** (2016) 007, [arXiv:1601.06393 \[hep-ph\]](#).
- [81] G. Branco, L. Lavoura, and M. Rebelo, “Majorana Neutrinos and CP Violation in the Leptonic Sector,” *Phys.Lett.B* **180** (1986) 264–268.

- [82] J. F. Nieves and P. B. Pal, “Minimal Rephasing Invariant CP Violating Parameters With Dirac and Majorana Fermions,” *Phys. Rev. D* **36** (1987) 315.
- [83] J. F. Nieves and P. B. Pal, “Rephasing invariant CP violating parameters with Majorana neutrinos,” *Phys. Rev. D* **64** (2001) 076005, [arXiv:hep-ph/0105305](#).
- [84] E. E. Jenkins and A. V. Manohar, “Rephasing Invariants of Quark and Lepton Mixing Matrices,” *Nucl.Phys.B* **792** (2008) 187–205, [arXiv:0706.4313 \[hep-ph\]](#).
- [85] G. Branco, R. Felipe, and F. Joaquim, “Leptonic CP Violation,” *Rev.Mod.Phys.* **84** (2012) 515–565, [arXiv:1111.5332 \[hep-ph\]](#).
- [86] S. M. Bilenky, S. Pascoli, and S. T. Petcov, “Majorana neutrinos, neutrino mass spectrum, CP violation and neutrinoless double beta decay. 1. The Three neutrino mixing case,” *Phys. Rev. D* **64** (2001) 053010, [arXiv:hep-ph/0102265](#).
- [87] J.-N. Lu and G.-J. Ding, “Alternative Schemes of Predicting Lepton Mixing Parameters from Discrete Flavor and CP Symmetry,” *Phys.Rev.D* **95** no. 1, (2017) 015012, [arXiv:1610.05682 \[hep-ph\]](#).
- [88] C.-C. Li, J.-N. Lu, and G.-J. Ding, “Toward a unified interpretation of quark and lepton mixing from flavor and CP symmetries,” *JHEP* **02** (2018) 038, [arXiv:1706.04576 \[hep-ph\]](#).
- [89] J.-N. Lu and G.-J. Ding, “Dihedral flavor group as the key to understand quark and lepton flavor mixing,” *JHEP* **03** (2019) 056, [arXiv:1901.07414 \[hep-ph\]](#).
- [90] P. Ballett, S. F. King, C. Luhn, S. Pascoli, and M. A. Schmidt, “Testing atmospheric mixing sum rules at precision neutrino facilities,” *Phys. Rev. D* **89** no. 1, (2014) 016016, [arXiv:1308.4314 \[hep-ph\]](#).
- [91] S. T. Petcov, “Predicting the values of the leptonic CP violation phases in theories with discrete flavour symmetries,” *Nucl. Phys. B* **892** (2015) 400–428, [arXiv:1405.6006 \[hep-ph\]](#).
- [92] **DUNE** Collaboration, B. Abi *et al.*, “Deep Underground Neutrino Experiment (DUNE), Far Detector Technical Design Report, Volume II: DUNE Physics,” [arXiv:2002.03005 \[hep-ex\]](#).
- [93] **Hyper-Kamiokande** Collaboration, K. Abe *et al.*, “Hyper-Kamiokande Design Report,” [arXiv:1805.04163 \[physics.ins-det\]](#).
- [94] A. Alekou *et al.*, “The European Spallation Source neutrino super-beam conceptual design report,” *Eur. Phys. J. ST* **231** no. 21, (2022) 3779–3955, [arXiv:2206.01208 \[hep-ex\]](#). [Erratum: *Eur.Phys.J.ST* 232, 15–16 (2023)].
- [95] D. Marzocca, S. T. Petcov, A. Romanino, and M. C. Sevilla, “Nonzero $|U_{e3}|$ from Charged Lepton Corrections and the Atmospheric Neutrino Mixing Angle,” *JHEP* **05** (2013) 073, [arXiv:1302.0423 \[hep-ph\]](#).
- [96] I. Girardi, S. T. Petcov, and A. V. Titov, “Determining the Dirac CP Violation Phase in the Neutrino Mixing Matrix from Sum Rules,” *Nucl. Phys. B* **894** (2015) 733–768, [arXiv:1410.8056 \[hep-ph\]](#).

- [97] I. Girardi, S. T. Petcov, and A. V. Titov, “Predictions for the Leptonic Dirac CP Violation Phase: a Systematic Phenomenological Analysis,” *Eur. Phys. J. C* **75** (2015) 345, [arXiv:1504.00658 \[hep-ph\]](#).
- [98] I. Girardi, S. T. Petcov, and A. V. Titov, “Predictions for the Dirac CP Violation Phase in the Neutrino Mixing Matrix,” *Int. J. Mod. Phys. A* **30** (2015) 1530035, [arXiv:1504.02402 \[hep-ph\]](#).
- [99] A. A. et al, “First measurement of reactor neutrino oscillations at JUNO,” 2025. <https://arxiv.org/abs/2511.14593>.
- [100] Z.-z. Xing and S. Zhou, “Tri-bimaximal Neutrino Mixing and Flavor-dependent Resonant Leptogenesis,” *Phys. Lett. B* **653** (2007) 278–287, [arXiv:hep-ph/0607302](#).
- [101] C. S. Lam, “Mass Independent Textures and Symmetry,” *Phys. Rev. D* **74** (2006) 113004, [arXiv:hep-ph/0611017](#).
- [102] P. Ballett, S. F. King, S. Pascoli, N. W. Prouse, and T. Wang, “Sensitivities and synergies of DUNE and T2HK,” *Phys. Rev. D* **96** no. 3, (2017) 033003, [arXiv:1612.07275 \[hep-ph\]](#).
- [103] G.-J. Ding, L. L. Everett, and A. J. Stuart, “Golden Ratio Neutrino Mixing and A_5 Flavor Symmetry,” *Nucl. Phys. B* **857** (2012) 219–253, [arXiv:1110.1688 \[hep-ph\]](#).
- [104] P. P. Novichkov, J. T. Penedo, S. T. Petcov, and A. V. Titov, “Modular A_5 symmetry for flavour model building,” *JHEP* **04** (2019) 174, [arXiv:1812.02158 \[hep-ph\]](#).
- [105] G.-J. Ding, S. F. King, and X.-G. Liu, “Neutrino mass and mixing with A_5 modular symmetry,” *Phys. Rev. D* **100** no. 11, (2019) 115005, [arXiv:1903.12588 \[hep-ph\]](#).
- [106] G.-J. Ding, S. F. King, C.-C. Li, and Y.-L. Zhou, “Modular Invariant Models of Leptons at Level 7,” *JHEP* **08** (2020) 164, [arXiv:2004.12662 \[hep-ph\]](#).
- [107] S. F. King, T. Neder, and A. J. Stuart, “Lepton mixing predictions from $\Delta(6n^2)$ family Symmetry,” *Phys. Lett. B* **726** (2013) 312–315, [arXiv:1305.3200 \[hep-ph\]](#).
- [108] S. F. King and T. Neder, “Lepton mixing predictions including Majorana phases from $\Delta(6n^2)$ flavour symmetry and generalised CP,” *Phys. Lett. B* **736** (2014) 308–316, [arXiv:1403.1758 \[hep-ph\]](#).
- [109] C.-C. Li and G.-J. Ding, “Implications of residual CP symmetry for leptogenesis in a model with two right-handed neutrinos,” *Phys. Rev. D* **96** no. 7, (2017) 075005, [arXiv:1701.08508 \[hep-ph\]](#).
- [110] J. A. Escobar and C. Luhn, “The Flavor Group $\Delta(6n^2)$,” *J. Math. Phys.* **50** (2009) 013524, [arXiv:0809.0639 \[hep-th\]](#).